DOKUZ EYLÜL UNIVERSITY
GRADUATE SCHOOL OF NATURAL AND APPLIED SCIENCES

DESIGN AND IMPLEMENTATION OF EMOTION AND NEUROLOGICAL DISORDER DETECTION SYSTEM USING EEG SIGNALS

by
Betül YÜRDEM

January, 2023
İZMİR

DESIGN AND IMPLEMENTATION OF EMOTION AND NEUROLOGICAL DISORDER DETECTION SYSTEM USING EEG SIGNALS

A Thesis Submitted to the
Graduate School of Natural and Applied Sciences of Dokuz Eylül University
In Partial Fulfillment of the Requirements for the Degree of Master of Science
in Electrical and Electronics Engineering Program

by
Betül YÜRDEM

January, 2023
İZMİR

M.Sc THESIS EXAMINATION RESULT FORM

We have read the thesis entitled **"DESIGN AND IMPLEMENTATION OF EMOTION AND NEUROLOGICAL DISORDER DETECTION SYSTEM USING EEG SIGNALS"** completed by **BETÜL YÜRDEM** under supervision of **ASSOC. PROF. DR. AHMET ÖZKURT** and we certify that in our opinion it is fully adequate, in scope and in quality, as a thesis for the degree of Master of Science.

Assoc. Prof. Dr. Ahmet ÖZKURT

Supervisor

Prof. Dr. Mehmet ENGİN

(Jury Member)

Prof. Dr. Mehmet KUNTALP

(Jury Member)

Prof. Dr. Okan FISTIKOĞLU

Director

Graduate School of Natural and Applied Sciences

ACKNOWLEDGEMENTS

I would like to thank my advisor, Assoc. Prof. Ahmet ÖZKURT, for his support and guidance on the studies we have done so far.

I would like to express my gratitude to my professors, colleagues, and friends from Dokuz Eylül University and İzmir Bakırçay University for their unwavering support throughout this process.

I am grateful to my beloved parents for their endless support, and to my little sister for her medical information assistance and patience.

In addition, I would like to express my gratitude to all professors on the team of the Dokuz Eylül University BAP project, numbered 2018.KB.SAG.005, who ensured the realization of the data recording process of this thesis, especially the project coordinator Prof. Dr. Arzu GENÇ. This BAP project is approved by Dokuz Eylül University Ethics Committee.

Betül YÜRDEM

DESIGN AND IMPLEMENTATION OF EMOTION AND NEUROLOGICAL DISORDER DETECTION SYSTEM USING EEG SIGNALS

ABSTRACT

In this study, various studies were conducted on the detection of emotions and diseases with electroencephalography (EEG) signals. Relationships between emotions and changes in brain activity were analyzed using EEG datasets found in the literature and recorded with a designed system. From the results, an algorithm was developed that provides personalized informative electrode selection. The designed system has been used to record EEG, acceleration of body movements, and user-controlled marking data. After hardware and software parts were realized and combined, data recording implementations were carried out for different tasks. In some of these implementations, EEG and marking data were recorded while the participants viewed images or answered the questions. Using the results obtained from the studies done with the dataset in the literature and the developed algorithm, emotion and mental state studies were carried out on this recorded data. Additionally, concentration mental state and anxiety emotion levels were used for analyses, and classifications were done with basic machine learning and thresholding methods. Another dataset recording implementation is for disease detection. Here, in addition to EEG and marking data, acceleration data were also recorded. During these recordings, the patients performed specific tasks they were told (such as walking and turning around). Then, studies were carried out using an interface developed for disease detection. In these studies, using concentration and anxiety levels and Hjorth parameters, detections were done before, during, and after the disease occurred.

Keywords: Electroencephalography, emotion and mental state detection, disease detection, concentration, anxiety, Hjorth parameters, machine learning, thresholding method, signal processing, data acquisition system

EEG SİNYALLERİ KULLANILARAK DUYGU VE NÖROLOJİK RAHATSIZLIK TESPİT SİSTEMİ TASARIMI VE UYGULAMASI

ÖZ

Bu çalışmada, elektroensefalografi (EEG) sinyalleri ile duyguların ve hastalıkların tespiti üzerine çeşitli çalışmalar yapılmıştır. Literatürde bulunan ve tasarlanan bir sistemle kaydedilen EEG veri setleri kullanılarak duygular ile beyin aktivitesindeki değişimler arasındaki ilişkiler analiz edilmiştir. Elde edilen sonuçlardan ise kişiye özel bilgilendirici elektrot seçimi sağlayan bir algoritma geliştirilmiştir. Tasarlanan sistem EEG, vücut hareketlerindeki hızlanma ve kullanıcı kontrollü işaretleme verilerinin kaydedilmesi için kullanılmıştır. Donanım ve yazılım kısımları gerçekleştirilip birleştirilen bu sistem ile farklı görevler için veri kayıt uygulamaları gerçekleştirilmiştir. Bu uygulamaların bazılarında, katılımcıya görsel gösterilirken ya da katılımcı sorulan soruları cevaplarken EEG ve işaretleme verileri kaydedilmiştir. Literatürdeki veri seti ve geliştirilen algoritma ile yapılan çalışmalardan elde edilen sonuçlar kullanılarak, kaydedilen bu veriler üzerinde duygu ve mental durum çalışmaları yapılmıştır. Ayrıca, konsantrasyon mental durumu ve anksiyete duygu seviyeleri analizler için kullanılmış ve temel makine öğrenmesi ve eşikleme yöntemleri ile sınıflandırmalar yapılmıştır. Veri seti kayıt uygulamalarından bir diğeri ise hastalık tespiti içindir. Burada EEG ve işaret verilerine ek olarak hızlanma verisi de kaydedilmiştir. Bu kayıtlar esnasında hastalar kendilerine söylenen özel görevleri (yürüme ve kendi etrafında dönme gibi) yerine getirdiler. Ardından hastalık tespiti için geliştirilen bir arayüz kullanılarak çalışmalar yapılmıştır. Bu çalışmalarda konsantrasyon, anksiyete ve Hjorth parametreleri kullanılarak hastalık oluşmadan önce, gerçekleşirken ve sonrasında tespit edilmeye çalışılmıştır.

Anahtar Kelimeler: Elektroensefalografi, duygu ve zihinsel durum tespiti, hastalık tespiti, konsantrasyon, anksiyete, Hjorth parametreleri, makine öğrenimi, eşikleme yöntemi, sinyal işleme, veri toplama sistemi

CONTENTS

Page

LIST OF FIGURES

Page

LIST OF TABLES

Page

ABBREVIATIONS

EEG	: Electroencephalography
BMI	: Brain–Machine Interfaces
KNN	: K-Nearest Neighbor
SVM	: Support Vector Machine
PD	: Parkinson’s Disease
FOG	: Freezing of Gait
GUI	: Graphical User Interface
2D	: Two Dimensional
LALV	: Low Arousal Low Valence
LAHV	: Low Arousal High Valence
HALV	: High Arousal Low Valence
HAHV	: High Arousal High Valence
1D	: One Dimensional
LA	: Low Arousal
HA	: High Arousal
LV	: Low Valence
HV	: High Valence
ECoG	: Electrocorticography
fMRI	: Functional Magnetic Resonance Imaging
MEG	: Magnetoencephalography
BSF	: Bandstop Filter
LPF	: Low Pass Filter
HPF	: High Pass Filter
BPF	: Bandpass Filter
DEAP	: Database for Emotion Analysis Using Physiological Signals
ECG	: Electrocardiogram
EMG	: Electromyogram
EOG	: Electrooculogram
WT	: Wavelet Transform
EMD	: Empirical Mode Decomposition

DWT	: Discrete Wavelet Transform
FT	: Fourier Transform
FFT	: Fast Fourier Transform
DFT	: Discrete Fourier Transform
STFT	: Short Time Fourier Transform
PSD	: Power Spectral Density
db4	: Daubechies Wavelet of Order 4
SEED	: Shanghai Jiao Tong University Emotion EEG Dataset
SAM	: Self-assessment Manikin
DLPFC	: Dorsolateral Prefrontal Cortex
LAD	: Linear Discriminant Analysis
WE	: Wavelet Energy
TWE	: Total Wavelet Entropy
CSV	: Comma Separated Values
MP	: Mean Power
THR	: Threshold Ratio

CHAPTER ONE
INTRODUCTION

The development of technology that will facilitate the use of devices in daily life or improve human health is becoming more popular day by day with brain data. The data about the activity of the brain is obtained from electric and magnetic signals produced during electrochemical communication between the neurons in the brain works to operate vital and other functions. Varied methods to measure these signals are used which can be basically classified by their invasive or not (Ghadiri, Nourafza, & Rasoolian, 2019). Among these methods, electroencephalography (EEG), which is non-invasive, is the one that provides the fastest and most practical data acquisition (Cimtay & Ekmekcioglu, 2020; Kim et al., 2015). Hence, the usage of this technology is also getting more popular among the studies about Brain-Machine Interface (BMI) likewise in the field of medicine (Chaudhary, Birbaumer, & Curado, 2015; Coyle, Garcia, Satti, & McGinnity, 2011; Kerous, Skola, & Liarokapis, 2018; Musk, 2019; Torres, Torres, Hernández-Álvarez, & Yoo, 2020; Vaid, Singh, & Kaur, 2015; Vasiljevic and de Miranda, 2020).

In this thesis, a system is designed to obtain data that helps to examine the relationship between mental states, emotions, and neurological diseases by observing the changes in brain activity. Various studies have been carried out with the help of the determined relationships. These studies are given below.

- Emotion analysis with an EEG dataset from the literature,
- Emotion detection with the results from the previous study. For this analysis, a dataset was recorded by the designed measurement system for this thesis,
- Person-based informative electrode selection for emotion detection,
- Mental state prediction,
- Disease detection with the changes in mental states and emotions.

Human emotions and mental states, or in other words, brain states are complex to understand and interpret cause the effects may differ from person to person for the

same conditions (Deak, 2011). It was observed from the literature research that to investigate the psychological status of human beings, different methods have been tried to record a relevant dataset in the studies. In order to stimulate the emotions of the participants, they were shown music videos and clips from movies (Duan, Zhu, & Lu, 2013; Koelstra et al., 2011; Zheng & Lu, 2015), music was played for them to listen to (Sarno, Munawar, & Nugraha, 2016), or some images from the literature were shown (Lang, Bradley, & Cuthbert, 2005) during the recordings. Additionally, for the mental state, participants were asked to solve mathematical problems and English questions, or recite numbers backwards (Liu, Chiang, & Chu, 2013; Maskeliunas, Damasevicius, Martisius, & Vasiljevas, 2016; You, 2021). During these recordings, different types of data were recorded by using methods such as EEG and functional magnetic resonance imaging for changes in the brain activities of the participants, by videotaping their faces for changes in gesture and facial expressions, or by measuring features such as temperature and heart rate for physiological changes (Adolphs, 2002; Deak, 2011; Herrington et al., 2005; Koelstra et al., 2011).

In the literature, there are many studies about mental states or emotions using EEG that cannot be underestimated. Since EEG signals are non-stationary, the features extracted have been usually used in studies instead of using raw EEG signals (Bazgir, Mohammadi & Habibi, 2018; Choi, Kim, Jin, & Yoon, 2014; Kıymık, Güler, Dizibüyük, & Akın, 2005; Kimmatkar & Babu, 2021; Rahman et al., 2021; Ray and Cole, 1985). Time domain features such as mean, variance, standard deviation, and Hjorth parameters; features in the frequency domain such as band power and power spectral density; and features obtained from Fourier and wavelet transforms are mostly used (Byun, Lee, & Han, 2017; Koelstra et al., 2011; Sarno et al., 2016; Shahnaz, Masud, & Hasan, 2016; Wu, Xu, Shu, & Hu, 2017). Methods such as K-nearest neighbors (KNN), regression trees, support vector machines (SVM), correlation analysis, and neural networks are used for mental state and emotion classifications (Li, Xu, & Zhu, 2015; Shahnaz et al., 2016; Suhaimi, Mountstephens, & Teo, 2020; Wu et al., 2017; You, 2021).

On the other hand, within the scope of this thesis, epilepsy and Parkinson's disease (PD) among neurological disorders were scanned from the literature. While the sudden electrical changes in neurons cause epileptic seizures in epilepsy, the degeneration of neurons causes a negative effect on the functioning of the muscles of the patients as a symptom of the damage to the brain in PD (Bloem, Hausdorff, Visser, & Giladi, 2004; World Health Organization [WHO], 2006). Since both diseases are caused by a problem in the brain, most of the detection studies in the literature were done with the help of EEG signals. EEG features used in emotion studies mentioned earlier are also used in such neurological disease studies. Some studies in the literature on the detection of epileptic seizures with EEG are given as follows: a comparison of different transforms in the frequency domain (Kıymık et al., 2005), using an algorithm for feature extraction and classification (Şen & Peker, 2013), proposing a method to channel selection (Coşgun, Çelebi, & Güllü, 2021), classification with features from cubic spline interpolation (Kuran, Er, & Kuran, 2021).

In PD, although its symptoms are temporary, their occurrence can cause life-threatening risks such as freezing and falling while walking. The freezing of gait (FOG) is one of the common symptoms among patients, and its trigger is more unclear than the others (Bloem, et al., 2004; Moore, MacDougall, & Ondo, 2008; Schaafsma, Balash, Gurevich, Bartels, Hausdorff, & Giladi, 2003). There are FOG detection studies were done while a neurologist is examining the movements of the patients by giving them various tasks (Bachlin et al., 2009; Moore, et al., 2008; Schaafsma, et al., 2003). It was observed that different types of physiological signals are also used in PD detection studies. Using acceleration signals obtained from motion sensors connected to the left leg of the PD patients, a freezing index was determined in a study (Moore, et al., 2008). The freezing index is calculated by dividing the 3-8 Hz band (freeze band) power to the 0.5-3 Hz band (locomotor band) power, then values above a chosen threshold indicate the FOG events (Moore, et al., 2008). Additionally, freezing index thresholding was also used for FOG detection using leg motion data (Bachlin et al., 2009). In addition to these, studies using only EEG signals such as FOG estimation in the time domain and frequency domain,

examining the changes in brain activity during FOG, and the relationships between lobes have been conducted (Gérard et al., 2022; Handojoseno et al., 2012; Handojoseno et al., 2018; Shine et al., 2014).

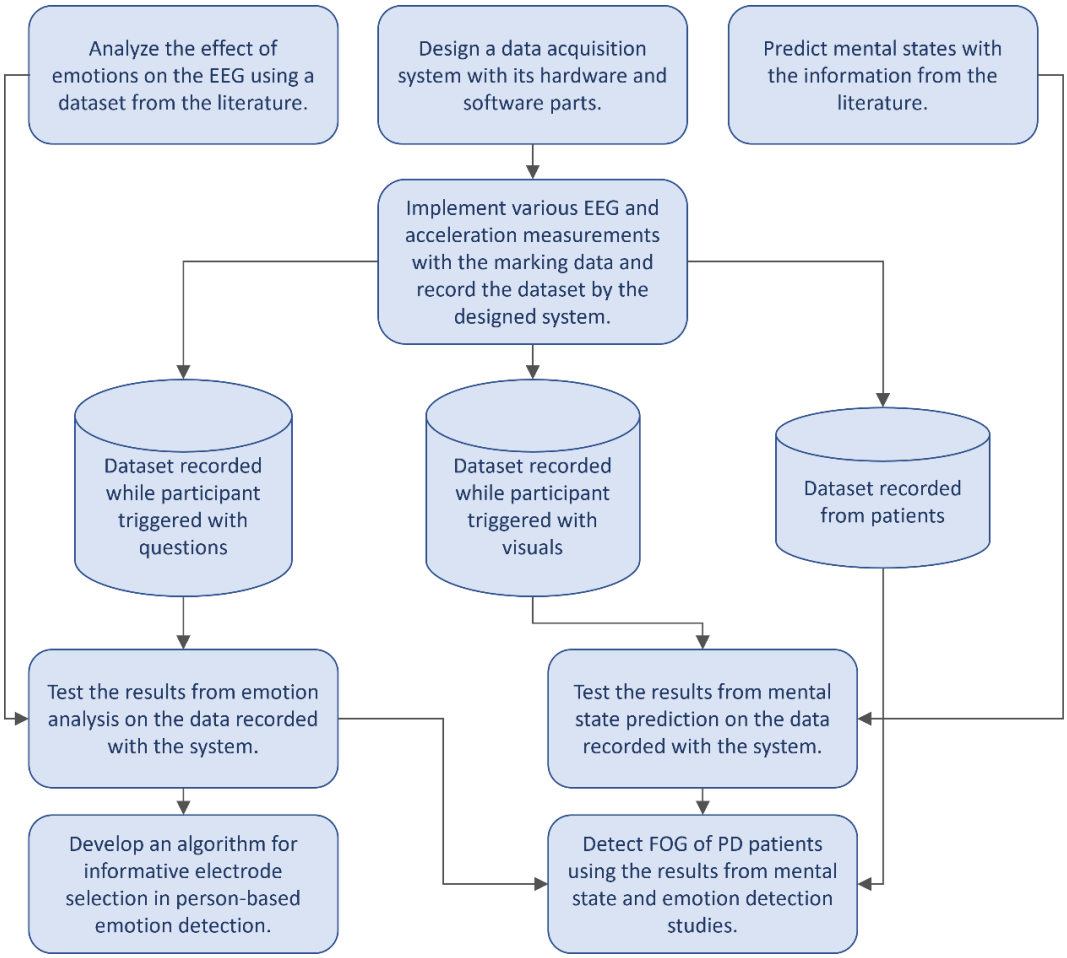

Figure 1.1 Flowchart of the studies in the thesis

Experimental studies within the scope of the thesis consist of the steps given in the flowchart in Figure 1.1. First, a system was designed with its hardware and software parts. This system includes different types of devices such as EEG measurement device, acceleration measurement sensor, computers, a button unit for data marking, and communication units. The simultaneous operation of all these devices throughout the system is provided by programs written in Python, Matlab, and Arduino languages. With this system, EEG, acceleration, and user-controlled marking data are measured and recorded. Detailed information about the system design is given in chapter three.

This system is designed to be used for studies on different subjects, and three different usage applications are included in this thesis. As given in the flowchart, these applications were carried out in the next step of system design. Meanwhile, studies on mental states and emotions were carried out using information and an EEG dataset in the literature. Within the scope of the thesis, these studies were basically done to determine the feasibility of detections with EEG and which features are more proper to use. After that, these inferences were used in the analysis of the data obtained by the designed system, and an algorithm was also composed to choose the most informative electrode by conducting emotion studies on a person-based basis.

The three mentioned datasets were recorded while the participants were viewing a displayed image, answering questions, and performing a task with special moves. The inferences for emotion by using the dataset in the literature were used in the test and analysis of the dataset recorded during triggering with questions. Then, the dataset recorded during triggering with images was used in the mental state analyses. And lastly, since there is a relationship between emotional changes and PD symptoms, disease detection studies in this thesis were done with the help of this relationship (Rahman, Griffin, Quinn, & Jahanshahi, 2008). Thus, the dataset recorded from patients while performing a special task was analyzed by the results obtained from both mental state and emotions.

The content of this thesis can be summarized with the main topics and the chapters are as follows:

In chapter two, medical information about the human brain and how it works, descriptions of some neurological disorders, the definition of mental states and emotions, and methods to investigate brain activity are given.

More theoretical information about the EEG measurement method, the signal processing steps, features, and extraction of them are explained in chapter three. Also, studies about emotion and disease detection with EEG are given.

The design of the data acquisition system is explained in two parts in chapter four. The first part is the hardware part in which the system equipment is described. Then in the second part, the software to connect all the system parts is explained step by step.

The implementation of this system for different cases is given in chapter five. These cases are mental state and emotion analysis triggered by images and questions, and detection of symptoms of neurological disorders.

In chapter six, all the applications performed within the scope of the thesis and their results are briefly explained. The studies are the emotion analyzes by using two separate datasets in the literature and recorded with the designed system, the generated algorithm for the informative electrode selection in emotion detection, and the detection of the FOG symptom with mental states and emotions from the data of PD patients. The details of the designed graphical user interface (GUI) for the analyzes are also given in this section.

Finally, the summary of the studies and their results, the conclusion, and recommendations for future work for this thesis are given in chapter seven.

CHAPTER TWO
MEDICAL BACKGROUND

Explanations about the medical information used in the content of the thesis are given in this chapter. These are the functioning of the human brain, its functions, mental states and emotions with their psychological and physiological effects, diseases that occur due to neurological problems in the brain, and the methods used to examine brain activities.

2.1 Human Brain

The human brain analyzes the environment, stores information, produces thoughts, and determines the physiological and psychological responses of the body to the events taking place in the person's environment (Guyton & Hall, 2006). There are special cells such as nerve and glial cells in the structure of the brain, so it is an electrochemical organ (Demiralp, 2021). Nerve cells or neurons can receive, process, and transmit impulses which are electrical signals that help communication in the central nervous system. There are four main parts in the structure of a neuron: dendrites, cell body, axons and synapses (Demiralp, 2021). There are almost 86 billion neurons, and they are connected to each other by synapses (Demiralp, 2021). Each neuron has about a thousand synaptic endings and ten thousand synaptic inputs (Malmivuo & Plonsey, 1995). A typical neuron structure and the flow direction of electrical signals in a neuron are shown in 2.1.

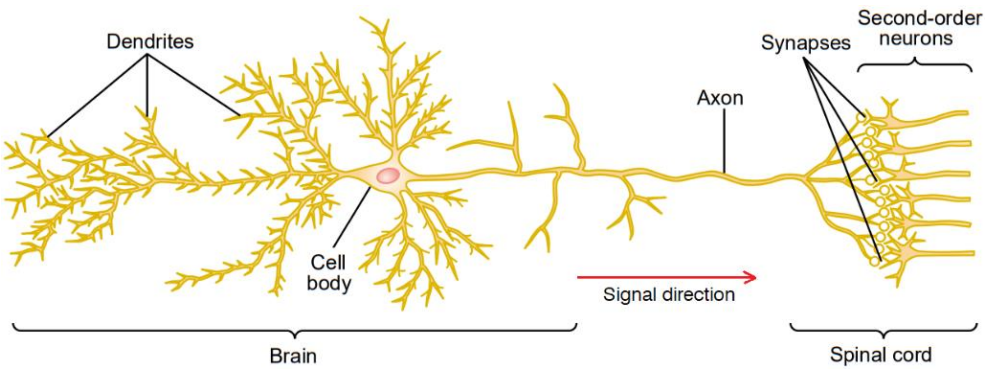

Figure 2.1 Neuron structure (Guyton & Hall, 2006)

The dendrites get the input signals, then the signals are processed in the cell body, and the axons transmit the output signals (Guyton & Hall, 2006). The synapses in the neurons are generally chemical synapses, and their structure allows the signals to be conducted in one direction (Guyton & Hall, 2006). Distribution differences of potassium, sodium, and chlorine ions throughout the neuron structure cause potential differences (Demiralp, 2021). To transmit the electrical signals, potential differences generated in the cell from dendrites to synapses provide the transmission of electrical current, and after the current passes from a region, the potential difference returns to its previous level (Bal, 2021).

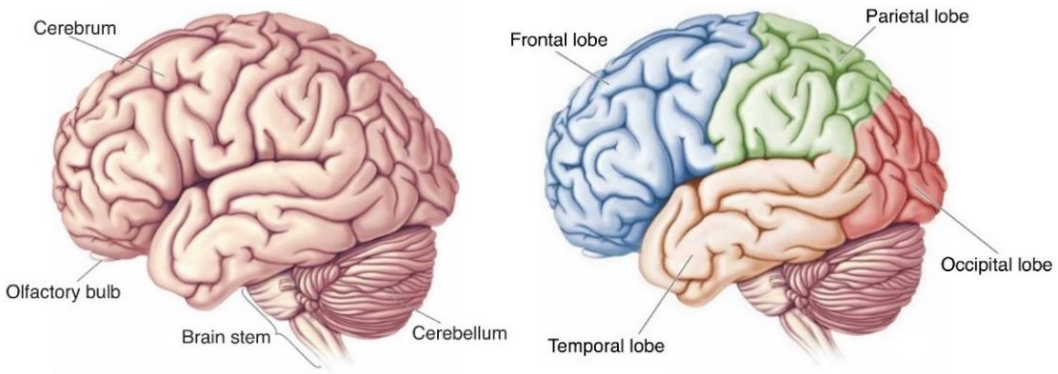

Figure 2.2 Human brain anatomy and lobes of the cerebrum (Bear, Connors, & Paradiso, 2016)

Among the main parts of the human brain, such as the cerebrum, cerebellum, brain stem, thalamus, and amygdala, the largest part is the cerebrum, or in other words cerebral cortex. It has two strongly folded hemispheres, and the frontal lobe, parietal lobe, occipital lobe, and temporal lobe are its main lobes (Malmivuo & Plonsey, 1995). The anatomy of the human brain and lobes on the cerebrum are given in Figure 2.2.

2.1.1 Motor and Sensory Controls

Each area of the brain has its own functions to control reactions such as motor and sensory. The cerebrum provides different functions such as a conscious sense, motor control, personal characteristic, learning, memory, communication, thinking,

planning according to the goal and the future (Demiralp, 2021). The general functions of the lobes are as follows:

- In the frontal lobe, planning of any movement, realization, thinking, information processing, emotion control, and evaluation,
- In the parietal lobe, touch, temperature, pain sensation, coordination of finger movements, coordination of space and movement,
- In the temporal lobe, sound and smell analysis, verbal memory, responsibility for remembrance, object recognition, and speech control,
- In the occipital lobe, color, movement, shape and depth analysis, visual associations, evaluation of sensations, interpretation, and classification of impressions are effectuated (Wróbel, 2018).

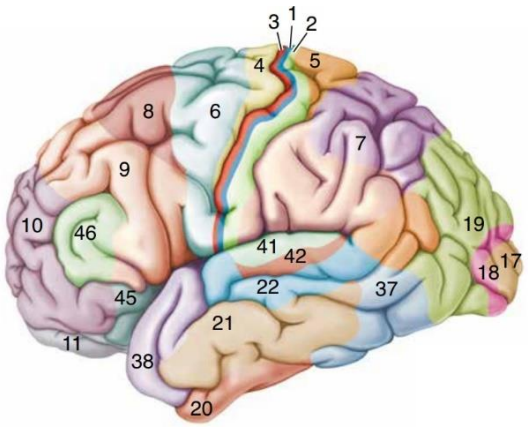

Figure 2.3 Brodmann's map (Bear et al., 2016)

Areas in the brain were first described by Brodmann (Bear et al., 2016). The function map of Brodmann is shown in Figure 2.3. In this map, each numbered area is for another function, and their functions are grouped as motor, sensory, and association. From sensory areas, 17, 18, 19 are visual areas, 1, 2, 3 are somatic sensory areas, and 41, 42 are auditory areas. Areas 4 and 6 are the motor control areas. The remaining areas are defined as association areas, as they can be identified as precisely responsible for neither sensory nor motor control (Bear et al., 2016).

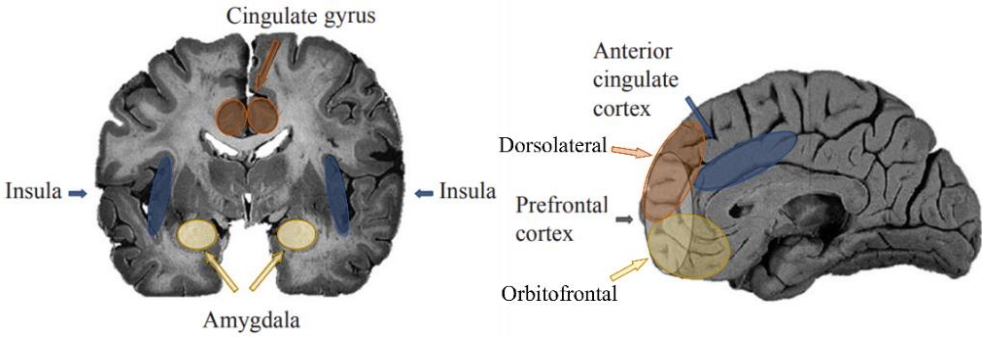

Figure 2.4 Important brain parts responsible for emotions (Deak, 2011)

As well as the cerebrum which forms the outside of the brain, there are important main parts like the amygdala, thalamus, hypothalamus, and hippocampus inside the brain. The amygdala is for fear emotion, and emotional memory. The thalamus is for transferring a big part of the sensory signals to the cerebrum. And the main functions of the hippocampus are learning, spatial memory, and consolidation of autobiographical memories in long-term memory (Demiralp, 2021). Implicated regions of the brain for emotion and memory are the amygdala, hippocampus, and hypothalamus (Suhaimi et al., 2020). These parts are shown in Figure 2.4.

2.2 Mental States and Emotion

Mental states and emotions occur as a response of the human brain to daily events besides physical responses, and hard to define and predict due to being subjective (Deak, 2011). The mental states are classified as concentration and relaxation, or attention and meditation states in the literature (Li et al., 2015; You, 2021). Its classification depends on the effort of the work with which people's minds are engaged (You, 2021).

Since the mental reaction of each person may vary, there are only empirical theories for emotion, which are discrete and dimensional emotions (Hamann, 2012; Zucco, Calabrese, & Cannataro, 2019). Discrete emotions can be defined by basic and non-basic emotions, and the basic emotions are recognizable from facial expressions, quickly detectable, and unique feelings. Thus, acceptance, anger,

anticipation, disgust, joy, fear, sadness, and surprise are some of the identified basic discrete emotions (Zucco et al., 2019).

Mostly known dimensional emotions were modeled by Russell and Plutchik (Koelstra et al., 2011). Plutchik's hybrid model was determined for different emotion pairs: anticipation-surprise, fear-anger, disgust-trust, and joy-sadness (Plutchik, 2001). Russell's simple but useful circumplex model consists of valence and arousal dimensions (Russell, 1980; Thammasan, Moriyama, Fukui, & Numao, 2017). In this model, the change in valence from a high value to a low value means that the emotion changes from pleasure to displeasure, while the change in arousal corresponds to a change in emotion intensity (Hamann, 2012).

In this study, Russell's model was used for emotion analysis and detection. The emotions classified according to arousal and valence values in the circumplex emotion model is given in Figure 2.5. With this model, two-dimensional (2D) emotions can be classified as low arousal low valence (LALV), low arousal high valence (LAHV), high arousal low valence (HALV), and high arousal high valence (HAHV) (Koelstra et al., 2011; Sarno et al., 2016).

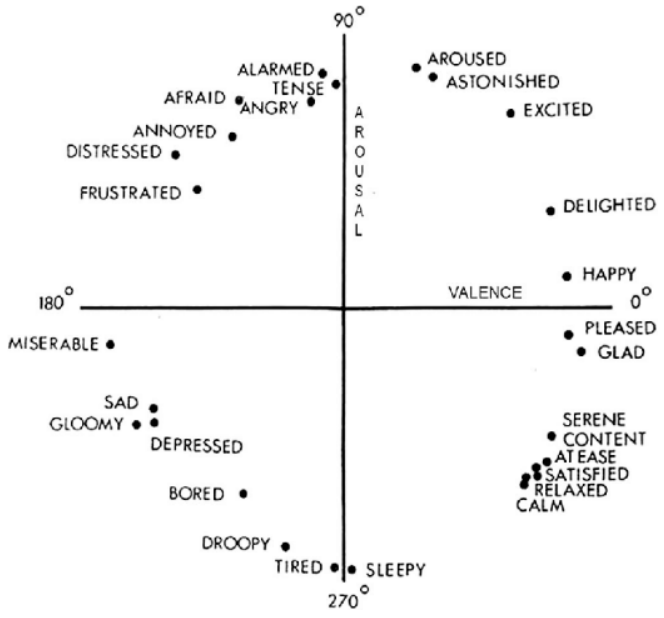

Figure 2.5 Russell's circumplex emotion model (Russell, 1980)

In Figure 2.6, 2D emotions' distribution on the same emotion model in Figure 2.5 is shown. For example, if a person's mood is classified as HAHV, the person's emotion can be classified as excited from this distribution. Besides 2D emotions, each dimension can be classified as one-dimensional (1D), like low arousal (LA) and high arousal (HA), low valence (LV) and high valence (HV).

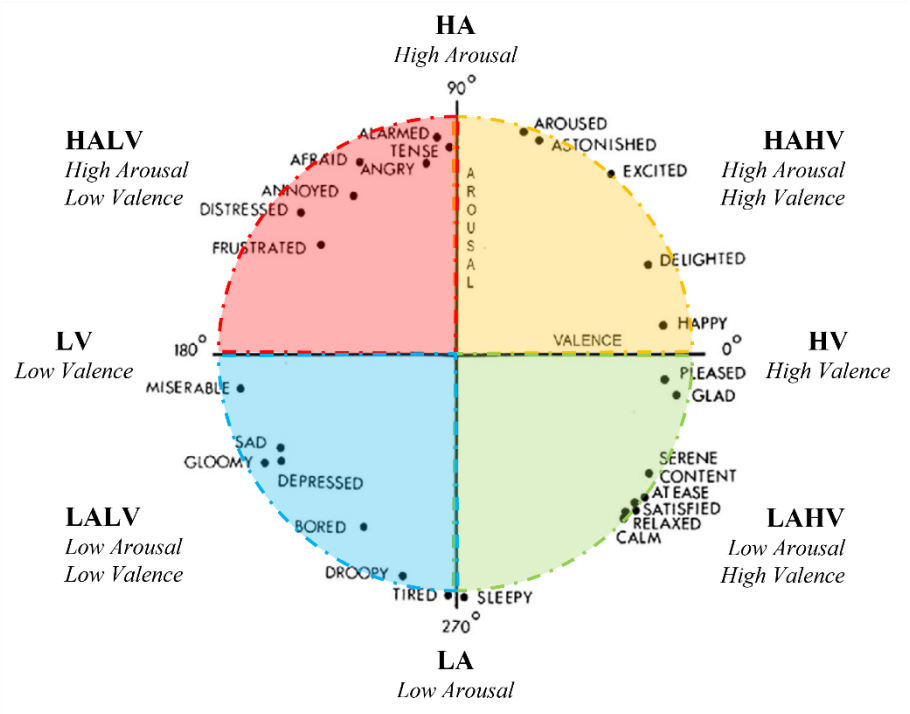

Figure 2.6 Distribution of 2D emotions on circumplex emotion model

In addition, emotional and mental states have physiological effects as well as psychological effects on people. Physiological factors such as respiration rate, blood pressure, vocal or facial expression, bioimpedance, movements in the muscular system, and temperature also undergo changes (Basu, Bag, Aftabuddin, Mahadevappa, Mukherjee, & Guha, 2016; Madden & Savard, 1995).

2.3 Neurological Disorders

Neurological diseases occur due to brain injuries, electrical over-discharge, or degeneration of neurons (Bek & Genç, 2021; Demiralp, 2021; WHO, 2006). Some of the common neurological disorders are dementia, epilepsy, multiple sclerosis, and

PD (WHO, 2006). From these disorders, epilepsy is seizures that occur due to the electrical over-discharge of neurons in the brain and cause normal brain functions to interrupt temporarily (Demiralp, 2021). Epilepsy seizures are classified into two main types based on their distribution in the brain, and they are focal and generalized seizures (Demiralp, 2021). Focal seizures begin in one area of the brain and affect that part, but in generalized seizures, discharges start from subcortical structures and spread to both hemispheres (Bek & Genç, 2021; Demiralp, 2021). In this thesis, epilepsy was examined only in the literature review of disorder detections done with EEG. In the application part of the thesis, studies on PD were carried out as disorder detection.

2.3.1 Parkinson's Disease

In PD, neurons in substantia nigra have degenerated. These neurons in the substantia nigra, which is bilaterally located in the deep structures under the cerebrum, produce and store dopamine. They transmit the dopamine to the striatum in the deep brain. The striatum gets the signals about movement from the cerebrum, and then the processed signals are transmitted to the muscles through the cerebrum, brainstem, and spinal cord. In this transmission, dopamine is used as a chemical carrier (Apaydın, Özekmekci, Oğuz, & Zileli, 2013).

The number of these cells gradually decreases over the years, and this causes slowness, tremors in the limbs, stiffness in the muscles, depression, sleep disorder, posture disorder, gait disturbance, freezing of gait (FOG), and falling in PD patients (Apaydın et al., 2013). The locations of the substantia nigra and striatum in a human brain and the comparison of the amount of transmitted dopamine for a healthy person and PD patient are given in Figure 2.7 and Figure 2.8, respectively.

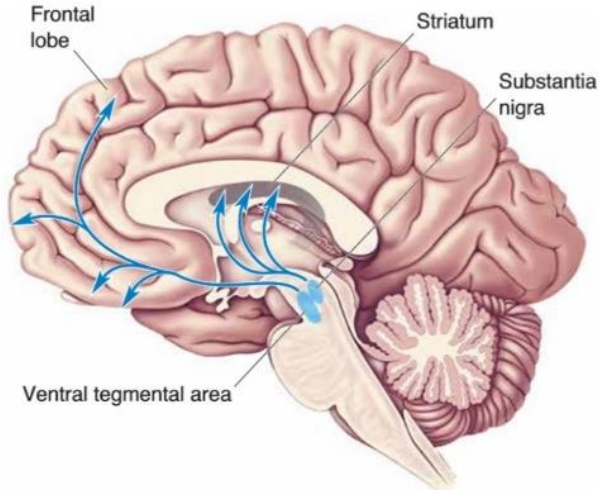

Figure 2.7 Dopamine system (Bear et al., 2016)

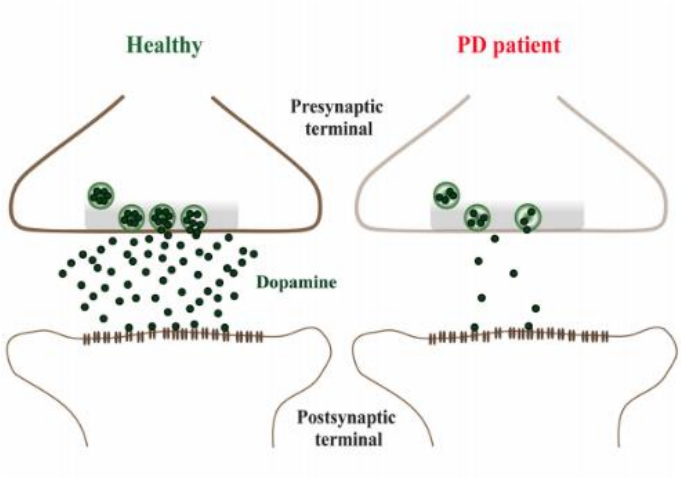

Figure 2.8 Comparison of dopamine transmission for a healthy person and a PD patient (Bridi & Hirth, 2018)

It has been observed that PD has an effect on emotions since PD causes damage in the amygdala region of the human brain, which has a very important role in the formation of emotions (Deak, 2011; Trnka, Hasto, Cabelkova, Kuska, Tavel, & Nikolai, 2018). When the amygdala structure was examined in PD patients, it was determined that there were losses on the left side of the amygdala with the increase in anxiety, and on both sides with the increase in depression (Trnka et al., 2018; van Mierlo, Chung, Foncke, Berendse, & van den Heuvel, 2015; Vriend, Boedhoe, Rutten, Berendse, van der Werf, & van den Heuvel, 2016)

PD affects the patients' daily life. Its symptoms cause difficulties in daily activities, and after all these inabilities, the patient feels less confident at doing something and even moving. Hence, understanding the symptoms and treating them is quite important. Among other symptoms of PD, FOG is one of the least figured out (Handojoseno et al., 2012). In the advanced stages of PD, this important clinical problem is manifested by taking extremely short steps, dragging the feet, or feeling as if the patient's feet are glued to the ground and unable to walk (Nutt et al., 2011). Within the scope of this thesis, only studies on the detection of FOG from PD were carried out and the results were examined.

2.4 Investigation of Brain Activity

As a result of brain starting to function, electrical signals are generated, and magnetic fields are induced by electrical currents that occur because of chemical transmission between the neurons. The human functions can be determined by the relationship of these activities with the variety of brain activity. The data obtained from these electrical brain activities is obtained to analyze the mental and physical activities of a person. Brain-machine interfaces (BMI) is a technology that aims to convert the signals obtained from the neuronal activity in the brain and use these obtained signals to control the external machines by the person only thinking (Chaudhary, Birbaumer, & Ramos-Murguialday, 2016; Waldert, 2016). In BMI, brain activity data is obtained by using different methods depending on where the electrodes are placed, such as invasive, semi-invasive, and non-invasive (Ghadiri, Nourafza, & Rasoolian, 2019).

In invasive methods, the electrodes are implanted into the cortex, and the most known types are local field potentials (LFP), single-unit activity, and multi-unit activity (MUA) (Chaudhary et al., 2016; Ghadiri et al., 2019). In another technique, semi-invasive methods such as electrocorticography (ECoG), the signals are measured with the electrodes on the surface of the cortex (Ghadiri et al., 2019). Although these two methods help to obtain the average signal of thousands of nerve cells and have a high spatial resolution, they require surgical operations to place the

electrodes (Kim et al., 2015; Musk et al., 2019). However, with the non-invasive method, the average signal of millions of nerve cells is measured from the external surface of the skull without surgery (Chaudhary et al., 2016; Musk et al., 2019).

For non-invasive methods, functional magnetic resonance imaging (fMRI), magnetoencephalography (MEG), and EEG can be said as the commonly used measurement methods (Kim et al., 2015; Rubin, Greenspan, & Brinkley, 2014). During the neural activity, fMRI detects the changes in blood flow in the brain, MEG catches the magnetic fields in the brain, and EEG measures the potential difference between regions on the surface of the brain (Kim et al., 2015; Malmivuo & Plonsey, 1995; Rubin et al., 2014). Although fMRI provides the highest spatial resolution, this method has two negative features compared to other methods: noisy operation and expensive devices (Deak, 2011). The MEG provides highest temporal resolution with higher spatial resolution than EEG, the EEG method is more practical, results faster than the other methods, and provides high precision in time (Cimtay & Ekmekcioglu, 2020; Kim et al., 2015).

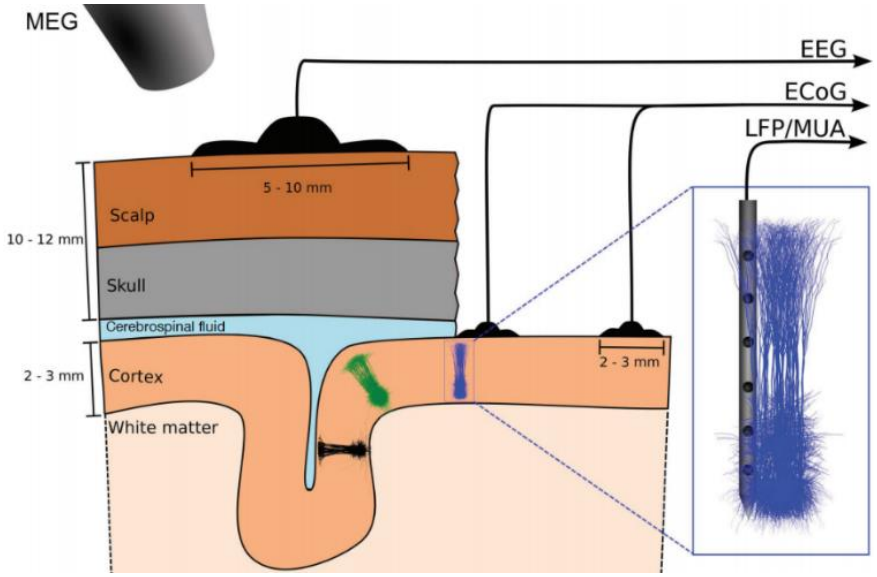

Figure 2.9 Illustration of non-invasive and invasive brain activity measurement methods (Hagen, Næss, Ness, & Einevoll, 2018)

The illustration of the measurement methods is given in Figure 2.9. The electrode placements for each mentioned measurement method can be seen in this figure. For

example, the electrodes of the ECoG, local field potentials, and multi-unit activity methods are under the scalp which means there is no other way to place these electrodes there without a surgical operation. However, the electrodes belong to non-invasive methods, which are EEG and MEG, placed on the scalp.

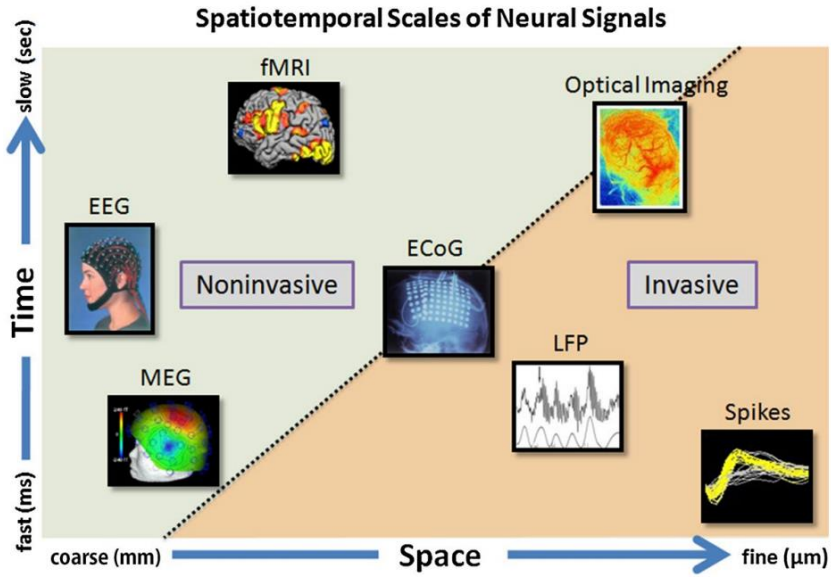

Figure 2.10 Comparison of non-invasive and invasive brain activity measurement methods in time and space (Kim et al., 2015)

In Figure 2.10, the temporal and spatial resolution comparisons of the mentioned methods are shown. From this figure, it can be said that MEG is faster than EEG, and fMRI. Therefore, MEG has the highest time resolution as the sampling frequency is the highest. From space feature comparisons, it appears that fMRI can improve data from smaller fields with high accuracy than MEG and EEG. MEG has a higher resolution for time. But it is also costly and impractical. It blocks the person's movements. Among the optical imaging and ECoG, which are semi-invasive methods, the ECoG has the highest time resolution and lowest spatial resolution. Lastly, from the measurement methods which are invasive, local field potentials has the lowest time and spatial resolutions.

CHAPTER THREE
EEG

Richard Caton published the results of the first known neurophysiologic experiment on rabbits and monkeys in 1875, and brain waves were discovered from fluctuating electrical brain activity by Adolf Beck with his study in which he placed electrodes on the surface of animals in 1890 (Emotiv, 2021). However, after almost half a century, in 1924, the EEG signals of human beings were recorded by Hans Berger, and he invented the device called the electroencephalogram, which allows the measurement of EEG signals (Britton et al., 2016).

Detailed information about the EEG measurement method, its circuit, brain waves, signal processing, feature extraction and summary literature search for studies with EEG are explained in this chapter.

3.1 Measurement Circuit

The electrical signals that fluctuate on the surface of the scalp result from chemical activity between nerve cells in the active brain. The average activity of neurons close to the placed electrodes can be observed by EEG. The general block diagram of an EEG measurement circuit is in Figure 3.1. With EEG channels, the potential difference between the reference probes and sensor probes are measured with differential amplifiers, and signals as much as the number of sensor probes is obtained (Bhagawati and Chutiai, 2016; Toresano et al., 2017). A notch filter as a band stop filter (BSF), and a low pass filter (LPF) with a high pass filter (HPF) as a bandpass filter (BPF) are applied to the signals to eliminate the distortion (Britton et al., 2016). The amplitude of EEG is on μV levels, so the gain of it is increased with post-amplifier (Webster, 2009).

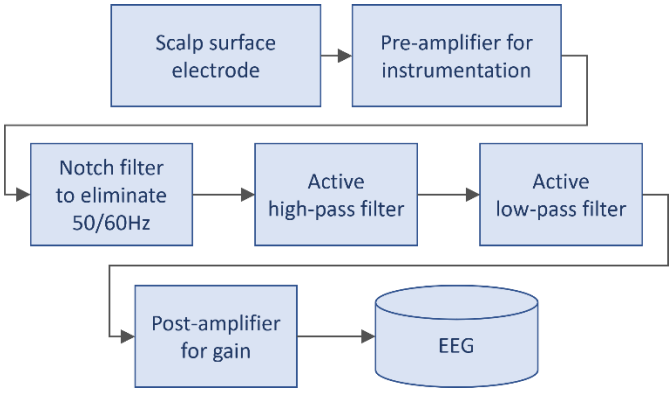

Figure 3.1 Block diagram of a typical EEG measurement circuit (Bitar & Tepe, 2021; Bhagawati & Chutiai, 2016; K and H products, n.d.; Lin, Lin, Chen, Lu, Chen, & Ko, 2010; Rabbani & Islam, 2019; Toresano et al., 2017)

3.2 Electrode Placement

The position of the electrodes is related to which areas of the brain to be examined. The average activity of the neurons for each EEG channel signal is measured by the voltage difference between two electrodes that are above these neurons. If these reference and sensor electrodes are placed closer or further to each other for different measurements, they measure different neurons' average activity (Britton et al., 2016). This may cause an error in the EEG measurement. Different standards are available to determine electrode positions to avoid errors in measurement. The common international electrode placement systems are the 10-10 system and the 10-20 system, and the electrodes are placed between 10% - 20% or 10% - 10% separation in these two systems from the center of the skull to the periphery (Acharya, Hani, Cheek, Thirumala, & Tsuchida, 2016). With these placement systems, the distances of between electrodes are defined so the error might be minimized.

Electrode locations of the international systems are given in Figure 3.2. As it can be seen from this figure, each electrode placement has a unique name which includes a letter and a number. The letter indicates which lobe of the brain the electrode is closest to. If the number is odd, the electrode is on the left hemisphere; if it is even, the electrode is on the right hemisphere (Britton et al., 2016). For example, O1 is on

the left of the occipital region and O2 is on the right. Also, some electrodes in the centerline of the scalp, such as Cz, Fz, and Pz, have the "z" letter instead of a number in their name (Britton et al., 2016).

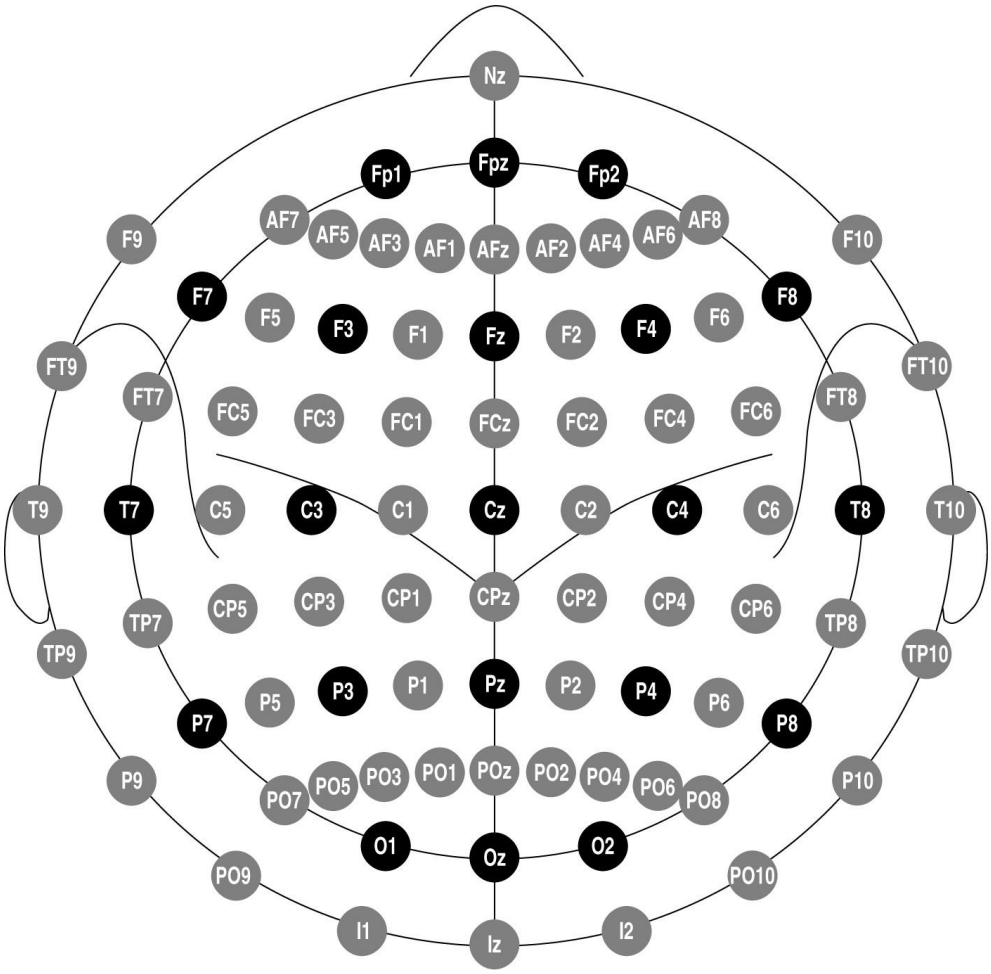

Figure 3.2 Electrode positions; black circles for the 10-20 system, and gray circles for the 10-10 system (Oostenveld & Praamstra, 2001)

The important point in EEG monitoring is the montage type means the method to display the EEG channels according to the difference signal between electrodes, and commonly used montage types are referential and bipolar (Acharya & Acharya, 2019). Of these, the bipolar montage which helps to obtain the signal between two nearby sensor electrodes, and the referential montage in which the difference signal between one reference electrode and other sensor electrodes are measured are the most used (Webster, 2009). The electrode connections of the differential amplifiers in the measurement circuit of these montages are given in Figure 3.3.

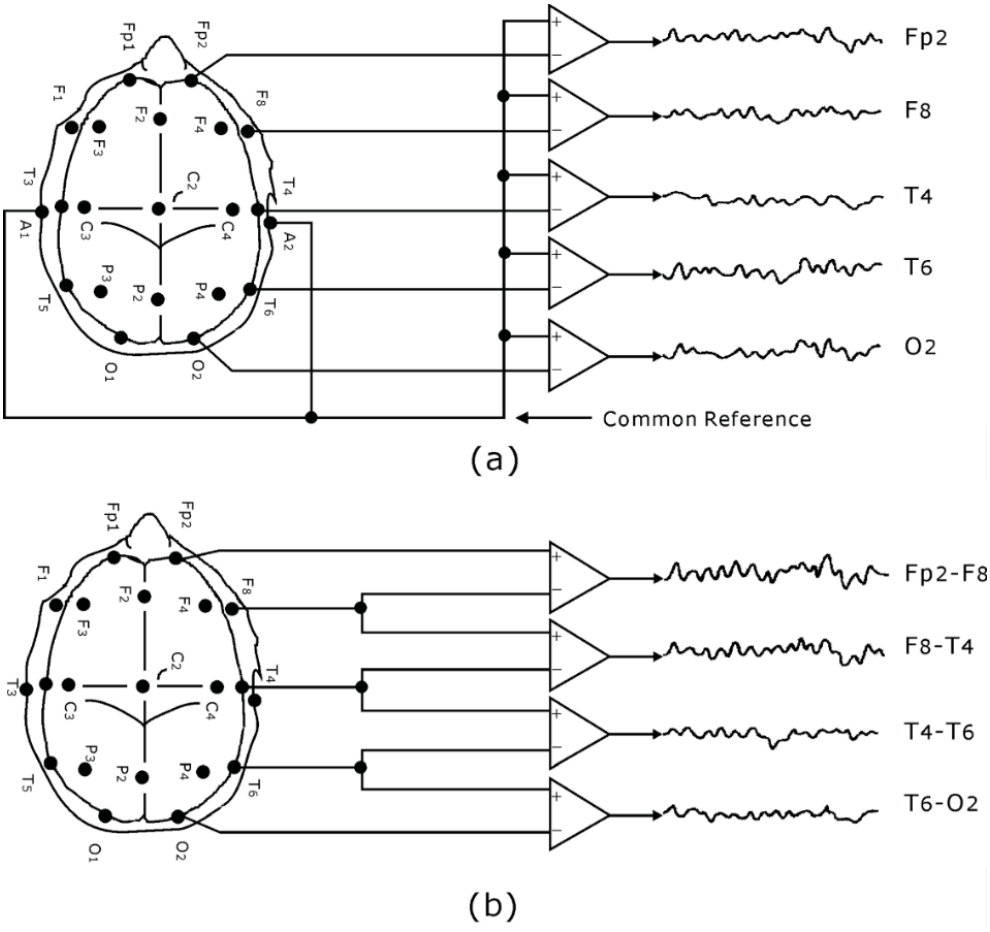

Figure 3.3 Montage types, (a) referential montage, (b) bipolar montage (K and H products, n.d.)

In Figure 3.4, EEG signals obtained from a device with the referential montage of 32 electrodes placed according to the international 10-20 system are given. These signals were obtained from the Database for Emotion Analysis using Physiological Signals (DEAP) dataset (Koelstra et al., 2011), and plotted by using Matlab as raw signals. The axes of the graphs displaying EEG usually have the same labels. The change in time is observed from the x-axis and the change in voltage from the y-axis. The overall patterns of the channel signals might seem similar, but a closer viewing would show that the signal amplitudes, polarities, or frequency components are different for each channel.

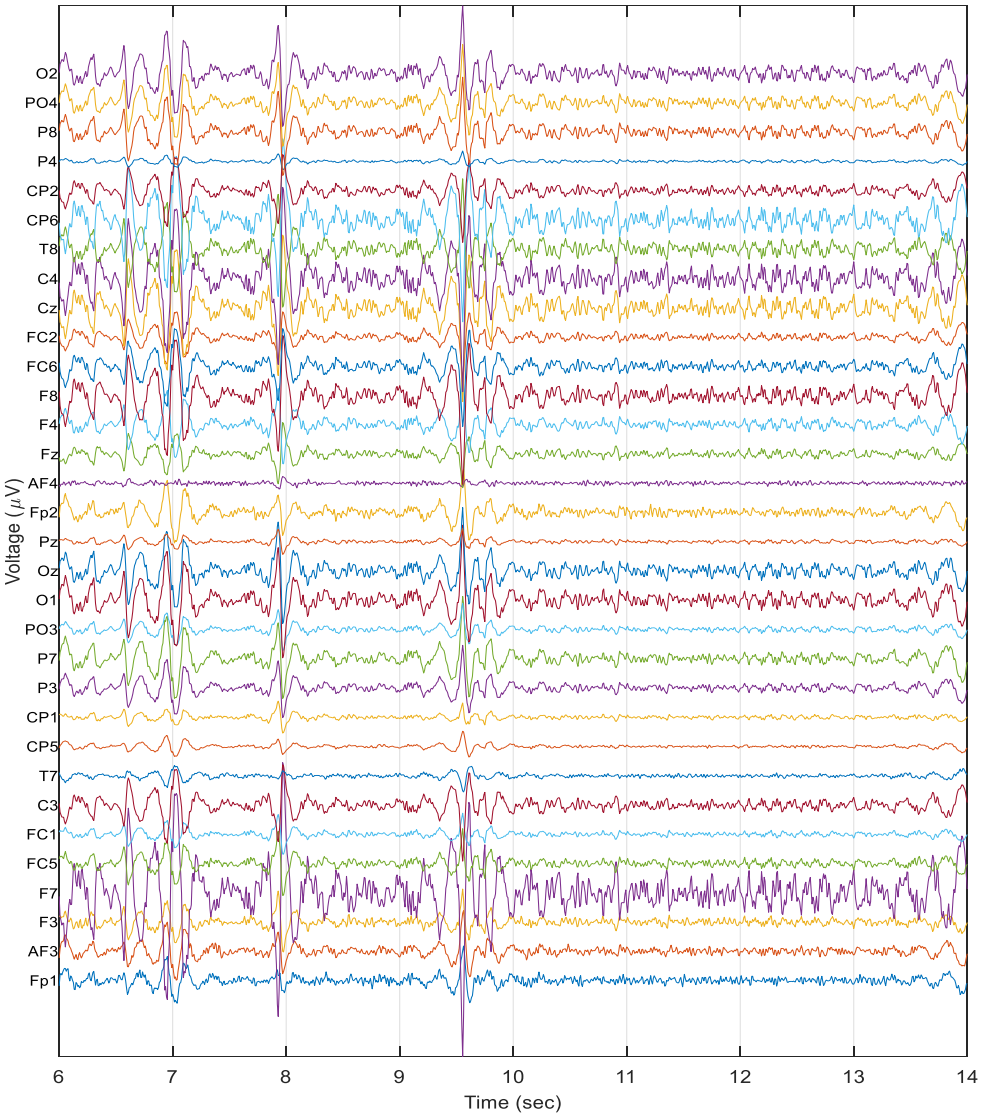

Figure 3.4 Sample signals of EEG from part of the DEAP dataset in literature with 32 electrodes placed according to international 10-20 system

3.3 Brain Waves

EEG signals are not periodic and their statistical parameters such as mean value, variance, and standard deviation change over time (Clark, Biscay, Echeverría, & Virués, 1995; Wong, Galka, Yamashita, & Ozaki, 2006). Therefore, these non-stationary signals are difficult to study. Brain waves derived from the frequency bands of EEG signals are analyzed in the observation of brain activities. There are five main brain waves: delta, theta, alpha, beta, and gamma (Bear et al., 2016). Also, it was observed in the literature that there are studies carried out with waves with

different frequency ranges (Choi et al., 2014). Information about the frequency ranges of the waves and their corresponding brain activities are given in Table 3.1.

Table 3.1 Features of brain waves (Choi et al., 2014; Posada-Quintero, Reljin, Bolkhovsky, Orjuela-Cañón, & Chon, 2019; Seo, Lee, & Crisan, 2010)

Brain wave	**Frequency range [Hz]**	**Brain activities**
Delta	< 4	Deep sleep, coma
Theta	4 – 8	Drowsiness, emotional
Alpha	8 – 12	Awake, relaxed
Low Beta	12 – 20	Active thinking, focus
High Beta	20 – 30	Anxious, stress
Gamma	> 30	Over-focused, energetic

Based on the information in this table, for instance, if the alpha waves are more dominant, it can be said that the person is awake, or if the gamma waves are more dominant, the person is over-focused on a task. In Figure 3.5, an original EEG signal and brain waves filtered from the same EEG are shown in the time domain. Delta and theta are low-frequency waves and have higher amplitudes than high-frequency alpha, beta, and gamma waves (Posada-Quintero et al., 2019).

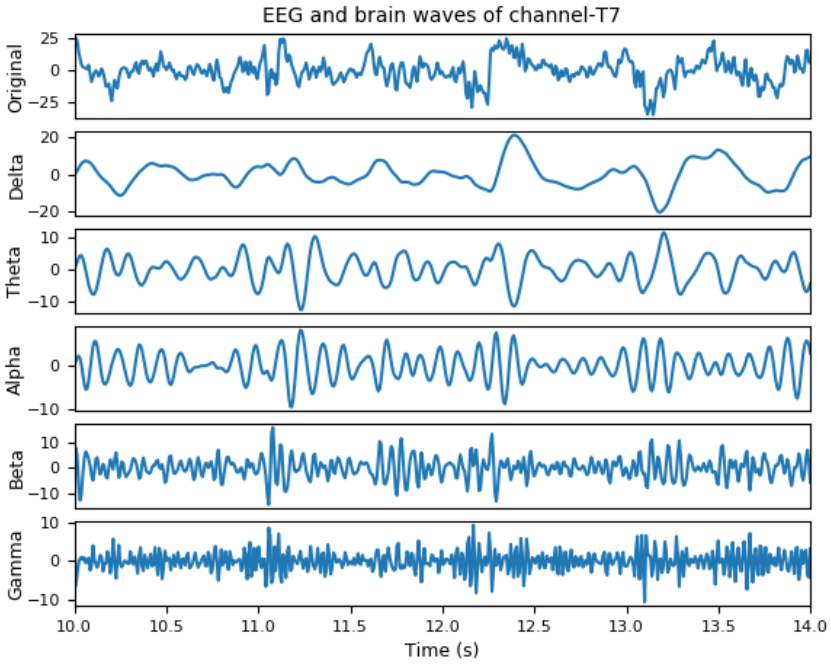

Figure 3.5 Original EEG signal of T7 channel and filtered brain waves from this study

3.4 Artifacts

In order to make more accurate EEG analyzes, the most accurate features must be extracted. For this, preprocessing needs to be applied to the raw EEG signals. The main reason for this is that other electrical signals generated in the human body or coming from the environment can also corrupt the EEG signals recorded during measurements (Britton et al., 2016). Commonly encountered internal artifacts are electrocardiogram (ECG), electromyogram (EMG), electrooculogram (EOG), eye movements, tongue movements, skin movements, and external artifacts are displacement of electrodes, EEG device movements, the poor ground connection, body and limb movements, and electromagnetic, optical, and vocalic interferences (Islam, Rastegarnia, & Yang, 2016). A recorded raw EEG signal containing samples of internal artifacts is given in Figure 3.6. The preprocessed EEG signal, which is excluded from EOG, ECG and EMG artifacts, is also given as pure EEG in this figure.

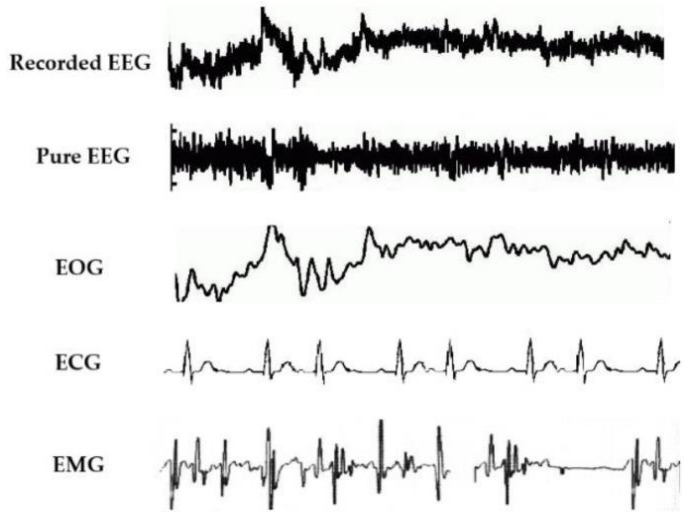

Figure 3.6 Internal artifacts observable from a raw EEG signal (Jiang, Bian, & Tian, 2019)

False information that artifacts caused are removed before analysis done with EEG. Although, these removals can cause information loss in data, their effect is reduced with this solution. Otherwise, a higher quality EEG device can be used as a precaution, but this method only helps to reduce some external artifacts, and there will still be artifacts in the recorded signal. At the artifact reduction steps, it is easier

to eliminate external artifacts from an EEG signal than internal artifacts (Anderer et al., 1999; Jiang et al., 2019; Urigüen & Garcia-Zapirain, 2015). Mostly used artifact reduction methods are LPF, HPF, BPF, BSF, adaptive filter, wavelet transform (WT), and empirical mode decomposition (EMD) (Urigüen & Garcia-Zapirain, 2015). Some artifacts and some methods from the literature to reduce them are given in Table 3.2.

Table 3.2 Artifacts and reducing methods in literature

Artifact	Method to reduce	Literature
Muscle artifact	LPF	Anderer et al., 1999
Sweat artifact	HPF	
Environmental line noise	BSF	Urigüen & Garcia-Zapirain, 2015
EOG artifact	Linear regression method Adaptive filter Principal component analysis	
EMG artifact	Adaptive filter	
ECG artifact	Recursive least-squares	
External artifacts	LPF, HPF, BPF or BSF	Jiang et al., 2019

3.5 Preprocessing

Definitions and explanations about preprocessing methods used in the literature are given in this section.

- **Filtering:** This method is used in processes such as removing brain waves from EEG signals and reducing artifacts. As mentioned earlier, there are different types of filters called LPF, HPF, BPF and BSF. Frequency components below a cut-off frequency with LPF and above a cut-off frequency with HPF are filtered out. BPF is used if a frequency range is to be filtered, and BSF is used if that range is to be rejected. BPF and BSF filters are formed by connecting LPF and HPF filters in series or in parallel (Alexander & Sadiku, 2009).

- **Wavelet Transform (WT):** With this method, the denoised EEG signal is tried to be obtained with main signal $y(t)$ which is called the mother wavelet

function. For this, scaling and shifting operations are applied to $y(t)$, and these values are the coefficients of WT (Kim, 2018). For the discrete-time sampled signals which are the EEG signals in this thesis case, the discrete WT (DWT) is applied (Islam et al., 2016). In Equation (3.1), the DWT formula is given where $x(t)$ is the original EEG signal.

$$DWT(j,k) = \frac{1}{\sqrt{|2^j|}} \int_{-¥}^{¥} x(t) y\left(\frac{t - 2^j k}{2^j}\right) dt \tag{3.1}$$

3.6 Feature Extraction

After preprocessing, various features are extracted from reliable EEG signals in the time or frequency domain. The extraction and formulas of these properties are given in this section.

3.6.1 Time Domain

- **Statistical Features:** The features calculated from the statistical parameters of the preprocessed EEG signal, $x(n)$, in the time domain are used. The formulas for calculating the smallest value in Equation (3.2), the largest value in Equation (3.3), the signal mean value in Equation (3.4), the standard deviation in Equation (3.5), the variance value in Equation (3.6), energy of the signal in Equation (3.7), and average power of a discrete signal in Equation (3.8) are given as follows (Proakis & Manolakis, 1996; Şen & Peker, 2013).

$$x_{min} = min[x(n)] \tag{3.2}$$

$$x_{max} = max[x(n)] \tag{3.3}$$

$$x_{mean} = \frac{1}{N} \sum_{n=1}^{N} x(n) \tag{3.4}$$

$$s = \sqrt{\frac{\sum_{n=1}^{N}(x(n) - x_{mean})^2}{N-1}} \tag{3.5}$$

$$var\big(x(n)\big) = s^2 = \frac{\sum_{n=1}^{N}(x(n) - x_{mean})^2}{N-1} \tag{3.6}$$

$$E_x = \sum_{n=-N}^{N} |x(n)|^2 \tag{3.7}$$

$$P_x = \lim_{N\to\infty} \frac{1}{2N+1} E_x \tag{3.8}$$

- **Hjorth Parameters:** Other features in the time domain are Hjorth parameters derived from statistical features (Oh, Lee, & Kim, 2014). The Hjorth parameters, activity, mobility, and complexity, are given in Equation (3.9), Equation (3.10), and Equation (3.11), respectively (Hjorth, 1970). In these equations, s_0 symbol is the variance, s_1 is the variance of the first derivative, and s_2 is the variance of the second derivative of the EEG signal.

$$H_{activity} = var(x) \tag{3.9}$$

$$H_{mobility} = \sqrt{\frac{var(x')}{var(x)}} \tag{3.10}$$

$$H_{complexity} = \frac{H_{mobility}(x')}{H_{mobility}(x)} \tag{3.11}$$

3.6.2 Frequency Domain

- **Fourier Transform (FT):** With FT, signals are transformed using sinusoidal functions with various frequencies as the basis function, and this transformation is defined in Equation (3.12) (Heckbert, 1995). The variable $x(t)$ in this equation represents the transformed continuous signal.

$$X(\omega) = \int_{-\infty}^{\infty} x(t) e^{-i\omega t} dt \tag{3.12}$$

- **Fast Fourier Transform (FFT):** As a result of EEG data recordings done in today's conditions, discrete signals are obtained no matter how high the signal frequency is. In addition to the transformation of continuous signals in Equation 3.10, a discrete FT (DFT) is performed for the discrete signals. For the calculation of DFT, there is an effectual algorithm called as FFT, and the definition of this is given in Equation (3.13) (Oppenheim, Buck, Daniel, Willsky, Nawab, & Singer, 1997):

$$\tilde{X}[k] = \frac{1}{N} \sum_{n=0}^{N-1} x[n] e^{-jk\left(\frac{2\pi}{N}\right)n}, \quad k = 0, 1, \dots, N-1 \tag{3.13}$$

where x[n] is the discrete signal and N is the length of this signal. For studies with EEG, the variable x[n] is the EEG signal obtained from a single electrode. As a result of this transformation, the frequency components of a signal can be examined. Also, the maximum frequency value on the FFT plot is determined as Nyquist frequency, which is the sampling frequency divided by two (Srinivasan, Tucker, & Murias, 1998).

In Figure 3.7, an example for FFT of an EEG signal is shown. In the first subplot, the preprocessed EEG signal of only the FC5 channel of a participant was plotted from the DEAP dataset. The change in the voltage of this signal, which is given for about 20 seconds, can be observed. In the second subplot, the obtained FFT result of this preprocessed signal is given. The amplitude values of the frequencies in the range of 0-64 Hz in the content of this signal, which has a sampling frequency of 128 Hz, can be observed separately. As mentioned in the description of this dataset in the literature, the signal was filtered with a BPF with cut-off frequencies of 4 and 45 Hz (Koelstra et al., 2011). This filtering process can be observed from the second subplot because the amplitude of the frequency components outside the 4-45 Hz range is 0.

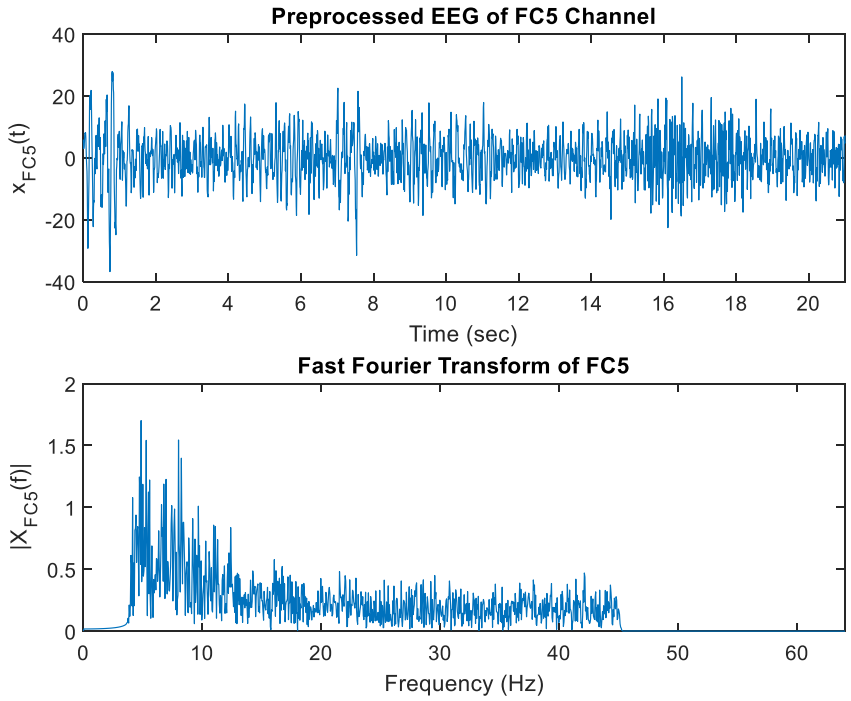

Figure 3.7 FFT example from the DEAP dataset in literature

- **Short Time Fourier Transform (STFT):** With FFT, amplitude information of all frequencies in the relevant signal can be observed. However, the changes in amplitude over time cannot be understood. STFT helps to analyze the amplitude change of all frequency components depending on time. Thus, it is often used for non-stationary signals. After the signal is divided by the windowing method, FT is applied to each segment and the process is performed. In Equation (3.14), the formula of the discrete STFT is given (Krishnan, 2021). In this equation, $\omega(n)$ is the window function.

$$STFT\{x[n]\} = X[n,\omega] = \sum_{m=-\infty}^{\infty} x(m)\omega(n-m)e^{-j\omega m} \tag{3.14}$$

An example for STFT is shown in Figure 3.8. The same data in FFT example used, but this time the change of the magnitude at different frequencies can be observed. The same data in the FFT example was used, but this time the change of the amplitude magnitude at different frequencies can be observed.

In Figure 3.7, the magnitude change only can be observed for the whole signal, and the time was unclear for changings. However, for different time ranges the magnitude change can be observed in Figure 3.8. For example, it can be understood from the values given in the magnitude color scale that the amplitude value between the 16th and 18th seconds is higher than the other times.

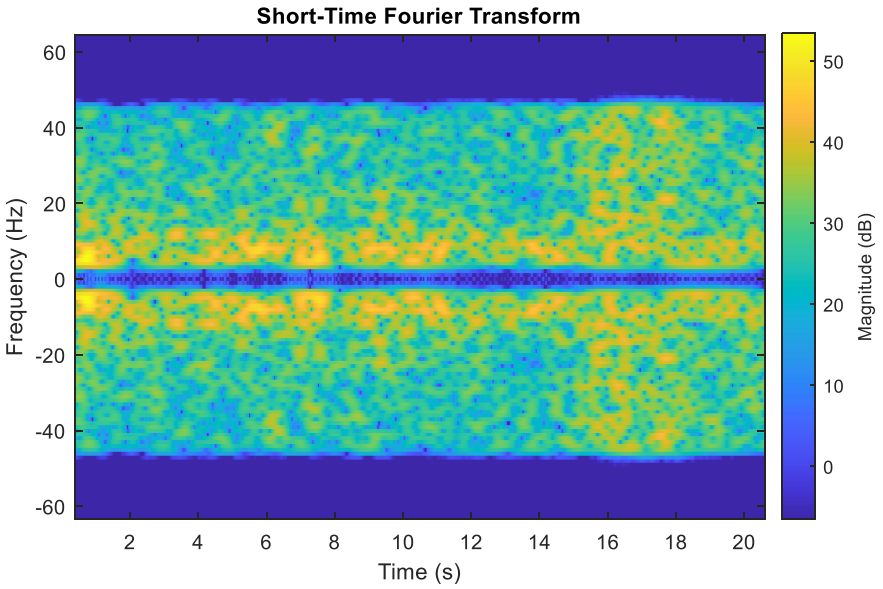

Figure 3.8 STFT result of the same data in FFT example

- **Power Spectral Density (PSD):** This method helps to examine the power distribution of a signal at each frequency component (Bansal & Mahajan, 2019). The PSD estimation is calculated with FFT of the autocorrelation of the EEG, and after the signal is divided into segments, FFT is applied to each segment, and the PSD signal is obtained from the average square of the FFT value calculated by making a correction between segments (Bansal & Mahajan, 2019). Its formula is given in Equation (3.15), where $\tilde{X}(f)$ represents FFT of $x(n)$ (Proakis & Manolakis, 1996).

$$S_{\tilde{x}\tilde{x}}(f) = \left|\tilde{X}(f)\right|^2 = \left|\sum_{n=0}^{N-1} \tilde{x}(n) e^{-j2\pi fn}\right|^2 \tag{3.15}$$

In Figure 3.9, the first subplot shows the PSD of EEG obtained from the T7 channel. Colored areas below the signal represent each sub-band, namely brain waves. The brain wave information is given in this plot. The second subplot also shows PSD signals of the same data. However, this time the brain waves are filtered from the original EEG signal, and then the PSD calculation was done for each brain wave. The sum of their distributions gives the signal in the first subplot.

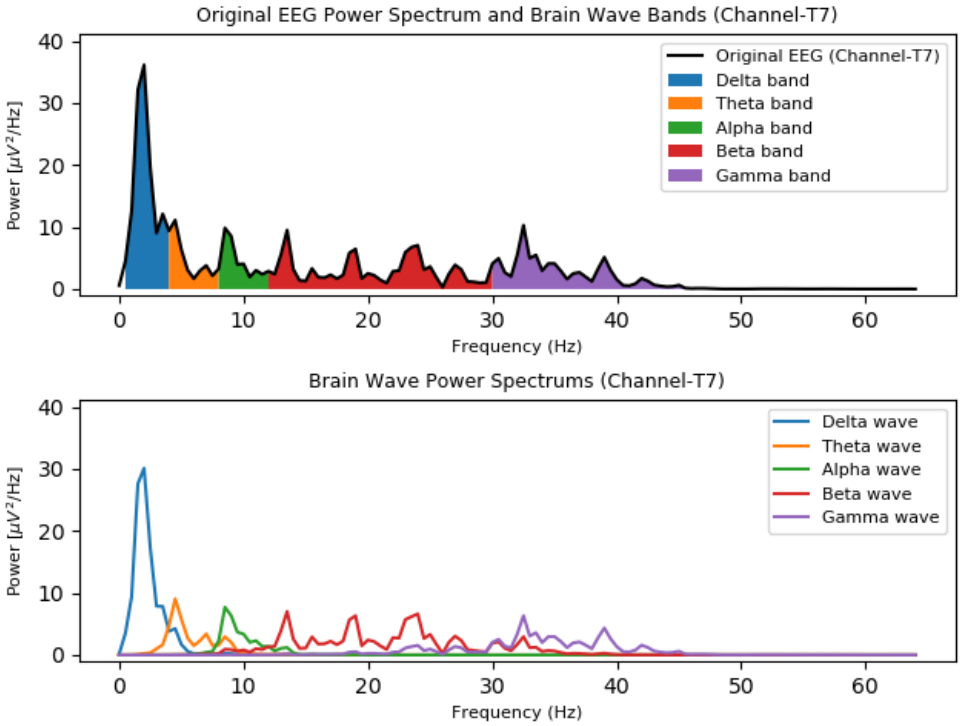

Figure 3.9 PSD of EEG signal of T7 channel and filtered brain waves

- **Wavelet Coefficients:** As it was mentioned in "Preprocessing" section, the brain wave signals are also obtained with DWT. The coefficients obtained by DWT using Daubechies wavelet of order 4 (db4), are used as the features, and it results better in classifications (Şen & Peker, 2013).

3.7 Literature Research for EEG

In the literature, EEG studies include various topics. Studies on emotions and diseases, which are also within the scope of this thesis, are some of them. The most

crucial obstacle of these studies is data. In this section, information is given about the datasets shared in the literature for emotion and the studies conducted on emotions and diseases in the literature.

3.7.1 Datasets

One of the most important issues observed in the literature for emotion detection is the dataset. It has been observed that the EEG dataset is generally used in studies in the literature for emotion detection. The datasets used in the studies are either recorded by the researchers by performing the procedures suitable for the study aim, or the data recorded for the closest purpose to the analysis in the literature are used. The participants' emotions were tried to be triggered by listening to music, examining images, or watching videos while EEG datasets were measured and recorded. Shanghai Jiao Tong University Emotion EEG Dataset (SEED), DEAP, MAHNOB-HCI, DREAMER, and LUMED are datasets built for emotion detection that are accessible as open-source in the literature (Cimtay, & Ekmekcioglu, 2020; Duan et al., 2013; Katsigiannis, & Ramzan, 2017; Koelstra et al., 2011; Soleymani, Lichtenauer, Pun, & Pantic, 2011; Zheng & Lu, 2015).

3.7.1.1. SEED Dataset

For the analysis of the emotions, 15 participants watched a total of 15 different movie clips, 5 for positive, 5 for neutral, and 5 for negative emotions. The recorded data includes EEG signals from 62 channels and eye movements. During the recording, the participants were given a 10-second start, then watched a 4-minute clip, and then rested for 20 seconds for each movie (Duan et al., 2013; Zheng & Lu, 2015). This process is given in Figure 3.10.

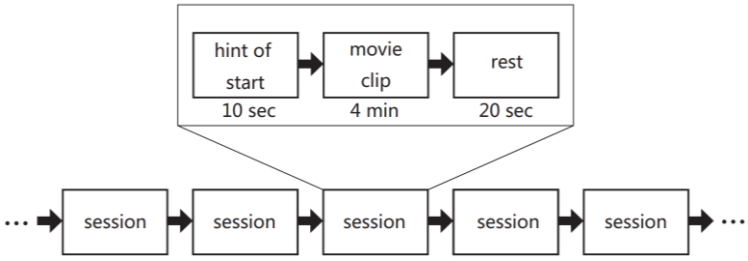

Figure 3.10 Process of viewing movie clips while recording the SEED dataset (Duan et al., 2013)

3.7.1.2. DEAP Dataset

In the DEAP dataset, 32 participants watched 40 different one-minute music videos, and the measured physiological signals were EEG of 32 channels (Fp1, AF3, F3, F7, FC5, FC1, C3, T7, CP5, CP1, P3, P7, PO3, O1, Oz, Pz, Fp2, AF4, Fz, F4, F8, FC6, FC2, Cz, C4, T8, CP6, CP2, P4, P8, PO4, O2), EOG, EMG, skin temperature, respiration pattern, blood volume pressure, and galvanic skin response (Koelstra et al., 2011). The sampling frequency of the EEG signals is 128 Hz. After watching the videos, participants were asked to rate the emotions triggered by the videos.

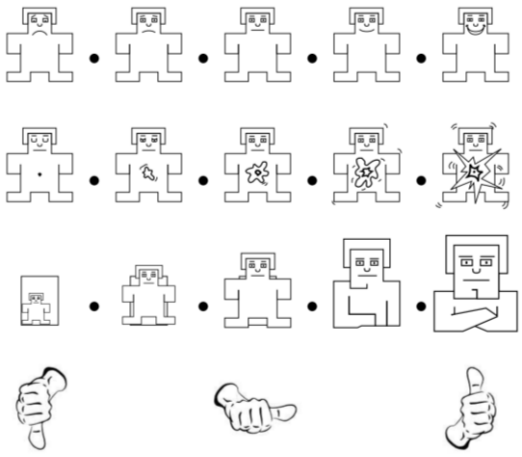

Figure 3.11 Used SAM images for valence, arousal, dominance, and liking categories, respectively (Koelstra et al., 2011)

A self-assessment manikin (SAM) for 5 different categories: arousal, valence, dominance, liking, and familiarity was used for the rating (Bradley & Lang, 1994; Koelstra et al., 2011). Images used for emotion categories in the SAM are given in

Figure 3.11. In this figure, the images at each row represent only one category. From top to bottom, the categories are as follows: valence, arousal, dominance, and liking. As a rating scale, discrete values on the scale of 1-5 were used for familiarity, and continuous values on the scale of 1-9 were used for other categories.

3.7.2 Studies

As far as it is observed in the literature and as it is tried to be done in this thesis, there are prediction and detection studies done with EEG signals for various subjects such as mental state, emotion, and neurological disorders.

3.7.2.1. Mental State

To classify the concentration and relaxation levels of the participants, a study was conducted using the common space pattern algorithm for feature extraction. As a result of the study done with the support vector machine (SVM), it was observed that using the gamma wave of F7-F8 electrodes proved the highest accuracy in discrimination of concentration and relaxation (Li et al., 2015). These two mental states are also tried to be determined in another study. EEG signals from the participants' Fp1 and Fp2 channels were measured while repeating the number told to them backward (You, 2021).

Additionally, brain waves are used for the detection of the mental state in an experimental study. It was reported that alpha wave activity has a significant relationship with attentional processes, and it was also stated that beta wave activity could be useful for investigating cognitive and emotional processes (Ray and Cole, 1985).

Beta increase while theta decreases during concentration, so it was observed with that concentration index in Equation (3.16). From the measured EEG signals, the index had been calculated for each of Fp1, Fp2, T3, T4, C3, C4, O1, and O2, and an

incrementation, especially in the indexes of the Fp1 and Fp2, was occurred during the concentration (Choi et al., 2014).

$$concentration\ index = \ power\ of \left[\frac{Low\ beta}{Theta}\right] \tag{3.16}$$

For anxiety, a reliable and high correlation has been found between the high beta of FC5 and FC6 probes in the anterior temporal lobe (Seo et al., 2010). Another important correlation has been found between theta wave bands and drowsiness, this wave increases when a person is sleepy and there is a slowdown in responses this person (Gorgoni et al., 2014).

In the light of these obtained information, an index in Equation (3.17) was derived for the detection of anxiety emotion (Yürdem, Akpinar, & Özkurt, 2019; Yurdem et al., 2020).

$$anxiety\ index = \ power\ of \left[\frac{High\ beta}{Theta}\right] \tag{3.17}$$

3.7.2.2. Emotion

Getting started analysis of the emotion studies, firstly, the team that saved the DEAP dataset for the emotion study analyzed the dataset. As a result of the analysis, it was observed that while the theta, alpha, and gamma brain waves were negatively correlated with the sense of arousal, the sense of valence was positively correlated with all brain waves (Koelstra et al., 2011). When the asymmetry of the lobes was investigated, it was determined that there was a higher increase in right temporal lobe beta and gamma brain waves (Koelstra et al. 2011).

The effects of stimuli familiarity were investigated in a study on the DEAP dataset in addition to their own recorded dataset were used. The average PSD values of twelve EEG channels for delta, theta, alpha, beta, and gamma waves, and also

fractal dimension values calculated from the Higuchi algorithm were used as the feature to perform classification for LA-HA and LV-HV emotions (Higuchi, 1988; Thammasan et al., 2017). In the results, it was observed that a higher accuracy was obtained on unfamiliar music videos by using SVM (Thammasan et al., 2017). For only detecting the valence emotion by decreasing the channel numbers to two, the time and frequency features on the DEAP dataset were helpful in to result that Fp1 and Fp2 channels are the chosen ones (Wu et al., 2017).

Again, by using the DEAP dataset, the features in the time domain were investigated by another research group. Afterward, they found that the power feature in Equation (3.8) is more helpful than other features with the Relief algorithm (Byun et al., 2017). In a study in which emotion detection was performed with the DEAP dataset, EMD was applied by filtering the beta wave from the EEG signals measured from the F3 and F4 electrodes of all participants, and an average of 94.98% success was achieved in the classification made with SVM using the entropy feature in Equation (3.18) (Zhang, Ji, & Zhang, 2016). In another study, after the application of DWT with "db4" to the EEG signals of some selected participants, the entropy values of the 5th order signal were used as features and the highest accuracy of 68.06% was obtained as a result of the classification made by the SVM (Al-Qammaz, Yusof, & Ahamd, 2017).

$$h(X) = \frac{1}{2}\log\left(2\pi e s^2\right) \tag{3.18}$$

Another emotion study was conducted to predict arousal and valence with the dataset recorded while participants were looking at pictures, listening to music, and watching videos (Sarno et al., 2016). The feature vector was constructed with the mean in Equation (3.4), standard deviation in Equation (3.5), and power in Equation (3.8) values calculated from the FFT of 14 EEG channels. In the results of the Pearson-correlation coefficient, it was obtained that the correlation between the powers of T7 and T8 with valence, and the correlation between the powers of AF3,

AF4, F7, FC5, T7, and T8 with arousal are higher than the other electrodes for high-frequency bands (Sarno et al., 2016).

To detect happiness and unhappiness, in a study done with the EEG measurement method, the conclusion has been reached that the high-frequency bands beta and gamma of T7 and T8 probes (Figure 3.2) on the temporal lobe are more reliable than the low-frequency bands. With the detection done on the participant-dependent model by the Gaussian SVM classifier using PSD as the feature, the highest accuracy obtained by the T7-T8 electrode pair was 72.90% (Jatupaiboon, Panngum, & Israsena, 2013a). Again, using the Gaussian SVM learning algorithm, the classification of the valence emotion was done in another study. According to the accuracy of different electrode pairs and brain waves, reductions in the used number of electrode pairs and waves were done to obtain the informative ones. Consequently, it was observed that F7-F8, AF3-AF4, F3-F4, FC5-FC6, T7-T8 electrode pairs (Figure 3.2) and gamma, beta, alpha, and delta waves help to provide the highest accuracy, respectively (Jatupaiboon, Panngum, & Israsena, 2013b).

To investigate the activity in the prefrontal cortex during pleasant and unpleasant stimuli processes with recorded fMRI data, it was observed that the activity in the left dorsolateral prefrontal cortex (DLPFC) was increased for the pleasant stimuli (Herrington et al., 2005). The location of the left and right DLPFC in an fMRI image is given in Figure 3.12 (a). In another study with EEG data to investigate the activity of the DLPFC region, the F3 and F4 electrodes in Figure 3.12 (b) were used as the corresponding ones (Yang, Gao, Shi, Ye, & Chen, 2017).

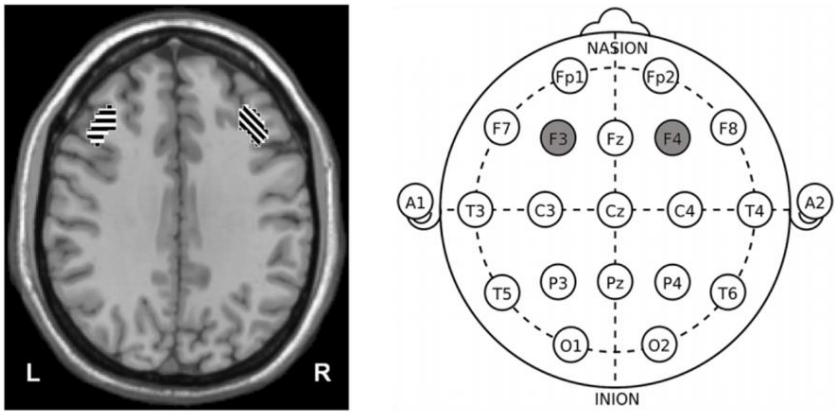

(a) (b)

Figure 3.12 (a) Marked regions are left and right DLPFC (Herrington et al., 2005), (b) Electrode placements in DLPFC (Yang et al., 2017)

Dimensional emotion classification for joy, sadness, anger, and pleasure was performed with a normalized hemispheric asymmetric alpha power index obtained from 12 different electrode pairs using the multilayer perceptron classifier (Lin, Wang, Wu, Jeng, & Chen, 2007). The normalized power index of 12 electrode pairs (ch_i) was calculated by Equation (3.19).

$$power\ index_{normalized}(ch_i) = \frac{asymmetry(ch_i) - min(ch_i)}{max(ch_i) - min(ch_i)} \tag{3.19}$$

Disgust, happiness, surprise, fear, and neutral emotions were classified by using Linear Discriminant Analysis (LDA) and K-nearest neighbors (KNN) classifiers with proposed energy features such as Recoursing Energy Efficiency (REE) in Equation (3.20), Logarithmic REE (LREE) in Equation (3.21), and Absolute Logarithmic REE (ALREE) in Equation (3.22), and conventional features such as power, standard deviation, and variance (Murugappan, Ramachandran, & Sazali, 2010). Alpha, beta, and gamma were decomposed using DWT with the “db4” wavelet function on D4, D5, and D6 decomposition levels. The total energy of three brain wave bands used in the proposed energy features was calculated by Equation (3.23). Using ALREE feature, the highest correct classification was obtained by KNN for disgust, happiness, and fear emotions, and by LDA for surprise and neutral emotions (Murugappan et al., 2010).

$$REE_{band_j} = \frac{E_{band_j}}{E_{total-3b}} \tag{3.20}$$

$$LREE_{band_j} = \log_{10}\left[\frac{E_{band_j}}{E_{total-3b}}\right] \tag{3.21}$$

$$ALREE_{band_j} = abs\left(\log_{10}\left[\frac{E_{band_j}}{E_{total-3b}}\right]\right) \tag{3.22}$$

$$band_j \in \{alpha, beta, gamma\}$$

$$E_{total-3b} = E_{alpha} + E_{beta} + E_{gamma} \tag{3.23}$$

3.7.2.3. Epilepsy

Besides detections like emotion, neurological disorders are also being tried to detect by using EEG signals. A study of epileptic seizures was performed with the Manhattan distance between the upper and lower envelopes of preprocessed EEG signals as the feature of SVM, KNN, and Decision Trees classifiers (Kuran et al., 2021). The envelopes were obtained by cubic spline interpolation using Equation (3.24) and (3.25), where $j = 1, 2, \dots, N$ and N is the length of the signal. After solving the variables a_j and b_j with the help of Equation (3.24) and its derivatives, these values are written in their places in Equation (3.25) and the main feature y_j is calculated (Kuran et al., 2021). After calculating these features, it was observed that the SVM method provided the highest accuracy for healthy participants who were awake and eyes open, and for epilepsy patients during seizures.

$$t(x) = a_j\left(x - x_j\right)^3 + b_j\left(x - x_j\right)^2 + c_j\left(x - x_j\right) + d_j \tag{3.24}$$

$$y_j = \ln\left(\frac{\left|a_j - b_j\right|}{2}\right) \tag{3.25}$$

The detection of epilepsy was also done by using the fast correlation-based feature selection and classification algorithm that the features are extracted from EEG signals (Şen & Peker, 2013). 36 features were calculated from 5 different categories: statistical, nonlinear, energy, time-frequency, and entropy. The fast correlation-based feature selection algorithm was used to find more informative features through relevance and redundancy analyzes, and the following features were obtained as the more relevant values: standard deviation of EEG signals, Petrosian fractal dimension, spectral entropy, the standard deviation of the beta wave, the mean of the alpha wave, mean curve length, and Hjorth parameters (Şen & Peker, 2013).

In order to predict before and between epileptic seizures, EEG channel selection was performed with the variance difference of these periods and weighted average sensitivity (WAS) parameters in the Rusboosted Tree ensemble classifier (Coşgun et al., 2021). After calculating the variance of each channel segment with Equation (3.6) and variance difference of segments for each channel with Equation (3.26), the channel selection was done by considering the highest value of WAS in Equation (3.27) (Coşgun et al., 2021). In these equations, channel number by ch, true-positive by TP, true-negative by TN, false-positive by FP, and false-negative by FN variables are indicated. Finally, for 26 symptoms, the false prediction rate per hour was 0.031 1/h, and the mean sensitivity was 71.80% (Coşgun et al., 2021).

$$var_{difference}(ch) = var_{before}(ch) - var_{between}(ch) \tag{3.26}$$

$$WAS\% = \frac{\frac{TP}{TP + FN} + \frac{TN}{TN + FP}}{2} \times 100 \tag{3.27}$$

When the comparison of STFT and WT methods was carried out as the subject of another study for the evaluation of the features, it was determined that STFT method was more useful because of the rapid occurrence of epileptic seizures and the rapid processing of the STFT method (Kıymık et al., 2005). By examining the changes in delta, theta, alpha and beta brain waves, it was stated that although the resolution of

the WT method is high, it will not be useful because the resulting time of the procedure is longer (Kıymık et al., 2005).

3.7.2.4. Parkison's Disease

The general goal of PD studies is to try to detect its symptoms before they occur. If this determination can be made, the patient can be warned in advance, and, for example, if freezing is in a situation that endangers the patient's life, safety can be ensured either by the patient or by other people around him/her. As a further level, a treatment to prevent freezing can be applied by detecting before it occurs. These studies were generally done by using data obtained from limb motion or brain activity.

Using wavelet energy (WE) and total wavelet entropy (TWE) of the EEG brain waves as features, a FOG detection was done with a three-layer Back Propagation Neural Network (BP-NN) using the Levenberg Marquardt algorithm for training. From this study, it was observed that the WE of the delta, theta, and alpha waves of the O1 channel, and WE of the delta, theta, alpha, beta, and gamma waves of the P4 channel, and TWE of O1 and P4 channels were important features for detection during FOG. However, of these important features, only P4 features performed better to detect 5 seconds before FOG occurred (Handojoseno et al., 2012).

In another study, their group also tried to detect FOG with directed transfer function (DTF) that helps to predict the causal effect of one channel on another at a given frequency, and partial directed coherence (PDC) that helps to improve and enhance the information of DTF by distinguishing direct and indirect flow between channels. Directed DTF (dDTF) and squared generalized PDC (sGPDC) were calculated and used to see the relations between O1, P4, Cz, and Fz electrodes at theta band (Handojoseno et al., 2014). Figure 3.13 shows which region on the brain affects which region during normal walking, onset, and FOG, and the thickness of each arrow between the two channels represents the strength of channel interactions (Handojoseno et al., 2014). For example, in the case of FOG in this figure, it was

observed that the region where the Fz electrode was placed was affected strongly by the region where the P4 electrode was placed for the dDTF parameter. With the sGPDC parameter, it was observed that regions where the O1 and Cz electrodes were placed also affected the Fz, but the effect of the P4 was higher than the O1 and Cz.

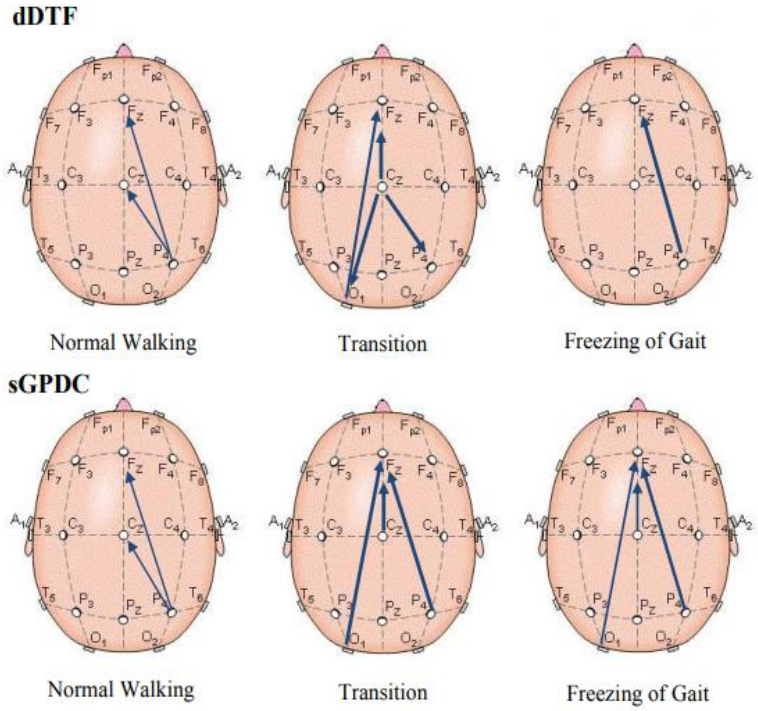

Figure 3.13 Interaction between EEG channels during normal walking, transition, and FOG conditions by using dDTF and sGPDC for theta wave (Handojoseno et al., 2014)

During the transition from walking to FOG, delta and theta brain waves, which represent low-frequency waves, have higher activity in the central and frontal lobes, and also, during the transition from FOG to walking, it was observed that the activity of theta and alpha waves in the central lobes with alpha and beta waves in the frontal lobes increased. For this, EEG signals of the O1, P4, Cz and Fz electrodes were measured, and then the PSD of each electrode was estimated with the FFT (Shine et al., 2014).

The relationship between theta wave and FOG was also observed in another study in which the participants performed tests based on visual attention on a computer. During tests, EEG signals with 512 Hz sampling frequency from 128 electrodes were recorded. After that, the signals were preprocessed and analyzed with toolboxes in

Matlab. As a result, it was observed that there is a high correlation of theta wave obtained from the signals in the orbitofrontal and occipitotemporal lobes of PDs with FOG (Gérard et al., 2022).

Comparison of a multimodal model and single-modal model to classify FOG was done by using the freezing index and the mean power of the theta wave of EEG signals of sixty channels measured from central and frontal lobes (Wang et al., 2020). As a classifier, RUSBoost classification was used because this classifier is useful for training datasets with an unbalanced number of samples (Seiffert, Khoshgoftaar, Van Hulse, & Napolitano, 2008; Wang et al., 2020). They measured the performance of the models by using Matthew Correlation Coefficient, and they observed the multimodal model was better than the single-modal model but not good enough to detect FOG (Wang et al., 2020).

CHAPTER FOUR
DESIGN OF DATA ACQUISITION SYSTEM

As part of this thesis work, a system was designed to measure and record EEG and acceleration data. This chapter describes the hardware and software design of the system. The system includes different types of electronic devices such as computers, sensors, and communication units. Communication between devices is done by different methods such as wireless communication and TTL serial communication over USB. The simultaneous operation of all these devices throughout the system is provided by programs written in Python, Matlab, and Arduino languages. In the system constructed in the study, it was desired to measure the data, transmit it to the computer with communication units and then save it with time information in real-time.

4.1 Hardware Design

In this section, the devices and communication methods of the system are explained. The block diagram of the data measurement and recording system is shown in Figure 4.1. In this figure, devices that measure and obtain the data are indicated in green blocks, units that provide the transmission of the data in blue blocks, and the computers that enable the system operation and record the data in gray blocks.

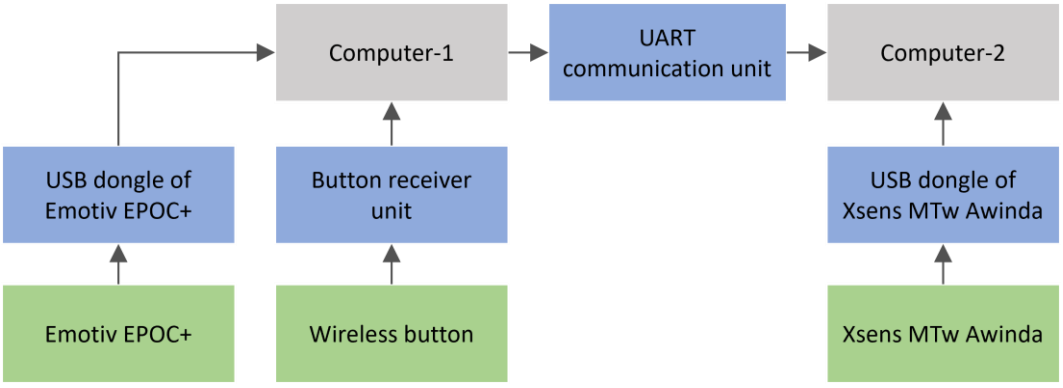

Figure 4.1 Block diagram of the data measurement and recording system

4.1.1 EEG Measurement System

In this subsystem, since the changes in brain activity are measured with the non-invasive EEG method, an EEG device can be placed without the need for a surgical operation. For EEG measurement, a device named Emotiv EPOC+ was used in the study. In Figure 4.2, the image of the EEG headset is shown.

Figure 4.2 Emotiv EPOC+ wireless EEG headset (Emotiv, 2022)

There are fourteen are sensor electrodes on the device (Emotiv, 2022). In Figure 4.3, the electrode locations are given. As a result of the measurements done with this device, the EEG signals of 14 different regions are obtained. The reference probes are given in yellow, and the sensor probes are given in green. The electrodes are located according to the international 10-20 system, and these channels are AF3, AF4, F3, F4, F7, F8, FC5, FC6, T7, T8, P7, P8, O1, and O2 (Emotiv, 2022).

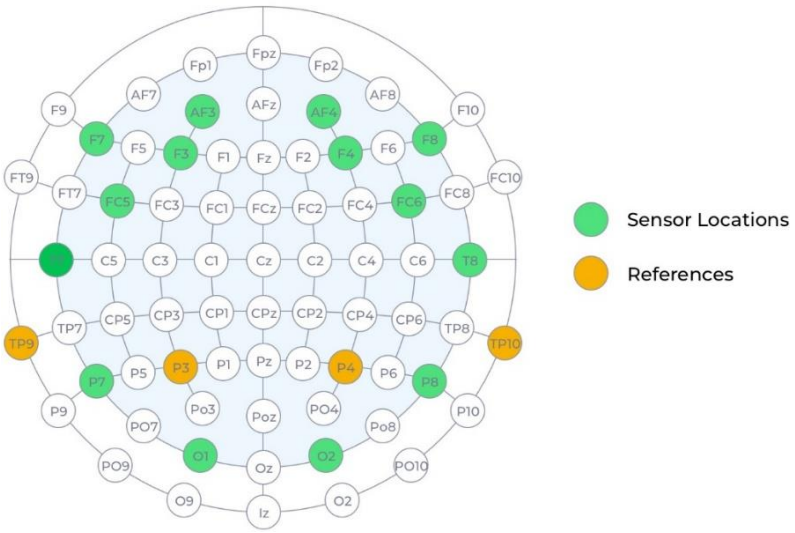

Figure 4.3 Probe locations (Emotiv, 2022)

With this device, there is no harm to patients since the signals are measured by the electrodes on the surface of the scalp. The data is sent from the headset to a USB dongle in real-time, the data transfer is done by using a proprietary 2.4GHz wireless protocol (Emotiv, 2022). Thus, there is no cable that might cause problems during measurements. Its universal USB dongle is shown in Figure 4.4.

Figure 4.4 USB dongle (Emotiv, 2022)

It is important that the electrodes of the EEG device should have been hydrated enough for robust EEG data acquisition. Thus, the data measurement quality increases. With the BPF in the EEG measurement circuit in the device structure, the data is filtered in the frequency range of 0.2-45 Hz and the components at the 50 Hz and 60 Hz frequency bands are stopped with the notch filter (Emotiv, 2022). The sampling frequency of the obtained EEG signals is 128 Hz. The technical specifications of this device are given in Table 4.1.

Table 4.1 Technical specifications of the Emotiv EPOC+ (Emotiv, 2022)

Number of channels	14
Sampling Method	Sequential
Sampling rate	128 SPS (2048 Hz internal)
EEG resolution	14 bits 1 LSB = 0.51μV
Bandwidth	0.2 - 45Hz, digital notch filters at 50Hz and 60Hz
Filtering	Built-in digital 5th order Sinc filter
Dynamic range	8400 uV(pp)
Coupling mode	AC coupled
Connectivity	Proprietary 2.4GHz wireless
Battery capacity	LiPo battery 680mAh
Battery life	12 hours
Sensor material	Ag/AgCl + Felt + Saline

4.1.2 Wireless Data Marker Button Unit

The key moments, like emotional changes or FOG events, occurring during recordings can be marked in the data with different methods in the designed system. These methods that enable this process to be carried out are a software property defined in the recording program and a wireless button unit that provides hardware marking in the designed system. In hardware marking, when the user observes the key moments according to the recording purpose of the data, the button is pressed and this information, which is sent to the receiver unit by wireless protocol, is transmitted to the computer via the USB port and these moments are marked in the recorded data. The data transmitted between button and the receiver consists of logic "0" and logic "1". The button and its receiver unit as communication system were designed and implemented. In Figure 4.5, the button and its receiver unit are given.

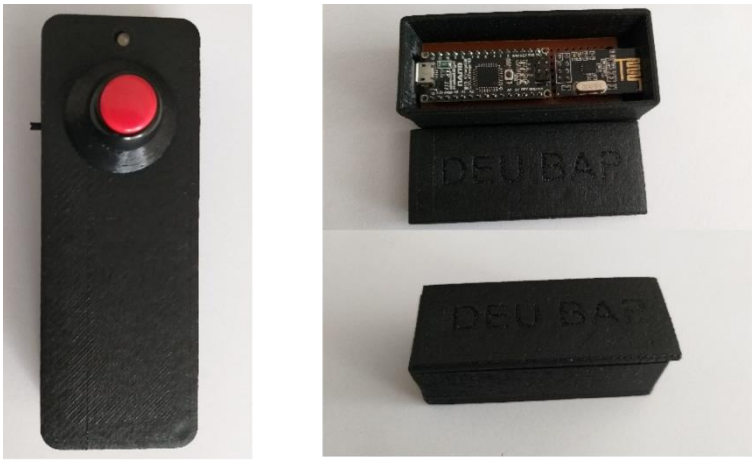

(a) (b)

Figure 4.5 (a) Wireless button, (b) Receiver unit (Personal archive, 2021)

The components that consist of the wireless button are a push button, a battery, a wireless communication module, and a microprocessor. There are a wireless communication module and a microprocessor in the receiver unit. Microprocessors in the button and receiver unit are controlled by codes written in Arduino language. The block diagram of the unit that provides hardware data marking is given in Figure 4.6.

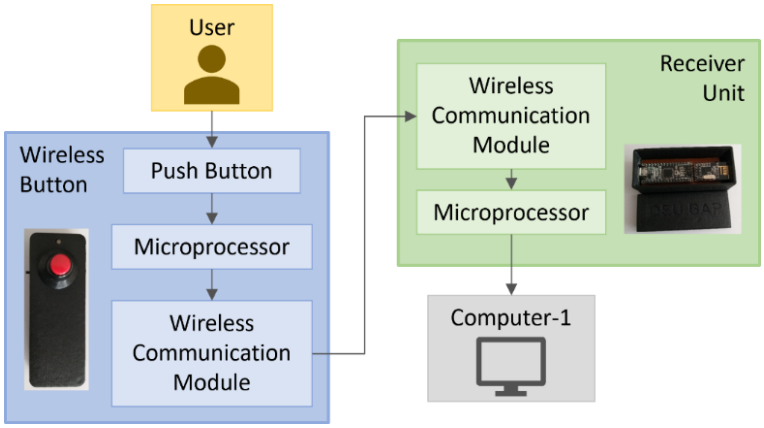

Figure 4.6 Block diagram of button system

4.1.3 Acceleration Measurement System

The data of the movement of the participant's limbs during walking are measured by this subsystem and then transmitted to the computer by the wireless method. The sensors used to measure movement data are Xsens MTw Awinda motion tracker sensors. This sensor provides angular velocity, acceleration, and magnetic field data, but only acceleration was recorded with the designed system. Communications of all sensors to each other, and to the computer are provided with the Awinda USB dongle (Xsens Technologies B.V., 2018). In Figure 4.7, the MTw motion tracker and the USB dongle are shown.

(a) (b)

Figure 4.7 (a) MTw motion tracker, (b) Awinda USB dongle (Xsens Technologies B.V., 2018)

The usage of these sensors during measurement is easy because of their wireless communication. Each sensor is placed on the human body with a velcro strap. Hence, these devices are not harmful to the patients. There are 6 sensors for getting the acceleration data from the patient's arms, feet, and waist. The sensors were placed as it is shown in Figure 4.8.

Figure 4.8 Placements of motion tracker sensors on a person during measurements

The sensors must be synchronized with the USB dongle to each other while measuring. The data transmission is done by a wireless protocol which is Xsens patented Awinda protocol (Xsens Technologies B.V., 2018). Acceleration data whose sampling frequency is 100 Hz for 6 sensors of X, Y, and Z axes are obtained and saved in real-time. The technical specifications of MTw Awinda are given in Table 4.2.

Table 4.2 Technical specifications of the MTw Awinda (Xsens Technologies B.V., 2018)

Performance for Acceleration	
Dimensions	3 axes
Full scale	± 160 m/s2
Alignment error	0.1 deg
Orientation Performance	
Dynamic Range	All angles in 3D
Static / dynamic Accuracy of Roll/Pitch	0.5 deg RMS / 0.75 deg RMS
Static / dynamic Accuracy of Heading	1 deg RMS / 1.5 deg RMS
Physical, Electrical and RF Properties	
Communication interface	Wireless 2.4GHz/USB
Wireless transmit range of MTw indoor / outdoor	~20m / 70m
Synchronization accuracy	< 10µs
Battery runtime	~6 hours
Housing dimensions of MTw	47 x 30 x 13 mm
Operating temperature range	0°C – 50°C
Weight of MTw	16 g
Update rate for 6 MTw's	100 Hz

4.1.4 Computers and Their Communication System

The whole system equipment is controlled with two computers which are Computer-1 and Computer-2. Computer-1 is the main computer used to control the system, it receives data from the EEG headset and the button unit. Computer-2 saves data from motion tracker sensors. To carry out working two computers synchronously, Computer-1 sends signals to Computer-2. This one-way communication takes place over the communication unit in Figure 4.9.

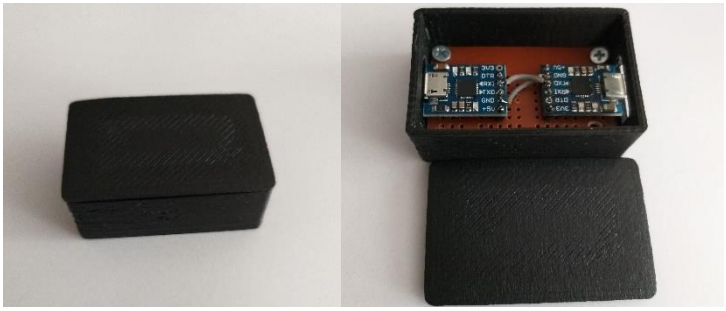

Figure 4.9 Unit for communication between computers (Personal archive, 2021)

Two computers are connected to this unit using the UART communication protocol. Since the data transmissions of sensors in the system are done with wireless communication methods, to prevent data loss, this communication system was done with TTL serial communication over USB. Its block diagram is shown in Figure 4.10.

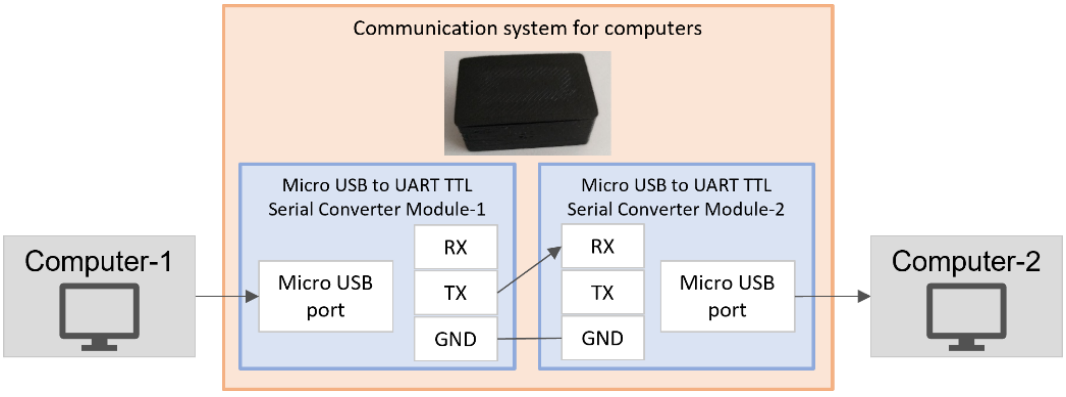

Figure 4.10 Block diagram of the communication system for computers

There are two micro-USB to UART TTL serial converter modules in this unit, and three used pins are RX, TX, and GND on these modules. For the one-way communication, the TX pin of the module connected to Computer-1 is attached to the RX pin of the module connected to Computer-2. These modules include a single chip CP2102 USB to UART Bridge. Technical specifications of this chip are given in Table 4.3.

Table 4.3 Technical specifications of the CP2102 (Silicon Laboratories, 2017)

Full speed	12 Mbps
Baud rates	300 bps to 1 Mbps
Receive buffer	576 byte
Transmit buffer	640 byte
Temperature range	-40°C to +85°C

4.2 Software Design

With the used equipment and the written codes, it has been tried to realize the proper and synchronous operation of the system. The block diagram of the data acquisition in system is shown in Figure 4.11. The main computer, Computer-1 has control over the other devices. It gets data from the EEG headset by its USB dongle, gets button data by the receiver unit, and sends signals to Computer-2 through their communication unit. This management is provided by a code written in the Python programming language. Computer-2 receives data from motion tracker sensors and signals for synchronization from Computer-1, these data transfers are done with a code written in Matlab programming.

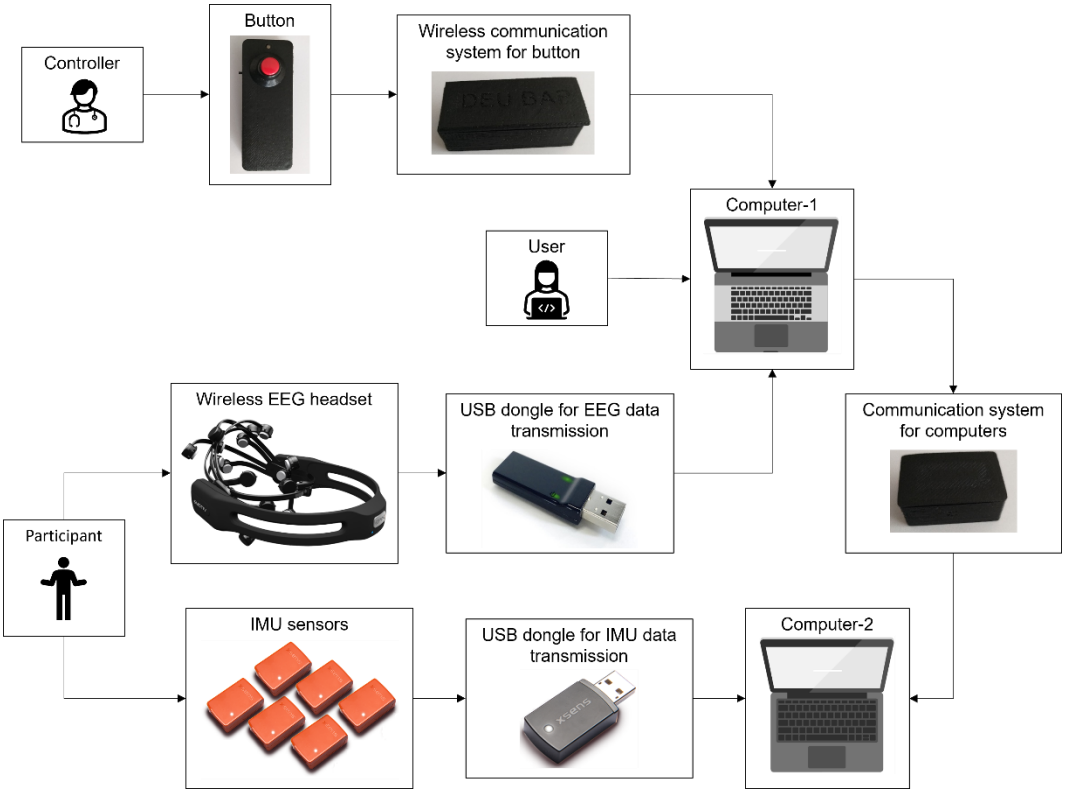

Figure 4.11 Block diagram of the data acquisition in the designed system

Before starting the measurement process, the sponges on the EEG electrodes are moistened with solution. Then the device is attached to the participant's head, and the quality of the EEG data is controlled on Computer-1 with EmotivPRO software released by the producer of the EEG device. In Figure 4.12, an example of the quality control on EmotivPRO is given. The green and orange color on the electrodes states that the quality is good and almost good. However, the red and black colors represent that quality is poor and very poor. An average quality percentage is calculated by this software. If it is lower than 95%, the user replaces the electrodes for the correct positions, or remoisten the sponges.

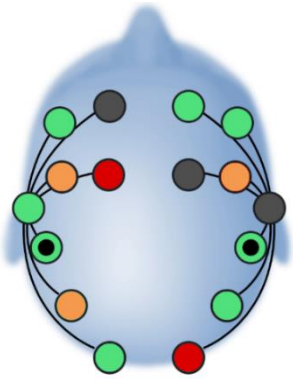

Figure 4.12 EEG quality control with EmotivPRO

On the other side, the six motion tracker sensors are synchronized with the code in Matlab on Computer-2. When it is ensured that the entire system and the participant are ready after the wireless button unit connections are done, the measurement process is started by the user via Computer-1. The flowchart of the Python-based software and graphical user interface (GUI) running on Computer-1 after the process starts is given in the Figure 4.13. With this program, real-time data measurement and saving processes are started and ended.

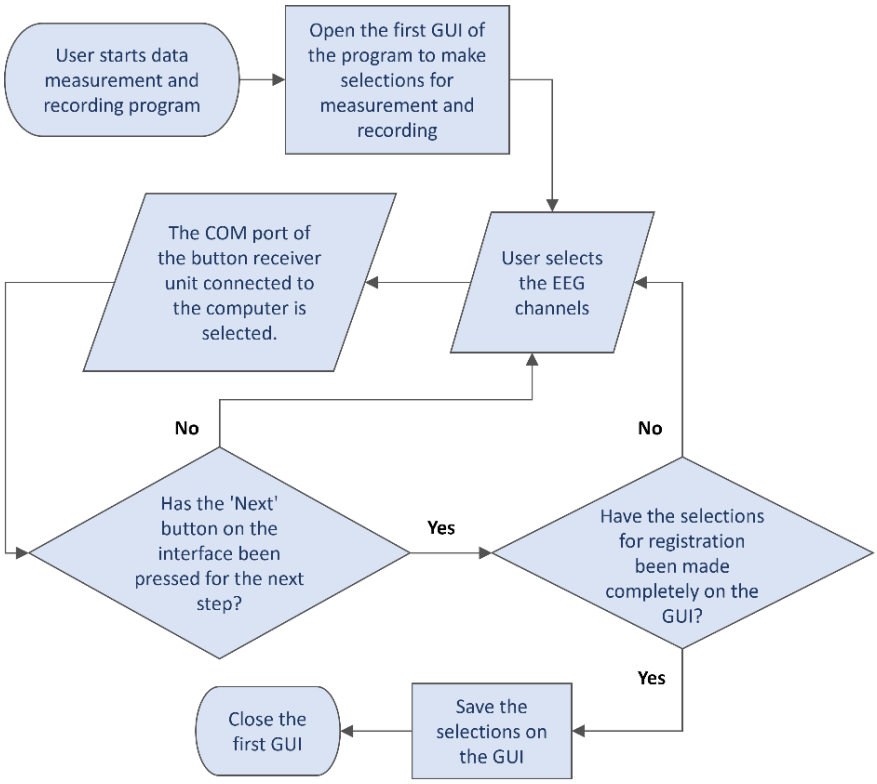

Figure 4.13 Flowchart of the first GUI opened by starting the system main program on Computer-1

The first GUI given in Figure 4.14 is shown the screen of Computer-1. To be recorded EEG channels and the COM port of the receiver unit are selected. Also, measurement of the acceleration data is optional, and if it is going to be recorded, the "Record Movement data" checkbox and the COM port of the communication unit must be selected. After that, the “NEXT” button on the GUI is pressed to pass to the next step of the process. If there is an incomplete selection, an error message will pop up.

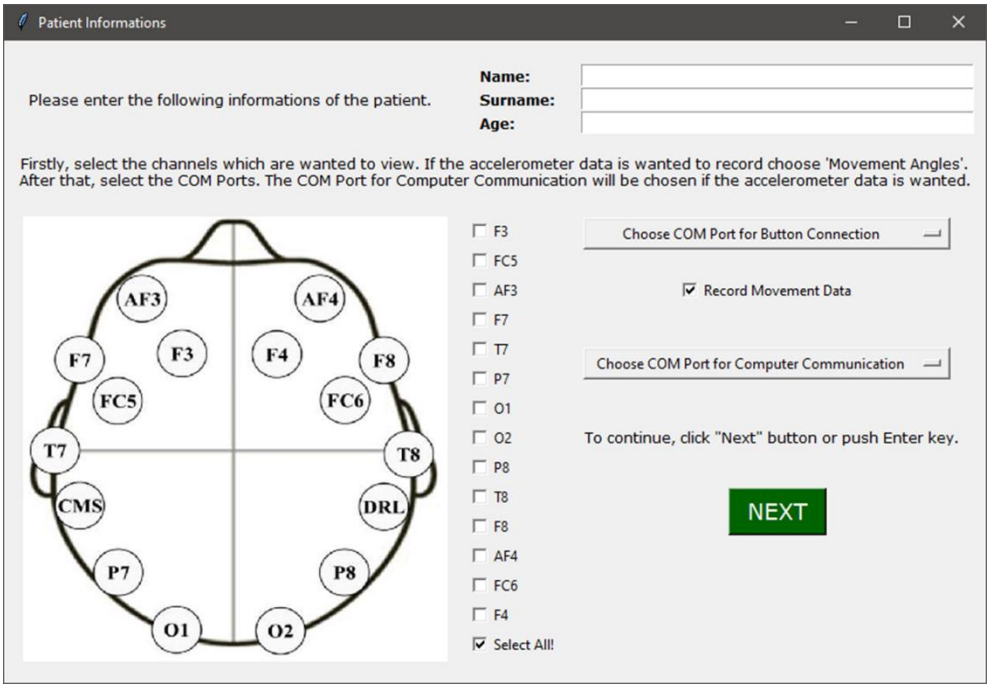

Figure 4.14 Screenshot of the first interface of the main GUI on Computer-1

In the next step, likewise the hardware, the software is also ready for measuring and recording. The GUI given in Figure 4.15 is shown on Computer 1. Before the user press the “Record” button, Computer-1 connects with other devices through COM ports selected on the first GUI. When the recording is started, the “Start Recording” string is sent from Computer-1 to Computer-2 through their communication unit. Then, the participant starts to do previously defined standardized tasks during measurement.

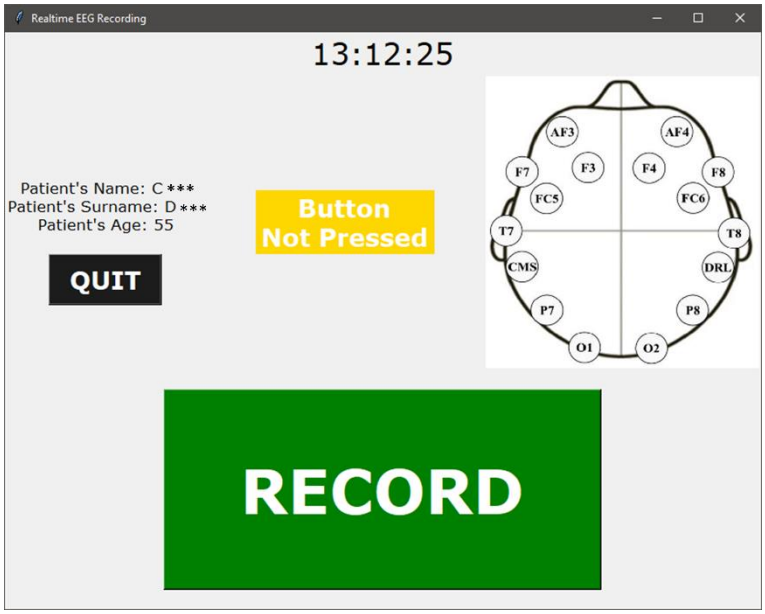

Figure 4.15 Screenshot of the main GUI on Computer-1 when recording has not been started, and the button has not been pressed yet

Until the user stops the recording, whole sensors measure and send the data to the connected computer. EEG signals are measured by the potential voltage difference between the reference and sensor electrodes on the EEG headset. The data is transmitted wirelessly to the USB dongle of the Emotiv EPOC+ connected to Computer-1. The data with a sampling frequency of 128 Hz is recorded synchronously with the time data at the time of recording in a comma-separated values (CSV) file. The flowchart of the second step of the process is given in Figure 4.16.

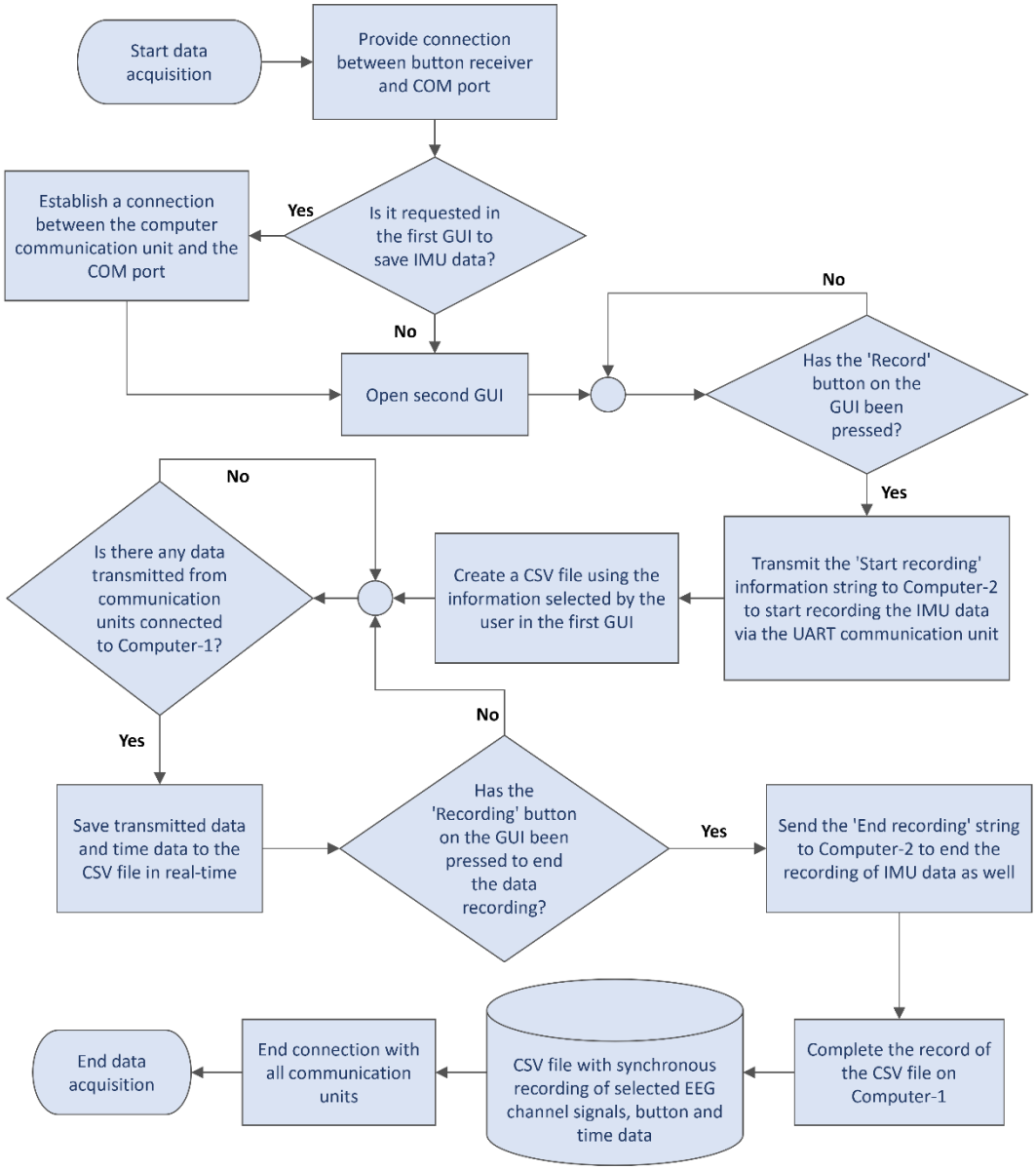

Figure 4.16 Flowchart of the operation of the data acquisition step

The data of the wireless data marker button unit transmitted consists of logic “0” or logic “1”. If there is no moment to be marked during recording, since the button is not pressed, logic “0” input is sent from the button to the receiver connected to Computer-1. If there is a moment to be marked, the user presses the button and the logic “1” input is sent. This button data is also saved synchronously with other data in the CSV file containing EEG and time data.

The 'Button not pressed' notice in Figure 4.17 (a), means that the button is not pressed, and the logic "0" data is transmitted. When the user presses the button to

mark the data at a key moment during the recording, the logic "1" data is transmitted and the 'Button pressed' notice is given on the GUI as in Figure 4.17 (b).

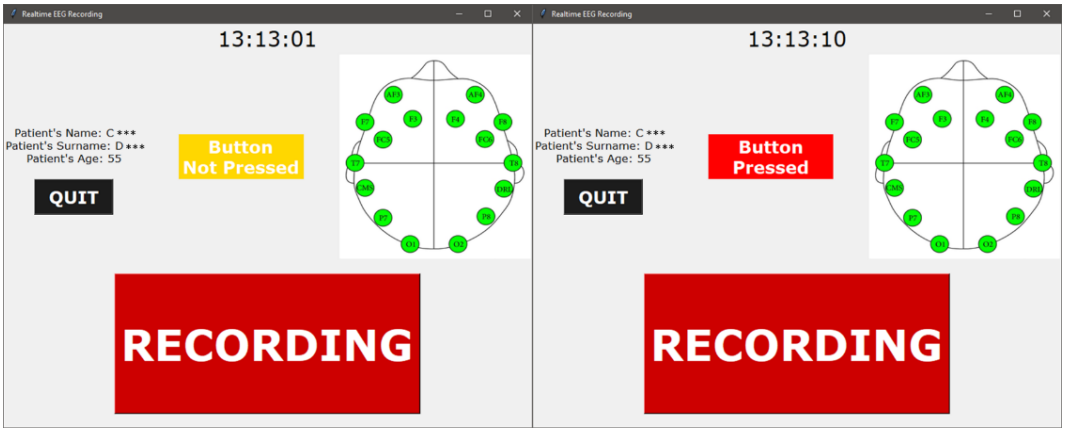

(a) (b)

Figure 4.17 Screenshot of the main GUI on Computer-1 when recording is started, (a) but the button has not been pressed yet, and (b) the button is pressed

With another method added to the system program, data can be marked with a software property during recording. This property is enabled for measurements done for a specific purpose. In these measurements, the participants are shown images to trigger their emotions. The process and generated data of marking in these measurements are given in Figure 4.18. With this software property, the logical state of the marking data is "0" while the participant looks at the black screen. However, when an image is shown, the marking data is logic "1".

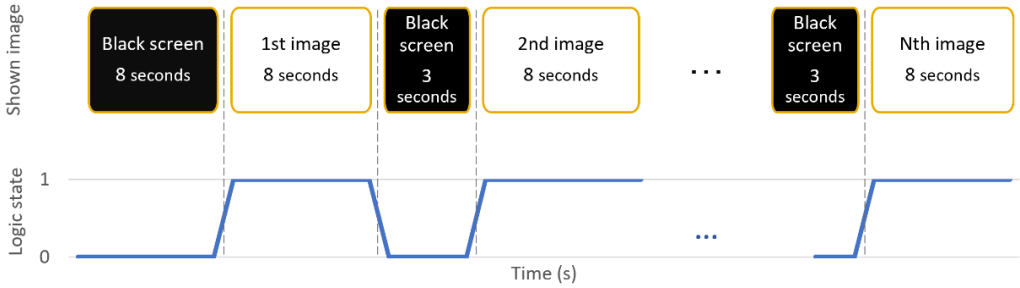

Figure 4.18 Process of measurements showing images and logical state of marking data

While the recordings in Computer-1 are performed in this way, if the recording of IMU data is selected in the first GUI, recordings are also done in Computer-2. The

six synchronized motion tracker sensors send their acceleration data with a sampling frequency of 100 Hz for the X, Y, and Z axes. These data are recorded in a matrix in the Matlab program on Computer-2 with time data in real-time. The flowchart of the program in Matlab program running on Computer-2 is given in Figure 4.19.

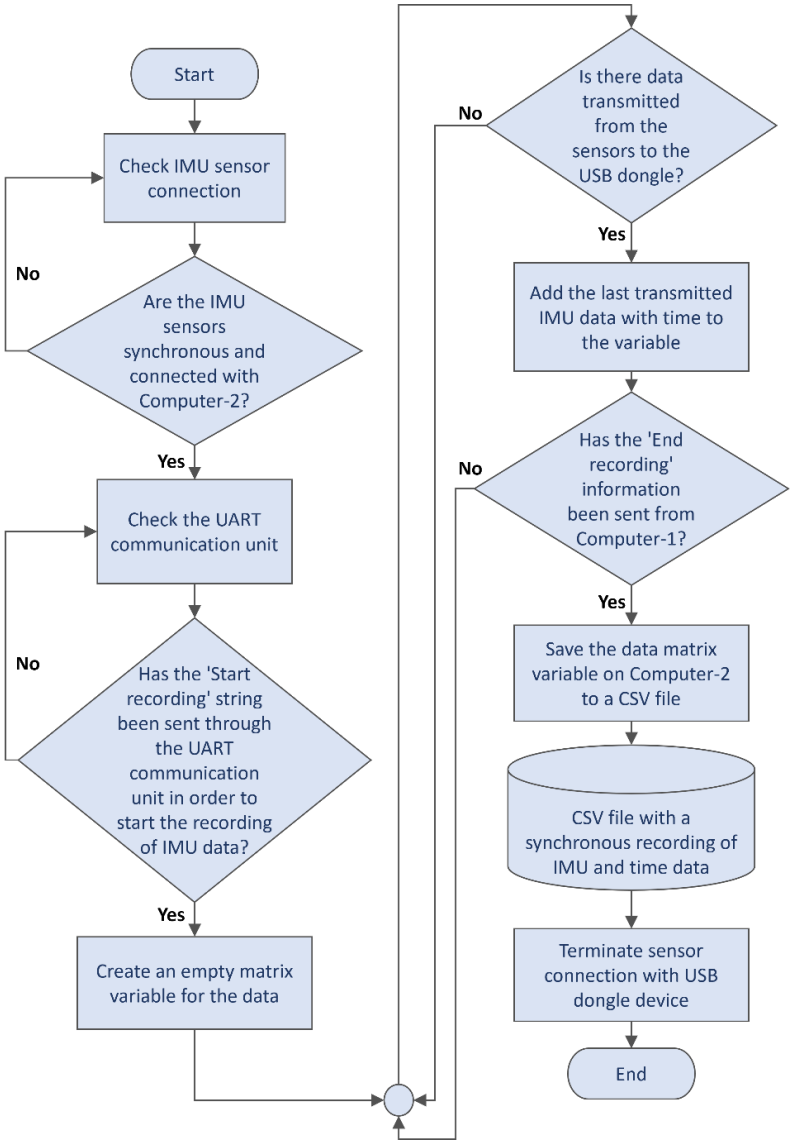

Figure 4.19 Flowchart of the process on Computer-2

After the measurement tasks are completed by the participant, the user presses the "Recording" button on the GUI (Figure 4.17) to end the data acquisition. After that, Computer-1 stops to get EEG and button data and saves the final CSV file. Then, it sends the “End Recording” string to Computer-2 via the UART communication unit, just as it was at the beginning before terminating the GUI on Computer-1.

Meanwhile, Computer-2 always checks if Computer-1 sends a message. When it receives the ending message, stops getting the acceleration data and saves the final matrix as a CSV file. Finally, connections between measuring devices, communication units, and computers are also terminated.

The collected data is saved in a CSV file separately for each record. The CSV file on Computer-1 contains time in the first column, button marking data in the second column, and signals of the selected EEG channels starting from the third column to the last one. The CSV file on Computer-2 contains the time and acceleration data of the X, Y, and Z axes for the six sensors.

The sampling frequency of the data in the CSV file in Computer-1 (Fs_1) is 128 Hz. The size of the data in the CSV files in Computer-1 (VB_1) can be calculated with Equation (4.1). Here, Nr_1 and Nc_1 represent the number of rows and columns, respectively. T_{rec_1} denotes the recording time in seconds. Ct gives the number of columns including time data. Cb is the number of columns including button data, and Nch is the number of recorded EEG channels. The Cb and Ct variables are always equal to 1.

$$VB_1 = Nr_1 \times Nc_1 = (T_{rec_1} \times Fs_1) \times (Ct + Cb + Nch) \quad (4.1)$$

Additionally, the size of the data in the CSV files in Computer-2 (VB_2) can be calculated with Equation (4.2). Its sampling frequency (Fs_2) is 100 Hz. This time, Nr_2 and Nc_2 represent the number of rows and columns on the data in Computer-2, respectively. T_{rec_2} denotes the recording time in seconds. Ct gives the number of columns including time data. S_a is the number of acceleration axes, and Ns is the number of IMU sensors. The Ct is always equal to 1, and S_a is equal to 3.

$$VB_2 = Nr_2 \times Nc_2 = (Trec \times Fs_2) \times (Ns \times (S_a + Ct)) \quad (4.2)$$

CHAPTER FIVE
IMPLEMENTATION OF THE SYSTEM

In this chapter, the recording implementations done by designing the data measurement and recording system are mentioned. With this system, which includes more than one sensor, EEG recordings can be done for different study subjects, and in this thesis, three different recording implementations were done with the help of this property of the system, the topics of which are FOG detection in PD and emotion analysis.

5.1 Experiment Performed While Displaying Images

In this recording implementation, images from the literature were shown to the participants to trigger them emotionally. These images were selected from International Affective Picture System (IAPS) which develops stimuli for experimental research on emotion and attention (Lang et al., 2005). Examples from shown images are given in Figure 5.1. From the first row to the second row, images trigger feelings of happiness, awe, sadness, and confusion, respectively.

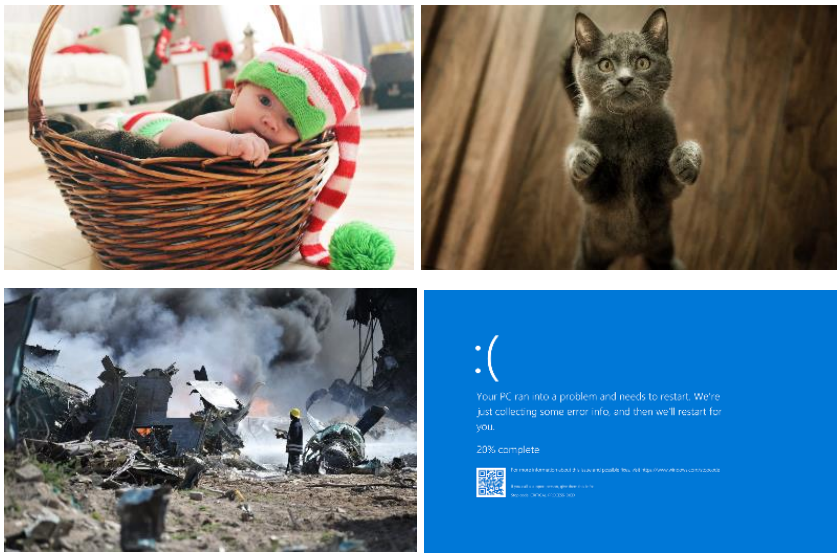

Figure 5.1 Some of images from literature shown during the implementation to trigger emotions (Lang et al., 2005)

The process given in Figure 4.18 was applied during each measurement. While the signals from 14 channels were measured with the EEG device, the marking data generated by the button were also recorded. The marking was done by enabling the software property. During the recording, logic "0" was added to the marking data when the black screen was displayed, and logic "1" was added to the data when emotion-triggering images were shown. Participants initially stared at a black screen for 8 seconds. Then, the triggering images for 8 seconds, and a black screen between each image for 3 seconds was shown on the screen.

Figure 5.2 Data acquisition done with the data recording system while showing triggering images (Yürdem et al., 2019)

Photographs taken during a recording for this implementation are given in Figure 5.2. During the display of the images, the lights of the room were turned off. With this, it is aimed that the participants can focus on the images more quickly and effectively.

5.1.1 Properties and Samples of Data Acquired Dataset

As a result of the measurements done for this implementation, the EEG dataset of 5 people was recorded. In Table 5.1, an example data part is given. As it was mentioned, the data contains time, mark, and EEG of 14 channels. Time data includes hours to microseconds. The column called "MARK" is the button label data, that is, for this application, the moments when the images are shown are marked as

logic "1", and the moments when the black screen is shown are marked as logic "0". The other columns give the EEG data of the 14 channels currently recorded, but only 7 of them are given in the table provided.

Table 5.1 Example data from recording done while showing triggering images (Yürdem et al., 2019)

TIME	MARK	AF3	F7	F3	FC5	T7	P7	O1	…
14:21:34.118914	0	4092.24	4073.88	4112.13	4076.94	4092.24	4096.32	4094.28	…
14:21:34.126909	0	4104.48	4078.98	4124.88	4083.06	4103.46	4101.93	4098.87	…
14:21:34.135019	0	4107.03	4081.53	4130.49	4101.42	4109.07	4107.03	4097.34	…
14:21:34.143017	0	4099.38	4081.02	4128.96	4080.0	4093.26	4098.87	4094.28	…
14:21:34.149835	0	4092.75	4077.96	4124.37	4077.45	4087.14	4093.77	4093.77	…
…	…	…	…	…	…	…	…	…	…
14:22:28.697284	1	4060.62	4084.59	4082.04	4070.82	4073.37	4090.71	4092.75	…
14:22:28.705251	1	4068.27	4083.06	4082.04	4056.03	4085.1	4094.79	4095.81	…
14:22:28.713273	1	4072.86	4082.04	4086.63	4048.38	4087.65	4100.91	4098.36	…
14:22:28.721353	1	4067.76	4083.06	4087.14	4046.34	4073.88	4097.34	4094.28	…
14:22:28.729322	1	4067.76	4087.14	4089.18	4052.97	4068.27	4096.32	4094.28	…
…	…	…	…	…	…	…	…	…	…

5.2 Experiment Performed While Asking Questions

Another emotion analysis was recorded using a different method with the designed system. This time, the participants were triggered by the questions asked. While participants were in a calm environment to trigger their emotions, other data were collected for emotion detection with given commands to them to imagine. Some of these commands are as follows:

- Imagine where you feel most comfortable with your eyes closed.
- Remember when you were very happy.
- Think of something that makes you angry.
- Think of a situation in which you are afraid.
- Examine the details of a bird painting.

An example photo from an implementation where the participant is asked to examine a bird painting is given in Figure 5.3.

Figure 5.3 Implementation from examining a bird painting, and the painting (Personal archive, 2019)

During the commands were given and the participants performed the commands, these moments were marked in the data with the wireless button unit. This application was done with 4 people and data was recorded.

5.2.1 Properties and Samples of Data Acquired Dataset

The recorded data consists of time, mark, and EEG data of 14 channels, as in the previous implementation in Table 5.1 where emotions were triggered by images.

5.3 Experiment Performed for Neurological Disorder Detection

In this study, which aims to determine the disease from the statistical properties of EEG data as well as emotion analysis, measurements were done with PD patients with FOG symptoms. The implementation, which was carried out in the company of a neurologist, was done by recording the EEG and acceleration data with the designed system while the patients were performing specifically determined tasks. The photographs of the whole data acquisition system equipment before different measurements are given in Figure 5.4.

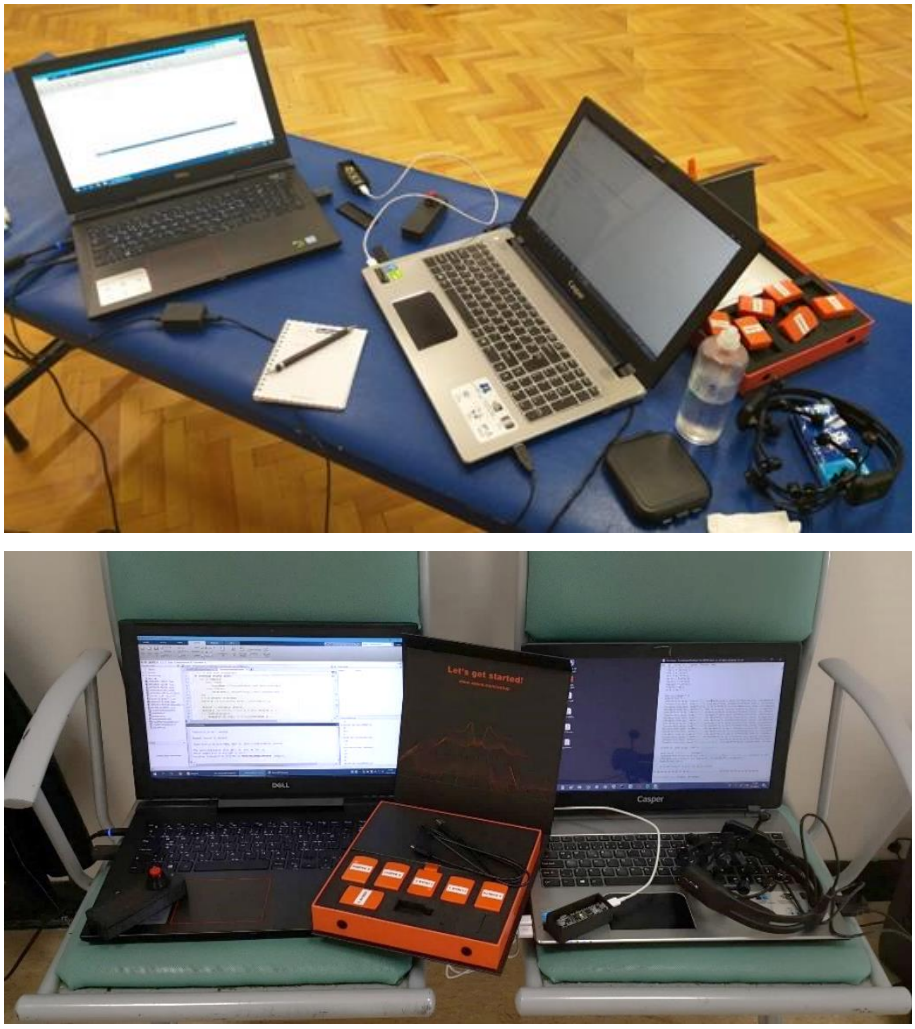

Figure 5.4 Data collection system before measurements done at different times (Personal archive, 2019)

The first thing to do at the beginning of the implementation is to hydrate the electrodes of the EEG device, as mentioned in chapter four. Then the EEG device and motion tracker sensors are connected to the computers. The devices are then worn by the patient with the help of the person who controls the system. After the electrodes of the EEG device are attached as indicated in the use of the device, the motion tracker sensors are placed on the body parts shown in Figure 4.8 with velcro strap. The first (left) of the photographs given in Figure 5.5 clearly shows the use of the EEG device and the second (right) clearly shows the use of motion sensors.

Figure 5.5 Sensors on the patients (Personal archive, 2019)

The button which is used to mark the FOG events is controlled by an experienced neurologist. In Figure 5.6, an example photo of the use of the wireless button providing data marking by the experienced neurologist is given.

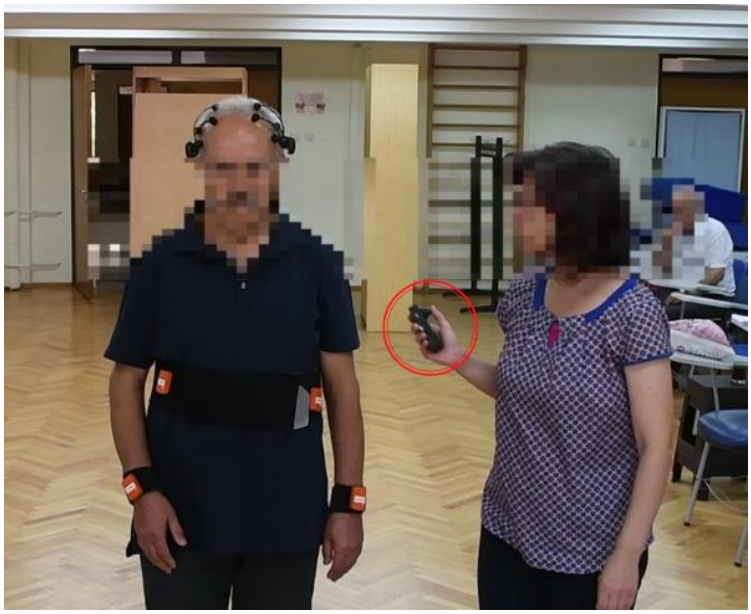

Figure 5.6 Using the button for data marking with an experienced neurologist (Personal archive, 2019)

As in the implementation procedure, after the quality of the signals of the sensors, motion trackers and EEG device is checked, the sitting patient stands up with the start command of the doctor and starts walking on parkour to perform the tasks. At that time, the user at the computers of the system starts the recording. The tasks that the PD patients were asked to do are given as follows, respectively:

- The patient stands up at the starting point.
- Starts to walk on a straight road for at least 5-10 meters.
- Passes through a narrow entrance such as a doorway.
- A few meters later, rotates 360 degrees around herself/himself slowly.
- Turns back and passes through the same narrow entrance.
- Walks up to 2 meters.
- Rotates 360 degrees around herself/himself several times.
- Walks back to the starting point.

It is aimed to trigger the patients and switch to the FOG state with the tasks such as passing through the door and turning. Thus, more data will be available for FOG analysis when the patient shows symptoms of FOG. The same procedure is applied 3 or 5 times depending on the patient's condition. Sample photographs from the implementations performed with PD patients is given in Figure 5.7.

The experienced neurologist determines if it is the FOG state or not. If the patient is frozen while walking, it means that the patient might be in the FOG state. If the neurologist decides that the patient is not in a FOG state, the button is not pressed, and the “0” string is sent from the button to the receiver unit which is connected to Computer-1. However, if the patient is in the FOG state, then the neurologist presses the button until the patient is no longer in the FOG state. During the button is pressed, the "1" string is sent.

Figure 5.7 Sample images from measurement processes (Personal archive, 2019)

This study, which was carried out within the scope of the BAP Project approved by the ethics committee, was carried out by a team mostly doctors. Within the scope of this Dokuz Eylül University BAP project, numbered 2018.KB.SAG.005, the data of healthy individuals as well as PD patients were measured. Measurements were taken from 18 PD patients and 10 healthy individuals. Although detailed investigations were done in the BAP project by other data analysis team. This thesis study only includes basic statistics and spatial studies on the EEG data received in the BAP project and independent fundamental studies about emotions.

5.3.1 Samples of Data Acquired for Disorder Detection

There are two data files for each measurement, the first CSV file includes EEG, button, and time data, the second file includes acceleration with time data. A sample CSV file part was shown in Table 5.1. The first column is the time data, the second column shows the button data which says if the patient is in FOG. The patient is in FOG if the button value is 1, but the patient is not in FOG state if the value is 0. The rest of the columns gives the EEG data.

In Figure 5.8, samples from EEG signals changing over time in seconds are shown on plots. There are fourteen channel EEG signals. Also, the FOG events which are determined by an experienced neurologist are indicated in this figure. From this plot, it can be said that the patient was in FOG state for three times. The first lasts from about the fifth to the twelfth second, the second lasts from about the fifteenth to the twentieth second, and the final one lasts from about twenty-fourth to the thirty-third second.

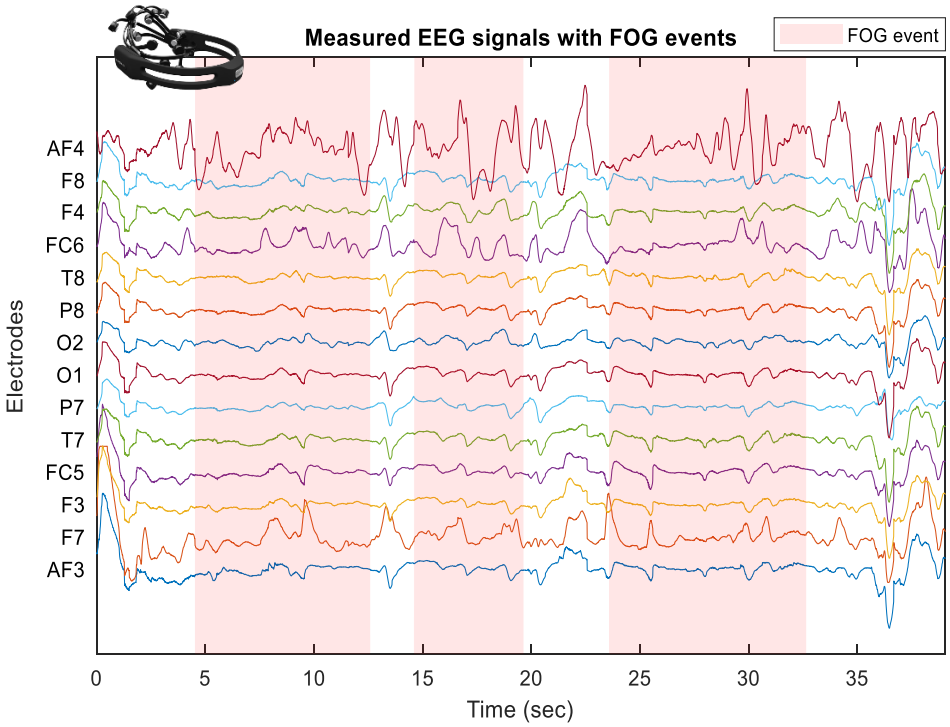

Figure 5.8 Sample EEG signals with FOG events

An example of the data obtained from six motion tracker sensors is given in Table 5.2, from the data of only three sensors. In this data, which is a part of the CSV file, there are time information for all six sensors, and acceleration data of three axes consisting of X, Y, and Z, respectively. These three sensors are the ones which were on the right wrist, left ankle, and left wrist.

Table 5.2 A part of a sample CSV file of acceleration data for 6 sensors

Right Wrist				**Left Ankle**				**Left Waist**				…
Time	**X axis**	**Y axis**	**Z axis**	**Time**	**X axis**	**Y axis**	**Z axis**	**Time**	**X axis**	**Y axis**	**Z axis**	…
09:49:31.460	7.37	-1.43	6.26	09:49:31.429	9.62	1.72	-0.66	09:49:31.460	-0.09	2.89	9.71	…
09:49:31.492	7.38	-1.58	6.18	09:49:31.476	9.62	1.73	-0.70	09:49:31.492	-0.08	2.83	9.70	…
09:49:31.507	7.46	-1.65	6.22	09:49:31.507	9.62	1.73	-0.70	09:49:31.507	-0.08	3.02	9.75	…
09:49:31.523	7.40	-1.45	6.31	09:49:31.523	9.60	1.70	-0.67	09:49:31.523	-0.09	3.08	9.76	…
09:49:31.539	7.29	-1.43	6.37	09:49:31.523	9.62	1.72	-0.66	09:49:31.539	-0.16	3.00	9.75	…
09:49:31.554	7.27	-1.47	6.38	09:49:31.539	9.62	1.72	-0.66	09:49:31.554	-0.13	2.82	9.64	…
09:49:31.554	7.24	-1.50	6.32	09:49:31.554	9.63	1.70	-0.65	09:49:31.570	-0.13	2.81	9.73	…
09:49:31.570	7.28	-1.54	6.33	09:49:31.570	9.60	1.70	-0.67	09:49:31.570	-0.16	2.83	9.72	…
…	…	…	…	…	…	…	…	…	…	…	…	…

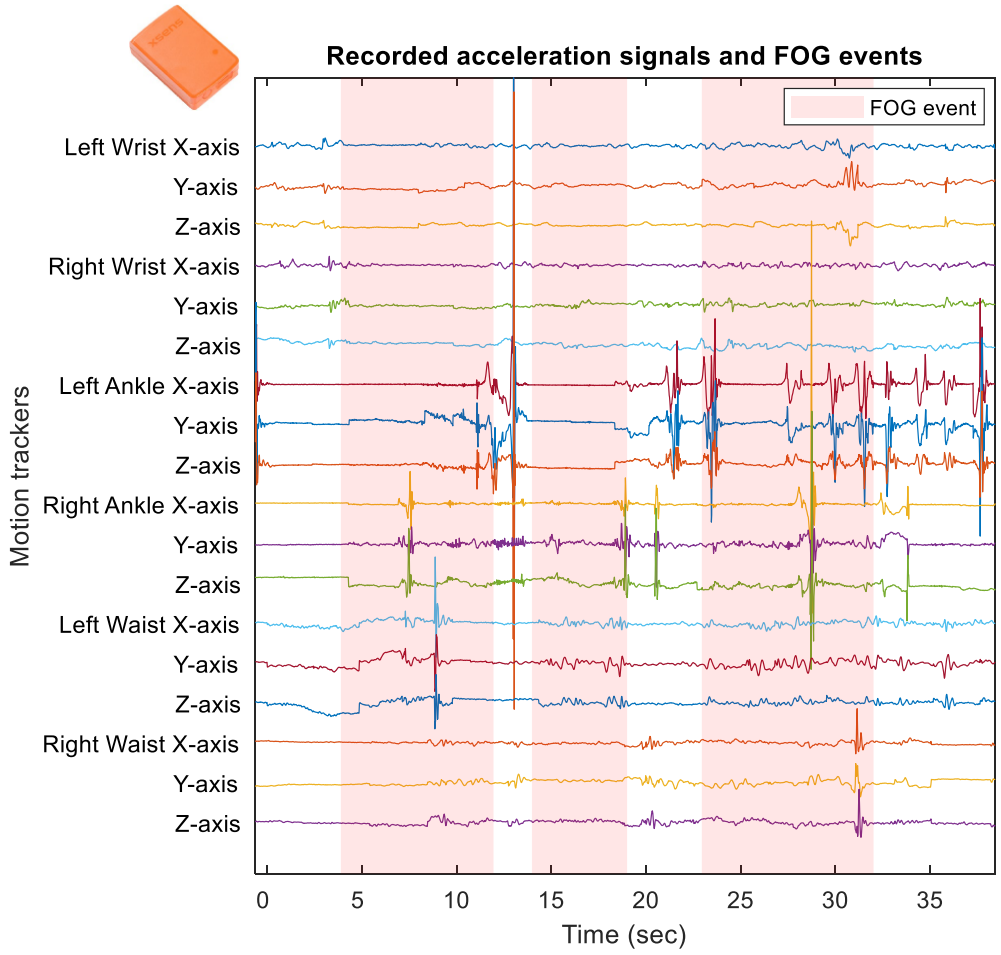

Figure 5.9 Sample acceleration data with FOG events

In Figure 5.9, the acceleration data recorded by motion tracking sensors which are in the same time interval EEG data in Figure 5.8 are given. The acceleration data in the X, Y, and Z axes were obtained from the six sensors connected to the wrists, ankles, and waist. The FOG events occurring simultaneously can be synchronized using the time data in both the EEG and acceleration data. Although there is no button data in the acceleration data, it can be observed that the FOG events and the acceleration data are synchronized in this plot.

CHAPTER SIX
APPLICATION AND RESULTS

Within the scope of this thesis, different analysis studies were carried out with the found and recorded datasets. The general purpose of these studies is to detect emotions or disorders with the changes in the activities of the brain regions. Regarding emotion, the following studies were accomplished using the DEAP dataset in the literature:

- General analysis of the dataset.
- Evaluation of music video ratings of participants.
- Classifying the music videos.
- Comparison of time and frequency domains of signals.
- Examining the distribution of the statistical changes in EEG signals for different emotions and participants.
- Study of regional changes in the brain during emotions.
- Study of changes in the brain over time during emotions.
- Examining the effect of features on the emotion detection.
- Examining the effect of brain waves on the emotion detection.
- Developing an algorithm for informative electrode selection.

The studies carried out with the recorded datasets by using the designed data acquisition system, consist of the following topics:

- Preprocessing the signals recorded by the designed system.
- Examining the changes in concentration and anxiety levels for different cases.
- Emotion classifications with basic machine learning methods.
- Testing results from the previous analysis and the informative electrode selection algorithm.
- Developing a GUI for EEG analysis and neurological disorder detection.
- Detecting emotion and neurological disorder by thresholding method.

The studies described towards the end were conducted to determine whether neurological disease symptoms are detected using mental state and emotion. FOG states were investigated under the knowledge of mental state levels and emotional changes.

The applications were accomplished with Python and Matlab programming. The application and results of all these studies are explained in the following chapter.

6.1 Emotion Analysis with the Dataset in the Literature

The previously described DEAP dataset was used in this analysis. The dataset consists of various types of biomedical signals, but preprocessed EEG signals from 32 channels were used in this thesis. Data were recorded from 32 participants while they were watching 40 different one-minute music videos. The sampling frequency is 128 Hz, and it was stated that artifacts were removed with a BPF with cut-off frequencies of 4 and 45 Hz in the preprocessing (Koelstra et al., 2011). In Figure 6.1, electrode positions of 32 channels of the dataset are given.

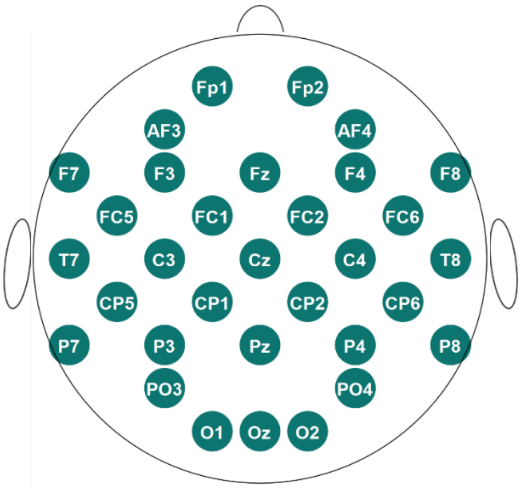

Figure 6.1 The electrodes positions in the DEAP dataset

This dataset also includes the ratings for emotions given by the participants under the influence of the music videos, and the average and standard deviation of all ratings. In the following sections, the studies done with this dataset and the obtained

results are given. First, the videos are classified into 2D emotions, and the reliable participants are determined by their rating results. Then, the effects of emotions on EEG signals in the time and frequency domains are investigated. As a result of the analyzes, studies were carried out for emotion detection.

6.1.1 Analyzing Emotion Rating Results

The forty music videos in this dataset were classified into LA, HA, LV, HV, LALV, LAHV, HALV, and HAHV emotions. For this classification, the arousal and valence emotion rating results were used. Both arousal and valence ratings ranged from 1 to 9. As an example, Figure 6.2 shows only two participants' ratings for 40 music videos. The numbers in these distributions indicate the video number, and its position consists of valence and arousal values.

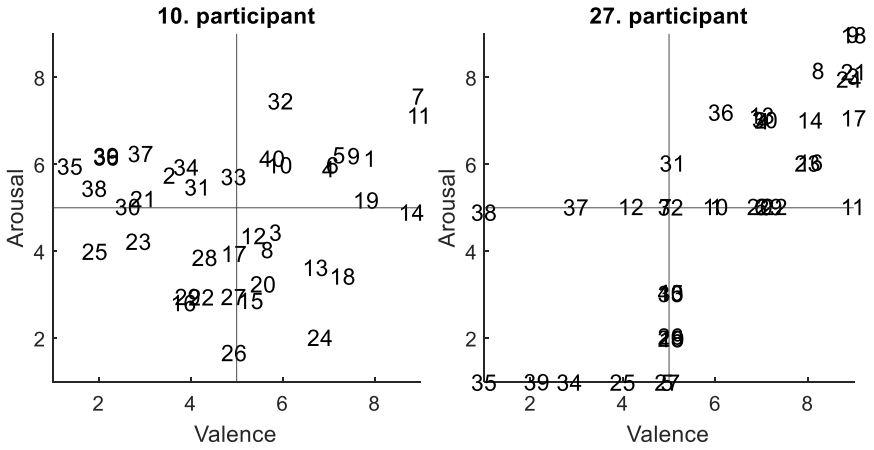

Figure 6.2 Ratings of 2 participants for 40 videos

As observed from this rating distribution, different ratings are given by the participants for the same video. In order not to cause erroneous results in studies, reliable participants were tried to be determined to be included in the analysis. For this purpose, the average arousal and valence emotion ratings in the dataset were determined as the reference, and then it was checked whether the users rated close to these ratings. Arousal and valence emotions were examined separately, and the threshold value was set to 5. For each video with close ratings, the participant was counted as having rated correctly, and the total number of correct ratings was

checked in the last step. For example, if the average valence rating of the checked video is less than 5, the participant must also have rated less than 5. As there are 40 videos in total, participants with more than 20 correct ratings for both emotions were determined as reliable participants. Only these participants were included in the analyses.

Table 6.1 Number of correct ratings of all participants for each emotion

Participant	Correct number of ratings for arousal	Correct number of ratings for valence	Participant	Correct number of ratings for arousal	Correct number of ratings for valence
1	23	22	17	32	33
2	**30**	**18**	18	31	27
3	32	26	19	35	33
4	**30**	**14**	20	37	23
5	28	25	21	31	20
6	28	27	22	33	24
7	30	29	23	29	22
8	32	28	**24**	**33**	**19**
9	29	24	25	31	22
10	34	34	26	30	21
11	34	31	**27**	**24**	**19**
12	33	27	28	33	32
13	31	26	29	33	29
14	34	33	30	29	20
15	36	27	31	28	31
16	23	24	**32**	**32**	**18**

In Table 6.1, the correct number of ratings for each emotion of all participants is given. Participants who did not have more than 20 correct ratings for either emotion and were not included in the analysis are 2, 4, 24, 27, and 32.

6.1.2 Emotion Classification of the Music Videos

The music videos are classified for 1D and 2D emotions for ease of analysis. The average ratings were used for this classification. Since ratings ranged from 1 to 9, between 1 and 5 were classified as low, and between 5 and 9 were classified as high arousal or valence. Figure 6.3 shows the average rating distribution of the videos and their 1D and 2D emotion classes.

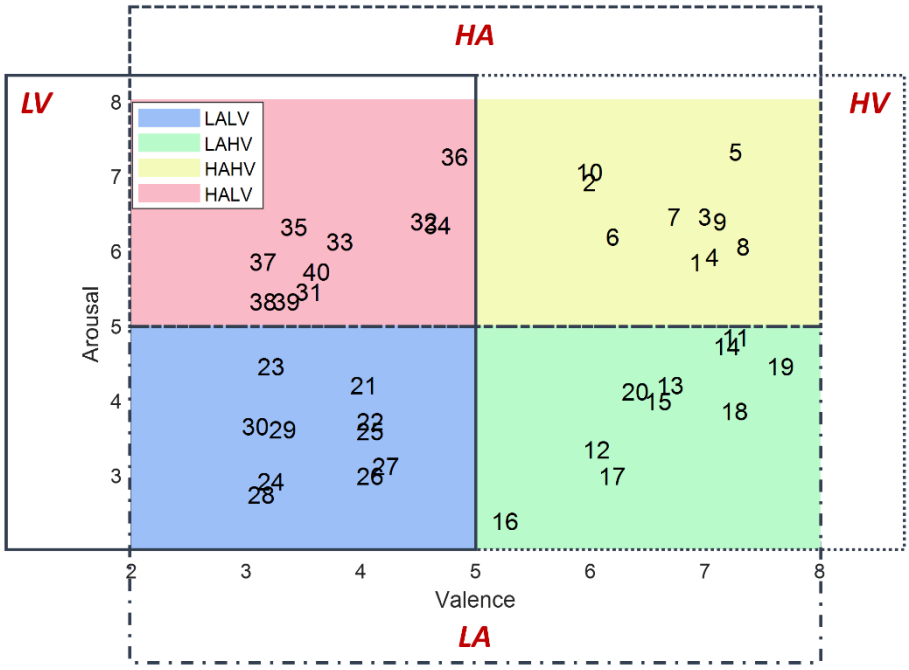

Figure 6.3 Emotion classes of videos according to ratings

When emotion classification was done from this distribution as 1D, the videos were examined separately for both emotions. All videos with arousal ratings less than 5 were classified as LA, while all the remaining videos with a rating greater than 5 were classified as HA. For valence emotion, all videos with a rating less than 5 are classified as LV, while others are classified as HV.

Accordingly, in the 2D emotion classification, the videos were classified according to both emotions. Arousal and valence values less than 5 were classified as LALV, both greater than 5 as HAHV, only arousal greater than 5 were classified as HALV, and only those with valence greater than 5 were classified as LAHV. The emotion classes of all videos are given in Table 6.2.

Table 6.2 Emotion classes of each music videos

1D Emotion	Videos in this class	2D Emotion	Videos in this class
LA	11-30	LALV	21-30
HA	1-10 & 31-40	LAHV	11-20
LV	21-40	HALV	31-40
HV	1-20	HAHV	1-10

However, it was observed that there was still a need for representative videos to be used as a reference for emotion analysis. For this reason, a video selection study was conducted for all emotions. The video closest to the center of each emotion region was chosen as the representation video of that emotion. In Figure 6.4, the flowchart of the representative music video selection is given.

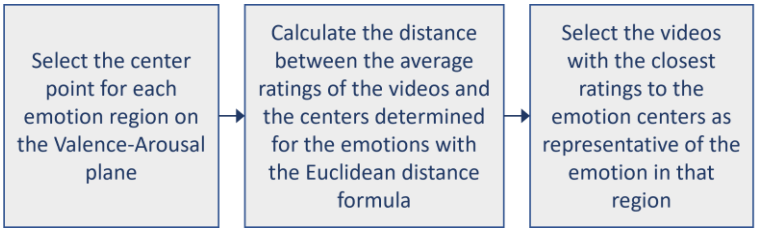

Figure 6.4 Flowchart of representative video selection

As given in this flowchart, first, the center points of these emotions were determined. The determined points are given in Table 6.3.

Table 6.3 Center point of each emotion region

Emotion	Valence	Arousal
LA	5	3
HA	5	7
LV	3	5
HV	7	5
LALV	3	3
LAHV	3	7
HALV	7	3
HAHV	7	7

After that, the distances between each video and the center points were calculated with the Euclidean distance in Equation (6.1). For this case, point a in the equation was determined as the center, and the valence value (a_1) and arousal value (a_2) are as in Table 6.3 for the relevant emotion. Point b is the average rating of the music video, and the average valence value is b_1 while the average arousal value is b_2.

$$d(a,b) = \sqrt{(a_1 - b_1)^2 + (a_2 - b_2)^2} \tag{6.1}$$

Finally, for each emotion, the video with the least distance from the relevant region was chosen as the representative of that emotion. The following equations provide mathematical representations of these video selection steps. In Equation (6.2), the main formula of the selection is given. n is the emotion (n = LA, HA, LV, HV, LALV, LAHV, HALV, HAHV), v is the video number (v = 1, 2, …, 40). The variables A_v and V_v are the average arousal and valence rates of videos, and their formulas are given in Equations (6.3), and (6.4), respectively, where p is the participant number. A_{c_n} and V_{c_n} are the center values of relevant arousal and valence emotion, $(A_{c_n}, V_{c_n}) = [(5,3),(5,7),(3,5),(7,5),(3,3),(3,7),(7,3),(7,7)]$.

$$video_n = \underset{v}{argmin} \sqrt{\left(A_{c_n} - A_v\right)^2 + \left(V_{c_n} - V_v\right)^2} \tag{6.2}$$

$$A_v = \frac{\sum_{p=1}^{32} (arousal\ rate)_{v_p}}{32} \tag{6.3}$$

$$V_v = \frac{\sum_{p=1}^{32} (valence\ rate)_{v_p}}{32} \tag{6.4}$$

Table 6.4 Selected representative videos for each 1D and 2D emotions

Emotion	Selected representative video	Emotion	Selected representative video
LA	16	LALV	24
HA	36	LAHV	18
LV	38	HALV	35
HV	11	HAHV	5

After performing these procedures, the numbers of the videos assigned for the relevant emotions are given in Table 6.4. These videos are only used to represent an emotion when it is desired to be analyzed.

6.1.3 Comparison of EEG in Time and Frequency Domain for Participants

Examples of EEG signals from the DEAP dataset are reviewed here. When the signal of a participant's CP6 channel was filtered with a band-pass filter for the music video number 12 representing the LAHV emotion, the signals in the time domain of

theta, alpha, beta, and gamma brain waves were obtained. By applying the FT to these signals with Equation (3.12), the amplitude values of the frequency components in the frequency domain were obtained.

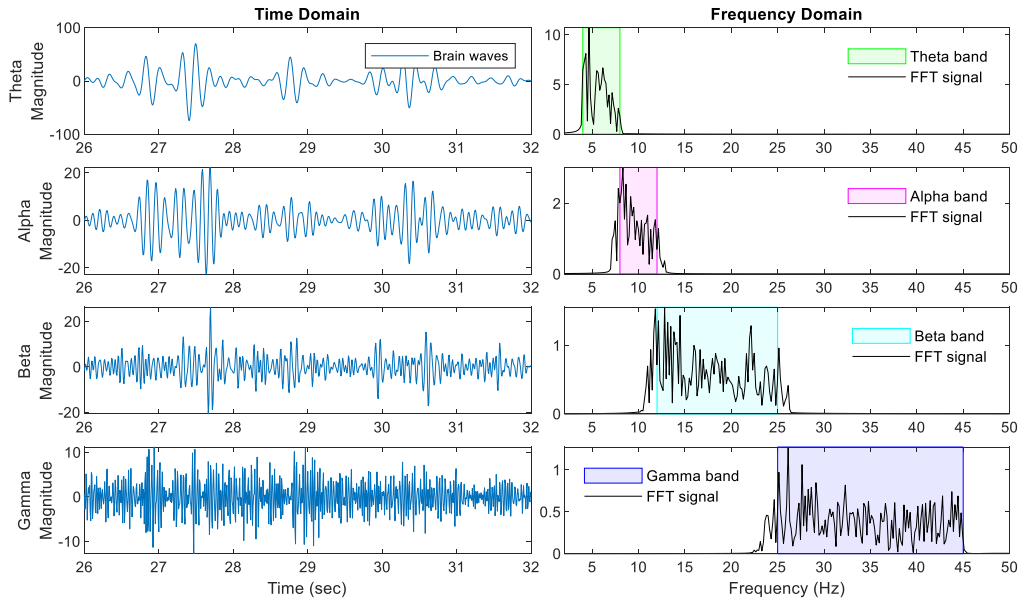

Figure 6.5 Comparison of brain waves in time and frequency domains

The signals of waves in time and frequency domains are given in Figure 6.5. From this comparison, it was observed that as the frequency value in the brain waves increased, the signal amplitude and power decreased.

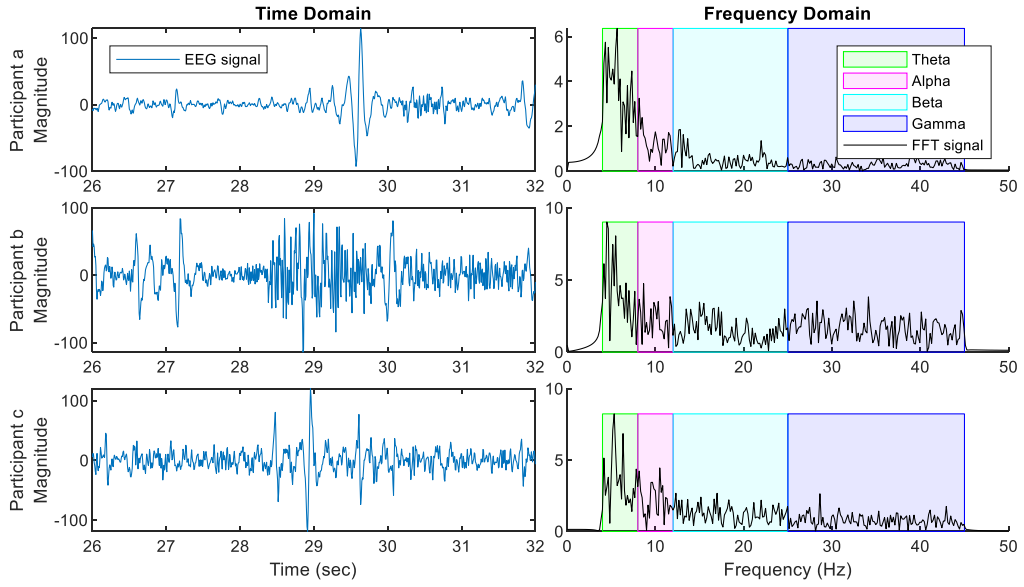

Figure 6.6 Comparison of participants' time and frequency domains of CP6 channel for 12th video

In Figure 6.6, three different participants are compared in time and frequency domains for the same video and channel in Figure 6.5. Participant b has a much higher amplitude in the time domain overall than the other participants. In the differences in the frequency domain, it is observed that participant-a generally has the lowest amplitudes in all bands and participant-b has the highest amplitudes in all bands.

6.1.4 Plotting the distribution of inter-channel EEG signals in Matlab

The amplitude distributions of the electrodes were formed with a code written in Matlab. For this, firstly, an 11x11 matrix was defined, and its element values were determined as given in the Figure 6.7. The value of the elements corresponding to the white cells is zero, the value of the light blue ones is equal to the proportional average value of the surrounding electrodes, and the dark blue ones are equal to the own value of the electrode at that point.

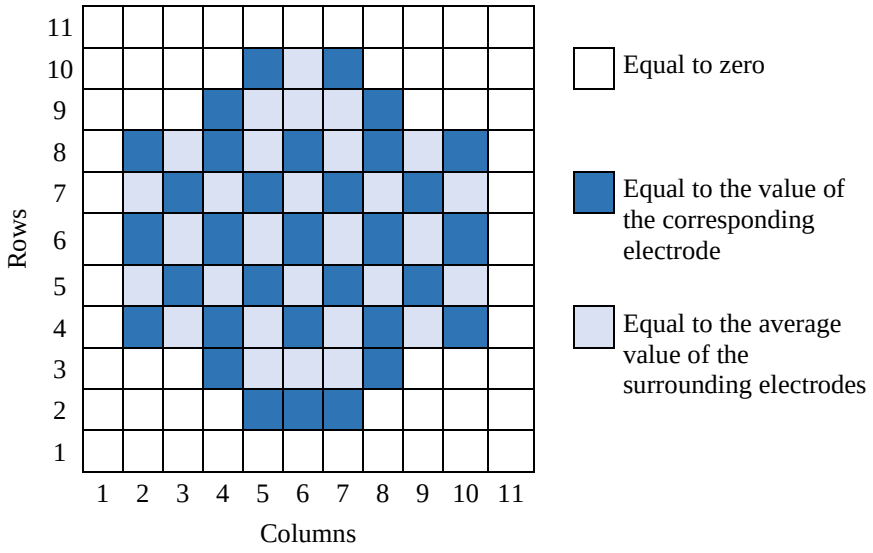

Figure 6.7 The electrodes positions and values for the EEG distribution plotting

Then, the effect of multiplying the average electrode value in the light blue points by a ratio to adjust the color transition between the dark blue and light blue points was examined. The change of this multiplying ratio, from 0 to 1, gives various distributions as in Figure 6.8. Since the observation of the distributions is better when the multiplication ratio is 1, the distributions in this thesis are drawn with this value.

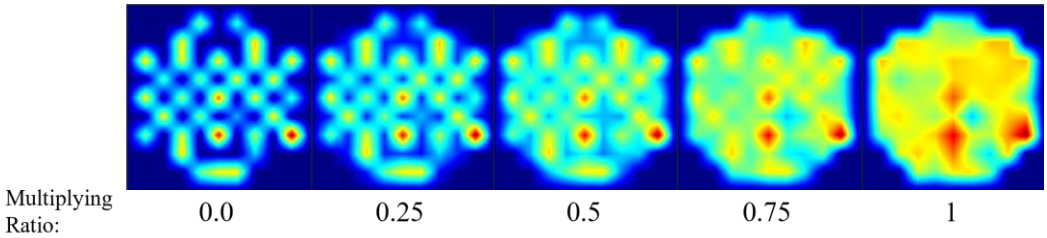

Figure 6.8 Changes in the distribution for different multiplying ratios

6.1.5 Emotion Analysis with Distribution of EEG in Time

After the emotions of the videos were determined, emotion analyzes were performed with EEG signals. First, it was desired to determine which region of the brain is more active or not for different emotions. In the first analysis, EEG amplitude changes were examined for only four representative videos representing 2D emotions. At this stage, the data has not been processed again because it has already been preprocessed as was told in the description of the data (Koelstra et al., 2011).

$$X_{k,l} = \frac{\sum_{p=1}^{32} \sum_{t=(l-1)\times Fs\times Tp)+1}^{l\times Fs\times Tp} x_{p_{v_k}}(t)}{Fs \times Tp} \tag{6.5}$$

The amplitude averages of the EEG signals of 32 participants at ten-second intervals for each channel for representative videos were calculated by Equation (6.5). In this equation, the k value is the channel number (k = 1, 2, …, 32), the N value is the length of the signal obtained from each channel, the Fs is the sampling frequency, the Tp variable is the duration of the time interval, the v variable is the selected video number($v \in \{video_{LALV}, video_{\text{LAHV}}, video_{\text{HALV}}, video_{\text{HAHV}}\}$), the l is the number of time intervals $\left(l = 1, 2, \dots, \left\lfloor \frac{N}{Fs\times Tp} \right\rfloor\right)$, $x_{p_{v_k}}(t)$ signal is the signal of the pth participant in the time interval selected from the EEG signal recorded from the kth channel in the vth video, and $X_{k,l}$ is the average EEG amplitude of channel k for the lth time slot.

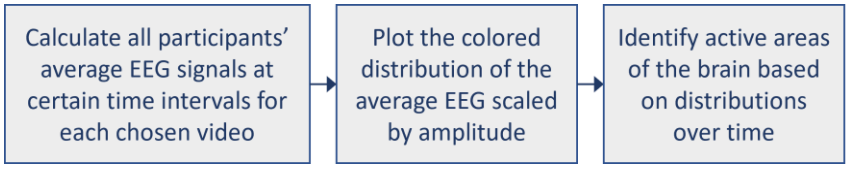

Figure 6.9 Flowchart of the first emotion analysis

In order to observe the changes in time, the colored distribution image scaled according to the amplitude was drawn. Then, the changes were observed for time intervals of ten seconds (Tp = 10). Flowchart of this analysis is given in Figure 6.9. With this analysis, the change in the mean EEG amplitude distributions of 4 videos over time was calculated and the scaled-colored distribution image given in Figure 6.10 was drawn and examined. The distributions in the first row belong to the music video number 5 representing the HAHV emotion, 18 representing the LAHV emotion in the second row, 24 representing the LALV emotion in the third row, and 35 representing the HALV emotion in the last row.

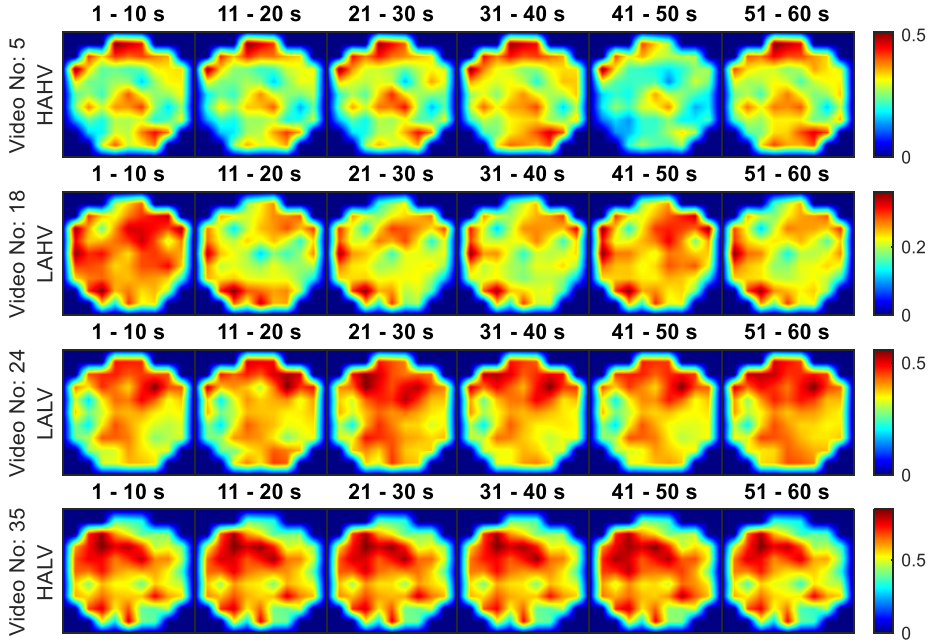

Figure 6.10 Time variation of mean amplitude distributions for selected videos

When these distributions were examined within themselves, according to the change in time, it has been observed that the amplitude sizes of some regions have increased or decreased partially, but there has not been a great change among the

active regions for some videos. For example, in the 35th video, there are no visible change between electrode amplitudes over time. In the 5th video, the average EEG amplitude in the frontal lobe also does not change much in 1-30 s interval, but in the 31-40 s interval, there is an increment, especially in the AF4 and F8 electrodes (Figure 6.1). Then again at the same points a decrease occurs. As can be seen from the color scale, the average value drops from about 0.4 to 0.2.

In the 18th video, a change is observed especially in the junction region of the frontal and parietal lobes, that is, in the middle region of the distribution pattern. From the color scale, while the average value of this region was red, that is, more than 0.2 in the 1-10 s interval at the beginning, it decreased below 0.2 in the 11-20 s interval and approached the green color. In other words, the average EEG signal amplitude value decreased. In the following periods, it can be understood that it passes very little by approaching the 0.2 value again. However, there was no increase as much as the 1-10 s interval.

6.1.6 Emotion Analysis with Distribution of EEG on the Brain

In this analysis, the flowchart of which is given in Figure 6.11, the amplitudes of the average EEG signals of each of the 40 videos were compared regardless of time. When $Tp = 60$ seconds, that is, a single time frame ($l = 1$) from the first to the last moment, the average value of the EEG channels of all participants was calculated by Equation (3.4). Then, the average amplitude distributions of the channels were plotted and interpreted. Afterward, the EEG averages obtained separately for 4 emotions from all participants in the related emotion group of the video were calculated and the distribution was drawn. From this drawing, it was tried to determine the active regions and informative electrodes according to the distributions.

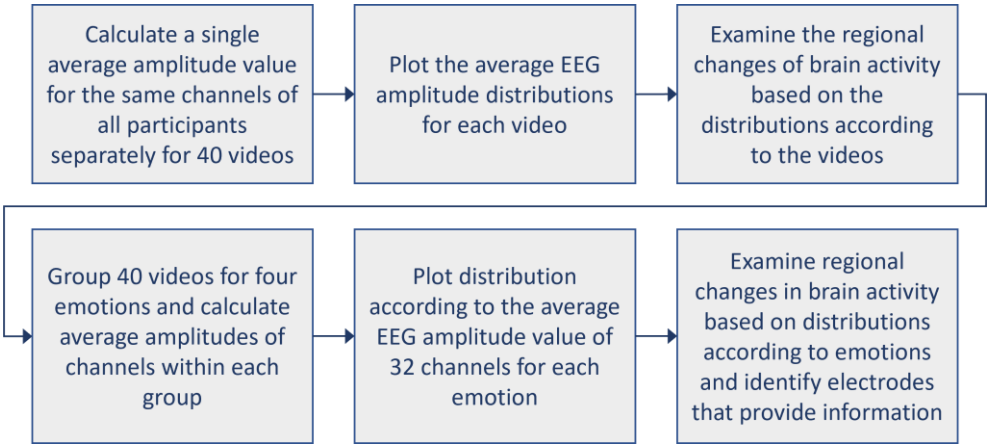

Figure 6.11 Flowchart of the second emotion analysis

The color scale in Figure 6.12, where the average distributions are given for all videos, is valid for all distributions. When the average variance of EEG between the videos were compared, it was observed that different activities took place for each video. For example, while the amplitude value in all channels is very low and almost 0.2 for the 3rd video, the 12th video has electrodes with the highest amplitude value of approximately 1.2.

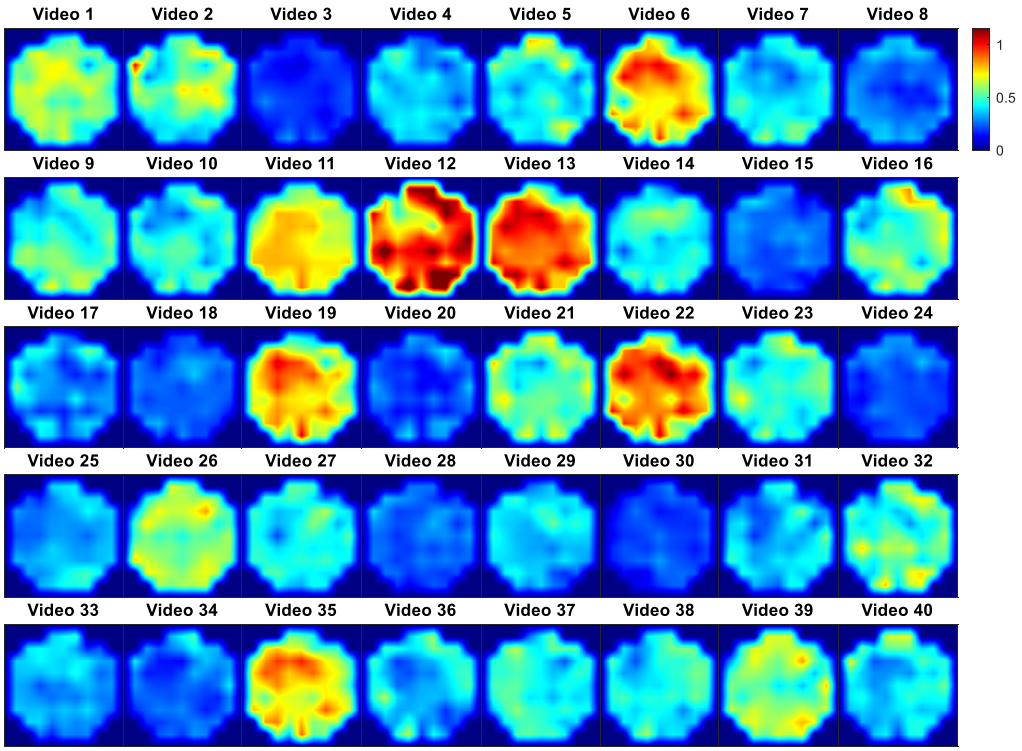

Figure 6.12 Average EEG amplitude distributions for all videos

Then the videos representing the emotions were compared. Just for the arousal, it can be said that while the average value of all electrodes is close to 0.5 in the 16th video representing the LA emotion, it is close to 0.25 in the 36th video representing the HA. For the valence, an increase in EEG amplitudes for HV was observed when 28 videos representing LV were compared with 11 videos representing HV.

To compare the emotions in the 2D emotion model, the EEG signal amplitudes obtained in 35th video, which is representative of HALV emotion, are higher than 5th video representing HAHV. It was observed that for video 24 representing LALV emotion and 18th video representing LAHV, almost all signals have lower amplitude than the 5th and 35th videos.

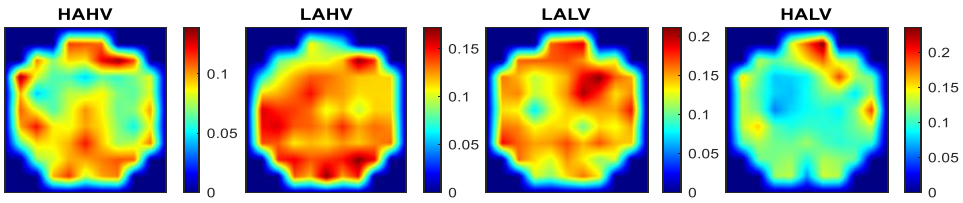

Figure 6.13 Average EEG amplitude distributions for each emotion

Afterward, the videos were grouped according to their emotional classes in Table 6.2. The average of the measured EEG signals during the videos in each emotion group was calculated. Then the amplitude distributions were plotted as in Figure 6.13.

Table 6.5 Comparison of channels and amplitudes for emotions

		HAHV	LAHV	LALV	HALV
The highest amplitude on EEG	Electrode	AF4	Oz	F4	Fp2
	Amplitude	0.1382	0.1717	0.2094	0.2354
Second highest amplitude on EEG	Electrode	F7	PO4	FC2	T8
	Amplitude	0.1377	0.1715	0.2022	0.1917

Then, the amplitude comparison of the emotions was done as a result of these distributions. First, it was observed that the highest amplitude signal was measured from the Fp2 electrode in the HALV sense. Electrodes with the highest amplitude for

other emotions were electrode F4 for LALV emotion, Oz for LAHV, and AF4 for HAHV. When the average signals obtained are compared, the electrode information with the highest first and second average values for emotions is given in Table 6.5.

6.1.7 Personalized Informative Electrode Selection for Emotion Detection

In the final analysis, done with the DEAP dataset, it was tried to detect emotion in a person based by selecting informative features and electrodes. This time, in addition to LALV, LAHV, HALV, and HAHV emotions, music videos were grouped for each arousal (LA or HA) and valence (LV or HV) emotion. Regions of these emotions in the 2D emotion model were shown in Figure 2.6, and the number of videos in each emotion class is given in Table 6.2. After that, an algorithm was then developed by comparing the features, brain waves, and electrodes with various analyzes. Detailed information about these stages and the results are given in this section.

6.1.7.1. Comparison of Features

As a result of the literature research, the mostly used features that are mean, standard deviation, variance (activity), mobility, and complexity were calculated for all channels with Equations (3.4), (3.5), (3.6), (3.9), (3.10), and (3.11). Then, the average value of the features obtained from the videos that were determined to trigger the same emotions were calculated and the results were observed for each channel.

First of all, the mean value feature was examined. For this, the average value of the EEG signals of all channels of the previously determined participants was calculated for the representative videos given in Table 6.4. The calculated mean values are given in Table 6.6. In this table, the values of the EEG channels with the highest value for each emotion are written in bold, and the emotions with the highest value for each EEG channel are highlighted in gray.

Table 6.6 Comparison of mean value feature with emotions for all electrodes

Electrodes	LA	HA	LV	HV	LALV	LAHV	HALV	HAHV
Fp1	0.1278	0.0397	-0.0496	0.0813	0.0486	0.3083	0.1358	-0.0122
AF3	-0.0259	-0.2341	0.0061	0.0452	-0.0801	-0.6373	-0.3063	-0.1875
F3	0.1631	-0.2118	**0.1109**	0.1645	-0.3291	-0.6135	-0.1699	-0.2859
F7	-0.4037	0.151	-0.1326	-0.0968	0.053	0.2001	0.1297	**0.6781**
FC5	0.0956	-0.2399	-0.062	0.0882	-0.1497	-0.241	-0.2447	-0.3216
FC1	-0.0077	-0.1162	0.0363	0.0677	-0.0488	-0.2434	-0.0421	-0.1356
C3	-0.0774	-0.1017	0.018	-0.0212	-0.0687	-0.2392	-0.1749	0.016
T7	-0.1081	0.1619	-0.0417	-0.0204	0.1554	-0.1107	-0.0333	0.224
CP5	0.0247	0.1451	0.0175	-0.2526	**0.3362**	0.4075	0.3375	0.1016
CP1	-0.0768	0.1132	0.0019	-0.0415	-0.0754	0.1196	0.1467	-0.0741
P3	0.061	-0.016	0.0568	-0.0061	-0.0225	-0.1388	-0.1567	-0.1555
P7	0.1343	-0.1607	-0.056	0.1072	-0.0736	-0.0158	-0.1445	-0.2428
PO3	0.0979	-0.1028	-0.0768	0.1604	-0.1667	-0.3155	-0.1723	-0.1506
O1	-0.0314	0.2525	-0.0727	-0.2412	0.2238	**0.5891**	**0.3846**	-0.1305
Oz	0.0549	-0.145	0.0029	0.0809	-0.1307	-0.2857	-0.229	-0.2896
Pz	-0.0725	0.1034	0.1008	-0.0477	0.0453	0.0007	0.0026	0.0466
Fp2	0.1117	0.0651	0.0741	-0.1009	0.2839	0.2779	0.1762	0.0398
AF4	0.065	**0.279**	0.0393	0.0123	0.1893	0.2696	0.2281	0.3329
Fz	0.0503	-0.2944	-0.09	0.218	-0.0825	-0.3608	-0.2657	0.0478
F4	**0.2923**	0.0447	-0.0439	**0.2789**	-0.1185	0.2946	0.1499	-0.2161
F8	-0.2048	0.0467	0.0871	-0.1312	0.0959	0.0254	0.1005	0.2769
FC6	-0.2553	-0.0437	-0.0976	-0.1325	0.0796	-0.0352	-0.1991	0.1742
FC2	-0.001	-0.0132	-0.0191	0.1532	-0.1074	-0.5414	-0.2858	0.0481
Cz	-0.2225	0.1384	0.0727	-0.1363	0.0292	0.057	0.0905	0.3134
C4	-0.1517	-0.1669	-0.0266	-0.0721	0.0424	-0.1352	-0.1547	0.312
T8	0.0979	0.1632	0.069	-0.0634	0.1829	0.303	0.1496	-0.1495
CP6	-0.0383	-0.0874	-0.0951	0.0368	-0.0075	0.2163	0.0112	0.2848
CP2	-0.0869	0.1326	0.0075	-0.0915	-0.084	0.3232	0.2056	0.1665
P4	0.0774	-0.205	0.0139	0.0742	-0.1932	-0.267	-0.1933	-0.1144
P8	0.0376	0.0696	0.0472	-0.0835	0.0702	0.0061	-0.0044	-0.1635
PO4	0.2118	0.1286	0.0796	0.0442	-0.1312	0.5125	0.3287	-0.1805
O2	0.0607	0.1045	0.0223	-0.0744	0.0338	0.2696	0.1996	-0.2525

The results from the table are examined within 1D and 2D emotions and between electrodes. First of all, from the values in bold, for arousal emotion, the F4 electrode has the highest value for LA emotion, while the AF4 electrode has the highest value for HA. In other words, it was determined that there was a change in the mean values of the EEG signals for the arousal emotion at approximately very close points in the right frontal lobe. for valence emotion, the F3 electrode for the LV and the F4 electrode for the HV emotions had high values. Here, it was observed that there was

a change between the right and left sides of the frontal lobe. When the 2D emotions were examined, the O1 electrode had the highest value for both LAHV and HALV emotions. The highest mean value was CP5 for LALV emotion and F7 for HAHV. As a result, it was observed that there was no distinguishing between LAHV and HALV for the mean value. However, it was determined that there were changes between the frontal and parietal lobes for LALV and HAHV emotions.

The inference obtained from the values highlighted in gray is that the HV emotion between LV and HV has the highest mean value in 7 different electrodes, and among 2D emotions, LAHV and HAHV have the highest mean value in 8 different electrodes. This can mean that the mean value feature among all electrodes has a higher value for the HV emotion in general.

The average values of the standard deviation, variance, activity, mobility and complexity values obtained from the EEG signals were calculated for all emotions, and the drawings were done in order to compare the features.

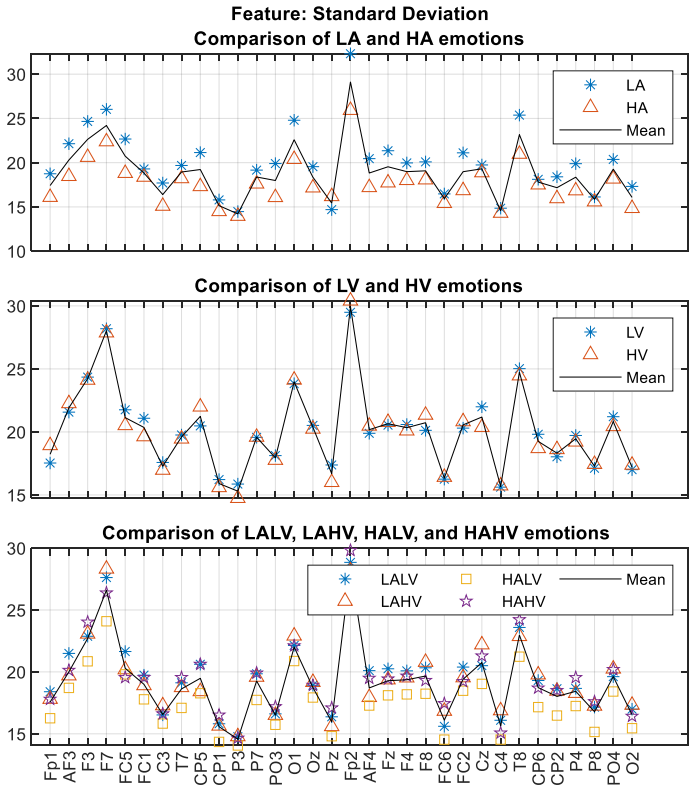

Figure 6.14 Comparison of standard deviation feature

In Figure 6.14, the calculated standard deviation values of each channel for each emotion are shown. It was determined that the P3, Pz, and PO3 electrodes would not be useful in detecting arousal emotion, P3, Pz, PO3, O2, P8, and CP1 electrodes in valence emotion, and P3, Pz, and PO3 electrodes in 2D emotion as the low value of the standard deviation would indicate very low changes in those signals.

There is also one more signal plotted in each subplot. This signal is the mean value of the standard deviations for the corresponding emotion. It has been observed that this signal can aid in the classification of 1D emotions, and plots have been done for 1D signals only from here on out.

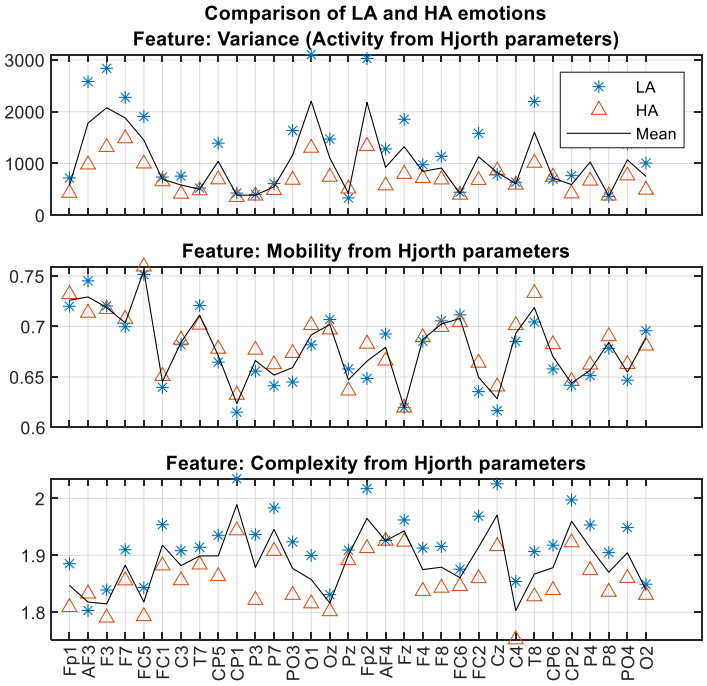

Figure 6.15 Comparison of Hjorth parameters for arousal emotion

After that, the signals of each feature for arousal emotion only were plotted as in Figure 6.15. Based on these results, it was desired to classify, and the electrodes in which the highest differences between the LA and HA feature values in the same electrode were observed for each property were tried to be determined. The electrodes for which this difference is greatest are Cz for standard deviation (Figure 6.14), F7 for activity, T7 for mobility, and Cz for complexity.

In Figure 6.16, the drawings for the same features are given for the valence emotion this time. First of all, it has been observed that the mean value signals take almost the same value as the arousal signals. Thus, it was thought that classification can be done using a single mean value signal. Before that, the electrodes observed to have the highest difference between LV and HV values are PO4 for standard deviation (Figure 6.14), F7 for activity, and Fp1 for mobility and complexity.

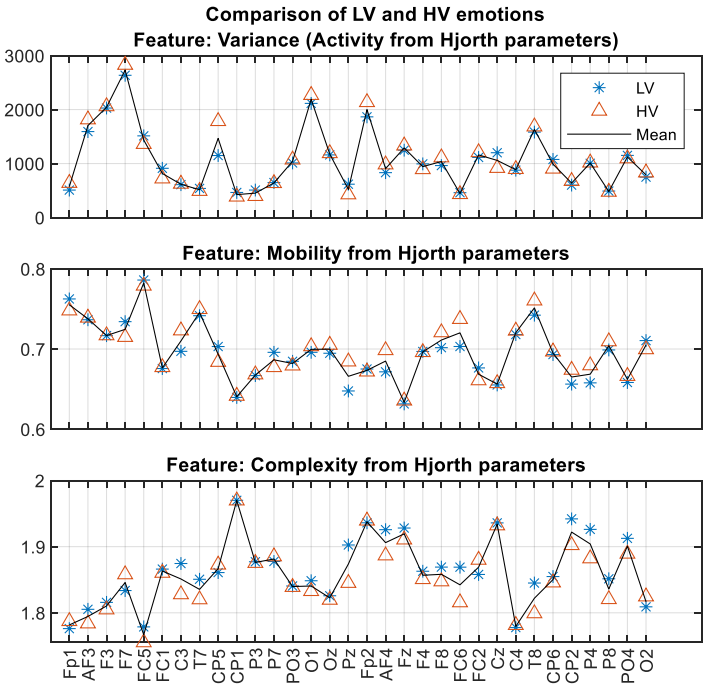

Figure 6.16 Comparison of Hjorth parameters for valence emotion

However, the majority information obtained from the participants was used instead of average values for emotion classification. For this, the standard deviation and Hjorth parameters of all channels in the selected videos for LA, HA, LV and HV were calculated. The differences between LA-HA and LV-HV was calculated and the electrode with the highest difference was chosen. After performing this operation for all participants, the most selected channel for each feature was selected. To determine which value is higher during classification, the mean value was calculated from the relevant electrode for LA-HA and LV-HV. The electrodes determined for both emotions, the mean values and the higher emotions are given are in Table 6.7.

Table 6.7 Features determined to have the highest value difference relative to the majority

Emotion	Highest difference obtained	Standard deviation	Activity	Mobility	Complexity
Arousal	Electrode	FC5	Fp2	FC5	FC5
	Mean value	10.28	2530	0.858	1.787
	Higher emotion	HA	HA	HA	HA
Valence	Electrode	Fp2	Fp2	Fp1	Fp1
	Mean value	34.24	1077	0.73	1.916
	Higher emotion	LV	LV	LV	LV

In the classification, the steps given in the flowchart in Figure 6.17 were applied. These results, which were obtained from the data of all participants, were tried and the percentage of accuracy was obtained. The features determined for the electrodes given in Table 6.7 were calculated for all participants and it was checked whether the feature value was lower or higher than the mean value given in the table. If it fits the given high emotion in the table, that classification was accepted as correct. These studies were tried on videos other than the videos in Table 6.2 and the classes of the videos were determined using Table 6.4.

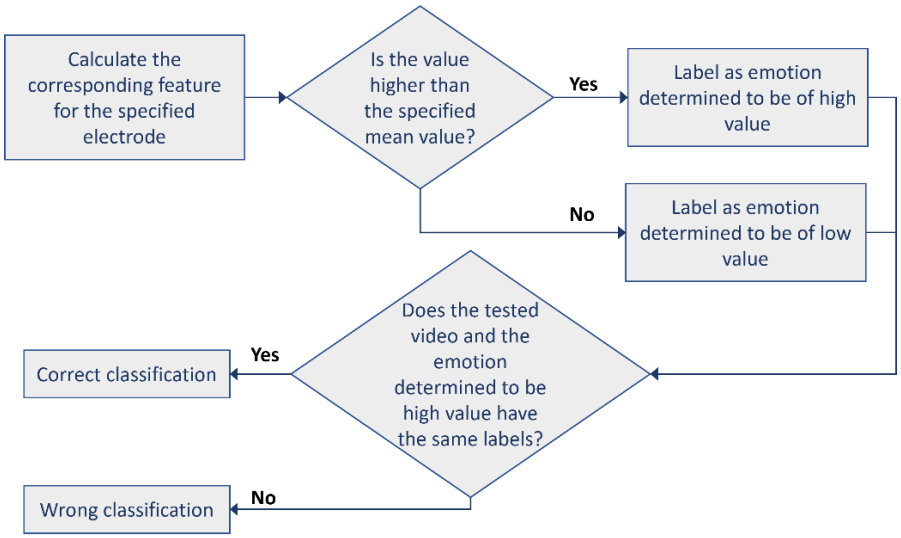

Figure 6.17 Flowchart of the 1D emotion classification

After the classification were done as it was mentioned, the accuracies of the classifications were calculated with the Equation (6.6) where $N_{correct}$ is the number of correct classifications and N_{false} is the number of false classifications.

$$accuracy(\%) = \frac{N_{correct}}{N_{correct} + N_{false}} \quad (6.6)$$

Accuracies for each emotion class and features are given in Table 6.8. Although the accuracy percentages are very low, if the features are compared with each other, the mobility feature provided the highest accuracy for arousal and valence emotions.

Table 6.8 Majority based 1D emotion classification accuracies

	Standard deviation	Activity	Mobility	Complexity
Accuracy of arousal emotion classification (%)	50.12	49.42	**51.16**	48.96
Accuracy of valence emotion classification (%)	49.88	49.31	**51.74**	48.03

The classification study done above was also carried out on a person basis. For this, the electrodes with the highest difference value for each feature and emotion, the mean values and which emotion had the highest feature value were recorded for the selected participants, as in Table 6.7. Then, classification was done as in Figure 6.17.

Table 6.9 1D emotion classification results with person-based values

		Accuracy for each feature (%)			
Emotion	Type of accuracy	Standard deviation	Activity	Mobility	Complexity
Arousal	Highest	62.5	62.5	**71.88**	65.63
	Average	48.84	46.18	**54.63**	46.3
Valence	Highest	65.63	65.63	**71.88**	59.38
	Average	43.4	43.06	**53.59**	45.95

The accuracy percentages in the person-based classification result are given in Table 6.9. In this table, the highest percentage of accuracy obtained from the classification results and the average percentage of accuracy of the participants are given for both 1D emotions. When the accuracy percentages of the participants were compared, it was seen that the highest percentage was obtained with the mobility feature for both emotions.

Finally, the inferences obtained in detecting emotions from comparing the features with different aspects are as follows:

- For arousal emotion, among the results obtained with the average values given in Table 6.9, it was observed that 54.63% of accuracy was obtained with the mobility feature.
- For the valence, as a result of the person-based values given in Table 6.9, the average highest accuracy of 53.59% was obtained with the mobility feature.
- The person-based classification (Table 6.9) resulted better than the majority-based classification (Table 6.8).

6.1.7.2. Comparison of Brain Waves

In the next study, comparisons of brain waves were done for emotion detection. The information obtained as a result of the previous study was also used in this study. Thus, the mobility feature was used to determine both arousal and valence emotions. For this study, first of all, the filters were designed using the frequency ranges of theta, alpha, low beta, high beta and gamma waves given in Table 3.1. BPF was calculated in Matlab with the Butterworth filter design function in order to filter these brain waves from the EEG signals. The transfer function of this filter is given in Equation (6.7). The coefficients in the transfer function of the BPF were obtained separately for each brain waves.

$$H(z) = \frac{B(z)}{A(z)} = \frac{b(1) + b(2)\,z^{-1} + \cdots + b(2n+1)\,z^{-n}}{a(1) + a(2)\,z^{-1} + \cdots + a(2n+1)\,z^{-n}} \tag{6.7}$$

Then, the features selected in the previous study were calculated for each brain wave of each channel. Figure 6.18 shows the values of the mobility feature calculated for each brain wave obtained from the representative video of the arousal. The highest mobility value difference between LA and HA emotions occurred at the high beta brain wave of F8, and the lowest occurred at alpha wave of O2 channel.

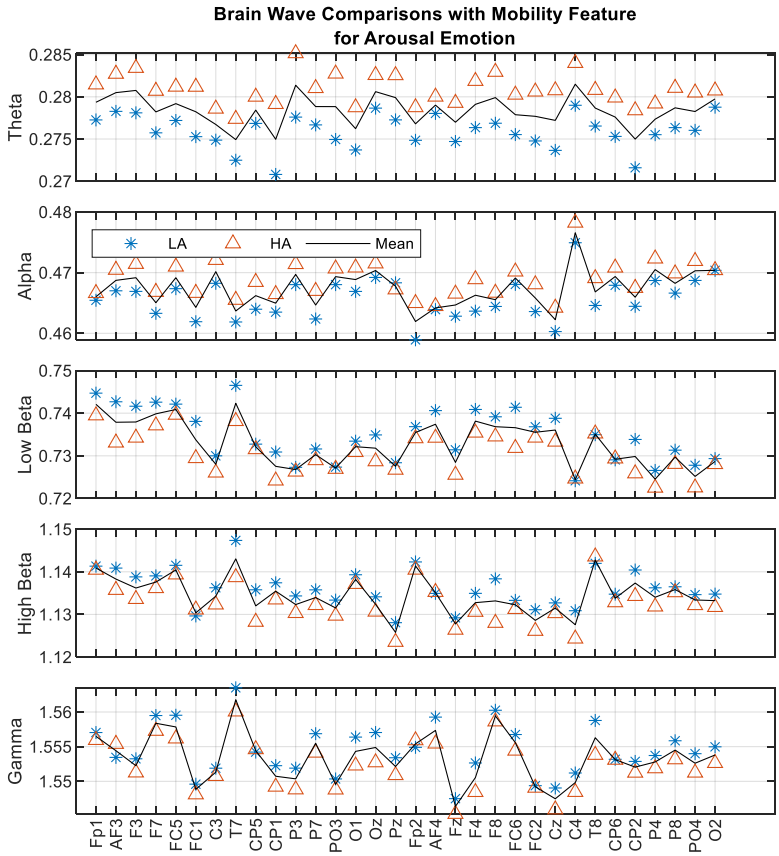

Figure 6.18 Mobility results of different brain waves to compare arousal emotions

According to these results, in Table 6.10, the electrodes with the highest mobility difference for each brain wave, the average value between LA and HA for this electrode and the emotion higher than this value are given. When the videos other than the representative videos were tested for the selected participants using these features, the accuracy percentages given in the same table were obtained. Although the percentage of accuracy is still not high enough to be relied upon, it is slightly higher than the average accuracies obtained from the original EEG signals in Table 6.8 and Table 6.9. Hence, by using the mobility features of the theta wave of the CP1 electrode, 52.78% accuracy were obtained.

Table 6.10 Electrodes determined to have the highest value difference for the arousal emotion

Arousal	Theta	Alpha	Low Beta	High Beta	Gamma
Electrode with highest difference	FC5	CP1	FC5	T8	FC5
Mean value	0.2758	0.4539	0.7564	1.1316	1.5829
Higher emotion	HA	HA	HA	HA	HA
Accuracy of classification (%)	51.04	**52.78**	50	51.62	49.31

In addition, for the valence emotion, the calculation results of the mobility feature from brain waves are given in Figure 6.19. As a result of these drawings, it was determined that the mobility difference value obtained from the high beta wave of the Pz channel is higher than the other waves. However, the high beta wave of the Fp1 channel provided the lowest difference between LV and HV.

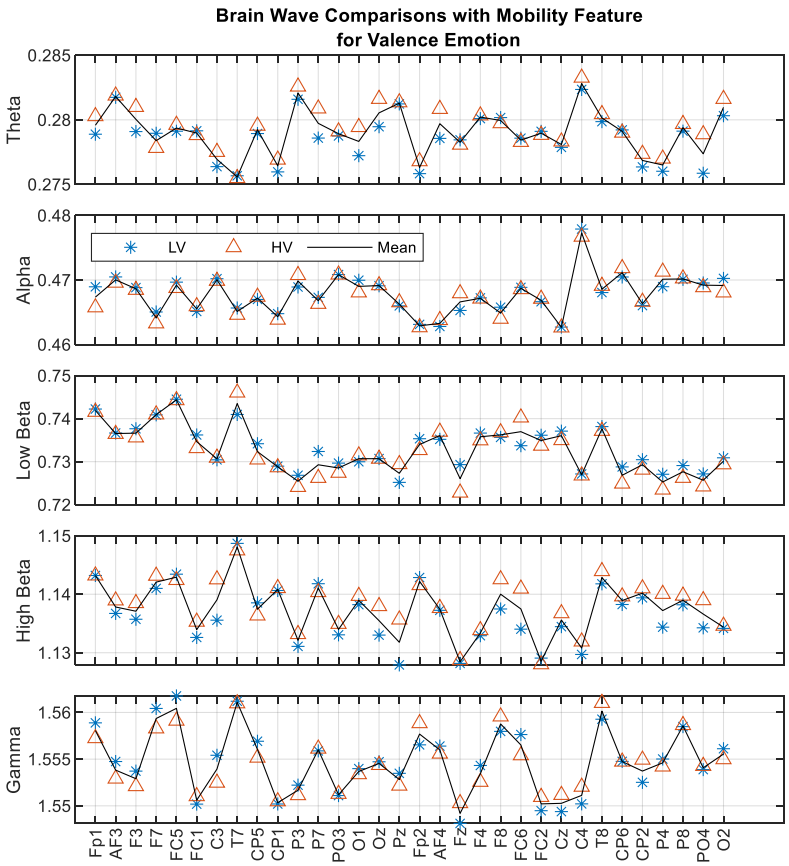

Figure 6.19 Activity results of different brain waves to compare valence emotions

As in Table 6.10, this time the electrodes determined as a result of the average mobility values for the valence emotion in Figure 6.19, the variable values required for classification, and the accuracies of classification for each wave are given in Table 6.11. The highest accuracy percentage was 54.98% and obtained by the mobility feature of the low beta wave of the Fp2 channel. Although it is slightly higher than the accuracy of the study done with the average features given in Table 6.8 and, it is still much lower than the person-based classifications given in Table 6.9

Table 6.11 Electrodes determined to have the highest value difference for the valence emotion

Valence	Theta	Alpha	Low Beta	High Beta	Gamma
Electrode with highest difference	C3	C4	Fp2	FC5	26
Mean value	0.2874	0.4817	0.7339	1.1626	1.5638
Higher emotion	LV	HV	LV	LV	HV
Accuracy of classification (%)	50.93	47.92	**54.98**	51,51	54,4

In the next stage, the difference between brain waves was examined by obtaining person-based features this time. The mobility value of all brain waves of all channels were calculated for arousal and valence emotions. Then, the electrodes where the calculated feature value has the highest difference for low and high emotions were determined as features. After the relevant features were saved, the testing was done by checking whether the calculated value was above or below the mean value.

Table 6.12 Results from person-based emotion detection for different brain waves

	Emotion	Theta	Alpha	Low beta	High beta	Gamma
The most chosen electrodes	Arousal	Fp2	Fp2	F7	F7	T7
	Valence	Fp2, AF4	Fp2	F7	F3, Fp2	T7
Highest accuracy (%)	Arousal	**72.5**	**72.5**	62.5	67.5	70
	Valence	72.5	72.5	**82.5**	77.5	72.5
Average accuracy (%)	Arousal	53.91	53.52	52.81	53.13	**55.39**
	Valence	53.91	56.25	57.66	**60.23**	58.83

The person-based emotion detection results are given in Table 6.12. From these results, the highest personal accuracy obtained from the theta and alpha waves of the Fp2 electrode was 72.5%, and the highest accuracy percentage on average with the gamma wave of the T7 electrode was 55.39% for the arousal. For valence, the highest accuracy was obtained from the low beta wave of the F7 electrode, and the highest accuracy on average was obtained from the high beta wave of the F7 channel. These accuracy percentages are 82.5% and 60.23%, respectively.

6.1.7.3. Informative Feature and Electrode Selection Algorithm

As a result of previous studies within the scope of this thesis, it has been observed that selecting informative features on a person-based basis in EEG studies provides higher accuracy. In addition, if this detection process is desired to be done in real-

time, the long-term use of EEG devices containing more than one electrode will not be useful as it will restrict the movements of the person being measured and disturb them. Besides, if the desired functions can be performed with fewer electrodes, having more electrodes will cause a delay in signal processing and cost loss.

For this reason, an algorithm has been developed that enables the selection of these features on a person-based basis. The flowchart of this algorithm is given in Figure 6.20.

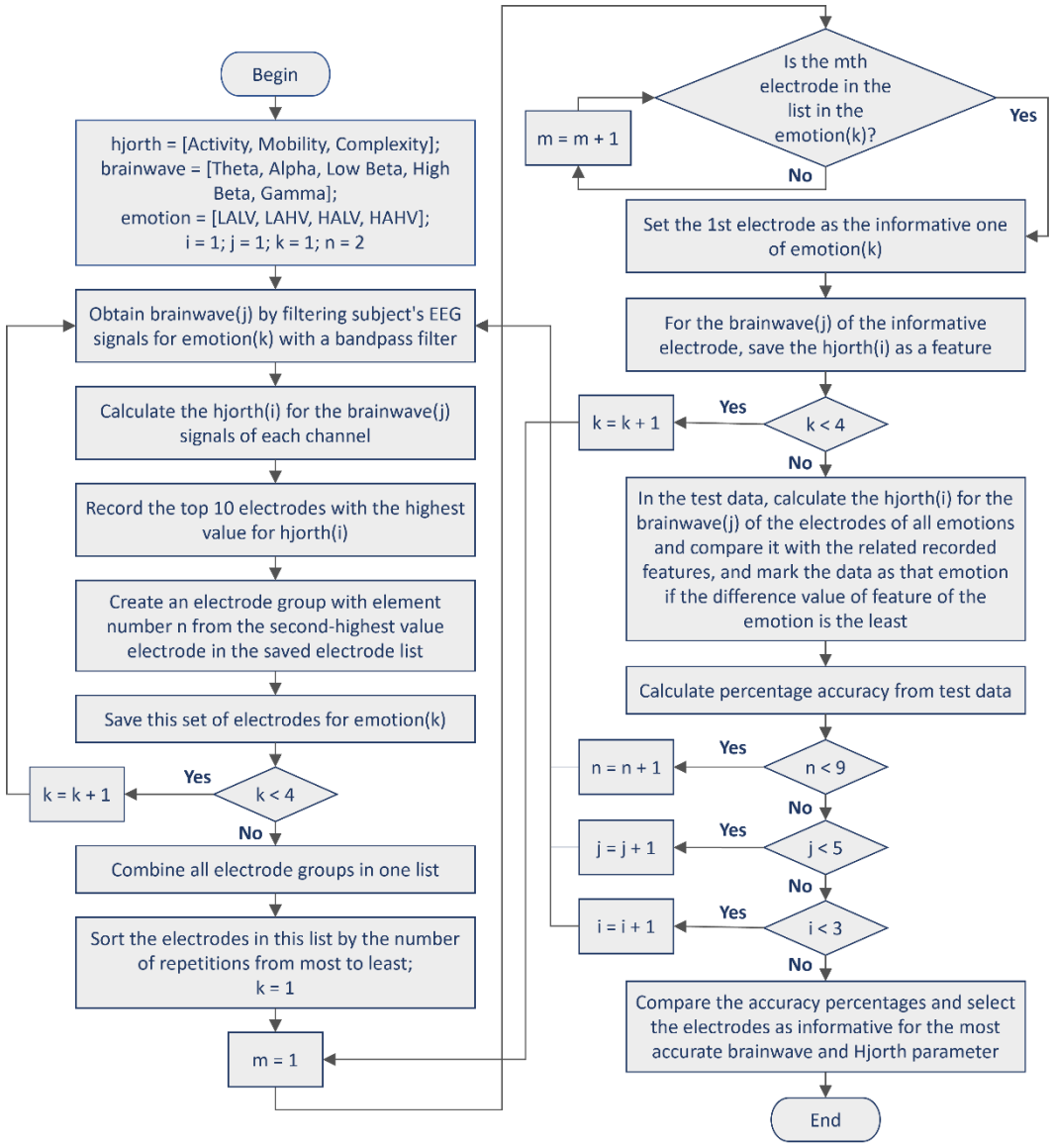

Figure 6.20 Flowchart of the algorithm of informative electrode selection (Yürdem & Özkurt, 2022)

At the beginning of the algorithm, in order to examine which brain wave is more useful in terms of providing information, the procedures described below are repeated, respectively, from theta wave to the gamma wave. Since the DEAP dataset is preprocessed, the brain wave is obtained directly from the original EEG signal by filtering it with BPF.

The feature is calculated after the brain wave is obtained from the EEG signals recorded during the representatively selected music videos. Since the use of Hjorth parameters as features generally provides high accuracy in previous studies, these parameters were determined as features. The activity, mobility and complexity properties are calculated by Equations (3.9), (3.10), and (3.11) were used, respectively.

After the calculation, the names of the first 10 electrodes with the highest feature values were recorded. However, this list was not used directly while generating the electrode selection algorithm. The first electrodes are omitted from this 10-electrode list, as some electrodes also have the highest value for different emotions. Then, firstly, 2-electrode groups are formed for all four emotions (LALV, LAHV, HALV, and HAHV) starting from the second highest value electrode. Then the electrode groups of all emotions are merged, and a single list is obtained. In Figure 6.21, a visual explanation of an example for using activity features of theta waves and forming a 2-electrode group is given for the part of the algorithm that has been described so far.

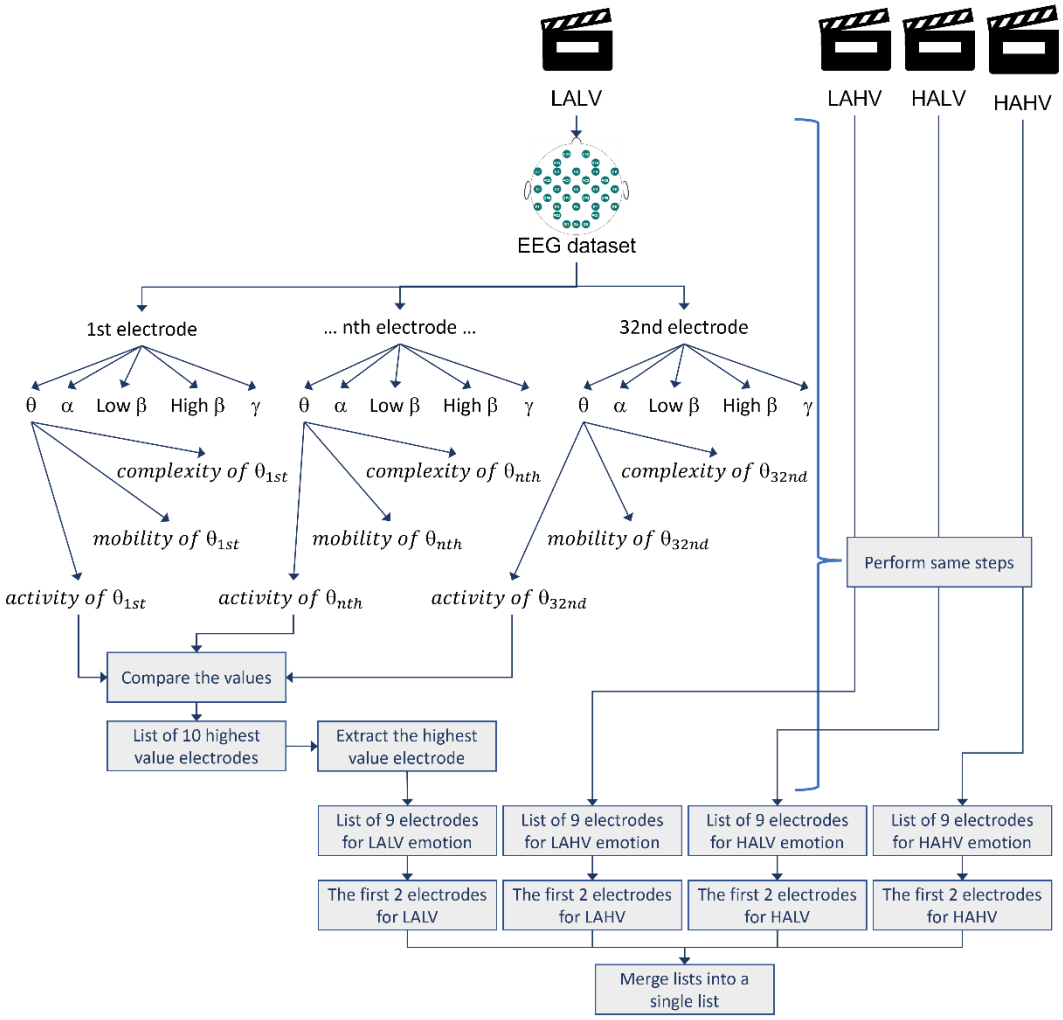

Figure 6.21 The first part of the algorithm's operation as an example for only features from theta wave and 2-electrode groups

In the next step, the number of repetitions of the electrodes in the merged list is determined. From the first electrode with a large number of repetitions, each electrode is checked for emotions in previously formed lists for each emotion. If an electrode in the merged list is in the list of the controlled emotion and no other electrode has been identified as such, then this electrode is selected as the informative electrode of that emotion. For each emotion, at most one electrode is designated as the informative electrode. As it was shown in Figure 6.20, this process was repeated by increasing the number of electrodes one by one from two to nine in the group consisting of 9 electrodes selected for each emotion.

An example of this algorithm is given below. For this example, for the mobility feature of a participant's gamma brain wave, groups containing three electrodes were formed and informative electrode selection was done. The mobility feature of all channels is calculated for representative videos. Then, the top 10 electrodes with the highest value are determined. The first 10 electrodes determined are given in Table 6.13. Of these electrodes, the ones with the highest value (i.e., those written in red) were excluded from the list as indicated in the algorithm. A group of the remaining 9 electrodes is then formed for each emotion. For this example, it was stated that there would be three electrodes in the groups. The groups formed from the electrodes written in bold in the table are also given here.

Table 6.13 Determined electrodes and the groups for informative electrode selection

	LALV	LAHV	HALV	HAHV
Top 10 electrodes with the highest value for the calculated feature (respectively)	**Fp1**	**Fp1**	**AF4**	**T7**
	F3	**AF4**	**CP1**	**P7**
	Fz	**P3**	**Cz**	**CP5**
	AF4	**FC2**	**Fp2**	**Cz**
	P3	Cz	FC1	CP1
	F4	Fp2	P3	FC1
	FC5	FC1	Fp1	Fp1
	FC2	CP1	P7	P8
	FC1	CP2	FC2	C4
	Cz	F8	Oz	Fp2
Groups containing three electrodes	[F3, Fz, AF4]	[AF4, P3, FC2]	[CP1, Cz, Fp2]	[P7, CP5, Cz]

For this example, when groups are merged, the new list is [F3, Fz, AF4, AF4, P3, FC2, CP1, Cz, Fp2, P7, CP5, Cz]. The Cz and AF4 electrodes are repeated twice in the list, while the others are not. If more than two repeating electrodes were found, these electrodes would also be removed from the relevant lists.

Then, starting from the first electrode of each emotion list, the other list was checked. This other list is the one in which the combined and more than two repeating electrodes are removed. The electrode with the highest feature value in both lists was accepted as the informative electrode for that emotion. Thus, for this

example, the informative electrodes for the four emotions were identified as F3 for LALV, AF4 for LAHV, CP1 for HALV, and P7 for HAHV.

Figure 6.22 shows the percentages of accuracy obtained by varying the brain waves and the number of members in the group for each 2D emotion. In these results of the informative electrodes selected from the groups with 2, 3, 4, 5, 6, 7, 8 and 9 electrode numbers. All calculations were done for the mobility feature.

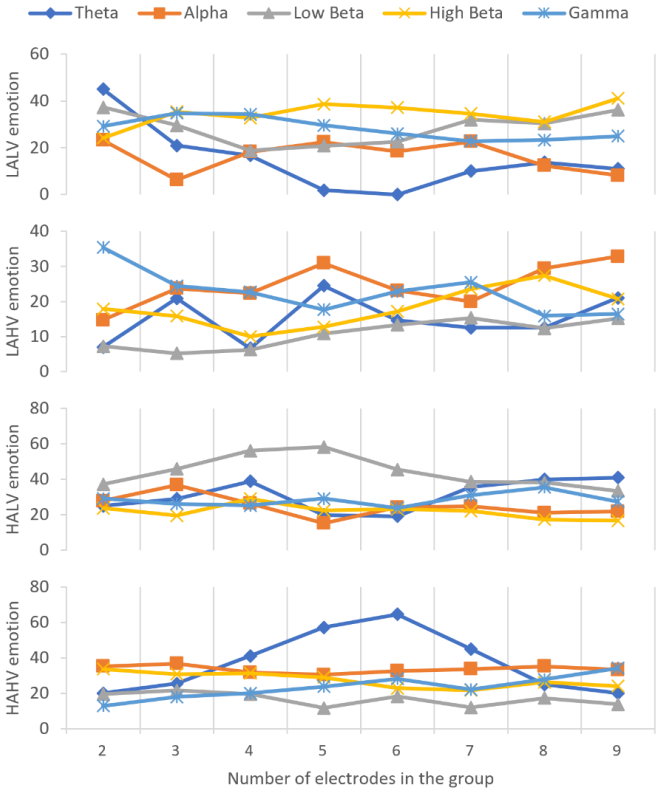

Figure 6.22 Comparison of brain waves for different number of electrode groups for 2D emotions using the mobility feature (Yürdem & Özkurt, 2022)

Based on these graphs, the highest average accuracies for LALV, HALV and HAHV, from which brain wave it was obtained and how many electrode groups were obtained are given in the Table 6.14. The highest accuracy was obtained for the HAHV emotion, while this percentage of accuracy was 64.62%, the number of electrodes in the group was 6, and the used wave was theta brain wave. In the table, the accuracy of LAHV emotion is the lowest among other emotions.

Table 6.14 The highest accuracies obtained as a result of the person-based emotion detection study

	LALV	LAHV	HALV	HAHV
Number of electrodes in the group	2	2	5	6
Brain wave	Theta	Gamma	Low Beta	Theta
The highest accuracy (%)	45	35.42	58.33	**64.62**

According to the results obtained from the person-based electrode selections, the number of informative group electrodes selected as the majority, the brain wave and the first two most selected electrodes are given in Table 6.15. In this table, the results obtained for the mobility parameter are given.

Table 6.15 Mostly selected informative electrodes as a result of the study

	LALV	LAHV	HALV	HAHV
Number of electrodes in the group	2	2	5	6
Brain wave	Theta	Gamma	Low Beta	Theta
1st most selected electrode	Oz	FC6	T8	Pz
2nd most selected electrode	FC6	T7	P8	PO3

From this table, it was determined that the theta wave of the Oz channel for LALV, the gamma wave of the FC6 channel for LAHV, the low beta wave of the T9 channel for HALV emotion, and the theta wave of the Pz channel for HAHV emotion were the most determined features among the participants.

6.2 Data Analyses with Recorded Dataset

After the studies with the dataset in the literature, studies were carried out with the datasets recorded with the data acquisition system constructed within the scope of this thesis. Since the datasets found in the literature were usually preprocessed, it was possible to proceed directly to the analysis or feature extraction stages in the studies (Koelstra et al., 2011). However, in these studies, the raw EEG dataset recorded with the system had to be preprocessed. In the following sections, the preprocessing process and the studies done with dataset recorded while asking questions and viewing images are given. In emotion detection studies, the results obtained from the previous studies done with literature dataset were used.

6.2.1 Preprocessing of the Recorded Dataset

For the clean signals used in the analysis, the following preprocessing steps learned from the literature were applied (Gorgoni et al., 2014; Handojoseno et al., 2013; Koelstra et al., 2011; Murugappan et al., 2010; Seo et al., 2010). These steps are given in Figure 6.23 as a flowchart.

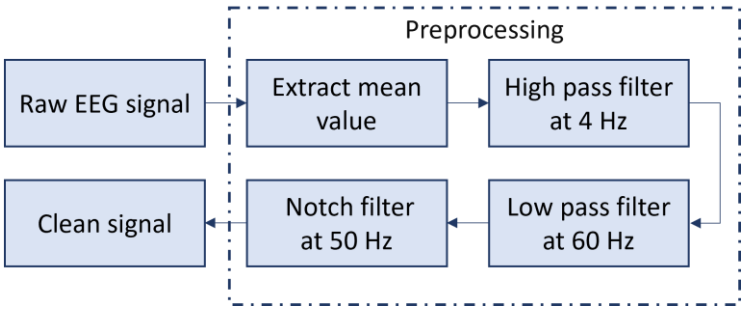

Figure 6.23 Flowchart of the preprocessing process done in this study

Firstly, the mean value which means DC offset is extracted from the raw EEG data. The signal is then filtered with an HPF with a cut-off frequency of 4 Hz to eliminate low-frequency noises and artifacts. After that, an LPF with a cutoff frequency of 60 Hz and a notch filter with a stopband frequency of 50 Hz are applied. With these two filters, high-frequency noises, environmental line noises, and artifacts are tried to be prevented. It was stated that filtering was applied for 50 and 60 Hz in the device, as indicated in the bandwidth property in the technical specifications of the used EEG device in Table 4.1. However, when the frequency domains of the obtained data were examined, it has been observed that high amplitude values are obtained in the 50 Hz frequency band. Hence, a Notch filter was applied in the preprocessing steps.

6.2.2 Studies with Dataset Triggered with Images

The analyzes done with the data recorded with the application, which is aimed to trigger the participants by showing the images, are given in this section. First of all, the changes in the concentration and anxiety signals during the recording were

examined, then the classification of the happiness emotion was carried out with basic machine learning methods such as KNN and SVM.

6.2.2.1. Examination of Changes in Concentration and Anxiety Levels

In this study, the EEG signals measured during the display of the images and the marking data obtained thanks to the software property activated in the recording system were used. Among these signals, the changes in the mental state of concentration and anxiety emotion were examined. Signals were calculated for these two states using Equation (3.16) for concentration and Equation (3.17) for anxiety. An example of this study is given in Figure 6.24.

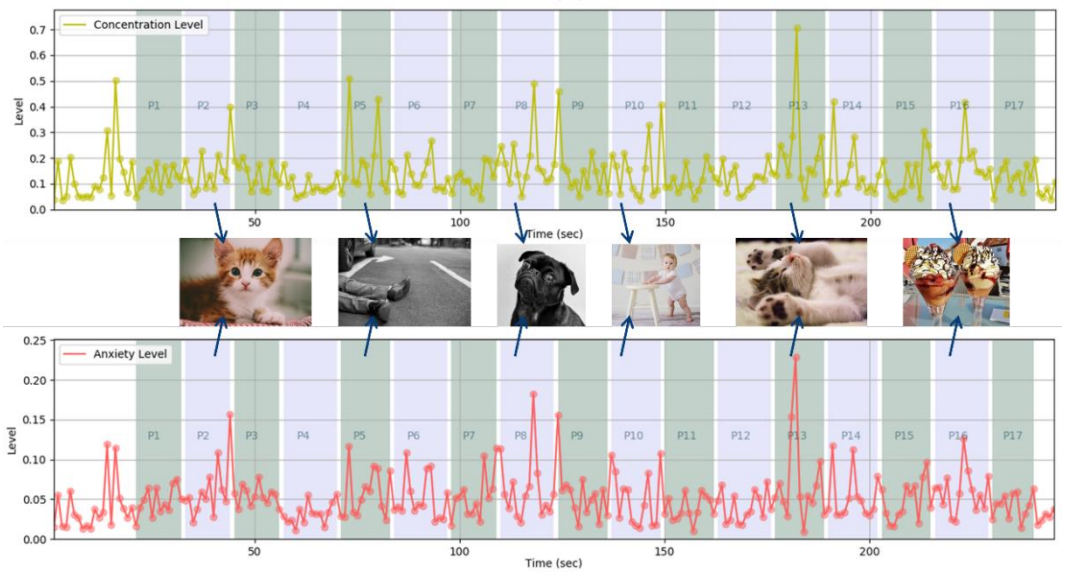

Figure 6.24 An example for concentration and anxiety changes (Yürdem et al., 2019)

In this example, the time intervals in which each image is shown are split. The second (P2), fifth (P5), eighth (P8), tenth (P10), thirteenth (P13), and sixteenth (P16) images are also given. Images P2, P10 and P13 were added to the study in order to trigger the feeling of happiness. A proportional change in concentration and anxiety levels was observed during these images. However, during the P5, which is intended to trigger the feeling of uneasiness, an average increase in the anxiety was observed, while a higher number of local peak values were observed in the concentration

compared to the other images. In other data samples, different level changes were observed for different emotions.

6.2.2.1. Classification with k-Nearest Neighborhood

With the KNN classification method, the feeling of happiness, which can be described as HA, was tried to be classified among all other emotions. The first classification was done by using features related to signal powers of all channels. After applying STFT to preprocessed signals, the features were extracted for brain waves. The first feature is calculated as mean power (MP) of all channels for each brain wave. The second one is the absolute value of MP difference of channel pairs (dMP_{ω_ε}) and calculated with Equation (6.8). This value is calculated for all brain waves (ω = [Gamma, Beta, Alpha, Theta, Delta]) and all electrode pairs, (ε_1, ε_2) = [(AF3, AF4), (F7, F8), (F3, F4), (FC5, FC6), (T7, T8), (O1, O2), (P7, P8)]. The MP_{ω_ε} means the MP value of ω wave of ε electrode.

$$dMP_{\omega_\varepsilon} = abs(MP_{\omega_{\varepsilon_1}} - MP_{\omega_{\varepsilon_2}}) \tag{6.8}$$

The accuracy percentages for different k value for the KNN are given in Table 6.16. When k is equal to 1, 73.8% accuracy was obtained. In Figure 7, the numerical and percentage confusion matrices are given, and the accuracy values are accentuated. However, when this value was increased, the accuracy was decreased. For example, when k was 3, the accuracy was 61.8%, and when k was 5, the accuracy was 59.6%.

Table 6.16 Accuracy of classifications using all features for different k values

k value	Accuracy (%)
1	73.8
3	61.8
5	59.6

After that, the features were used in classifications separately. As can be observed in the previous study, higher accuracy was obtained when the k value was 1. Hence, this value was also used in these classifications. When only MP of all channels for each brain wave were used as feature, the accuracy was 72.3%. However, difference of MP between the pair electrodes provided higher accuracy of 74.2%.

To see, the difference between the effects of brain waves, this time, high and low frequency waves were separated. For high frequency waves, only the MP difference of gamma, beta, and alpha waves were used as the features, and when the k parameter was 1, the obtained accuracy was 77.2% which was better than the previous one. After that, only the MP difference of theta and delta waves were selected as the features, and the obtained accuracy was 72%. So, it can be said that the high frequency brain waves that are gamma, beta, and alpha waves are more informative.

In the next step, the effects of the electrodes were examined. Hence, they were separated into two groups which are frontal–temporal (F and T) electrodes and other electrodes. The ones in the F and T lobes are AF3, AF4, F7, F8, F3, F4, FC5, FC6, T7, and T8 and the other ones are P7, P8, O1, and O2. These electrodes and their groups are given in Figure 6.25.

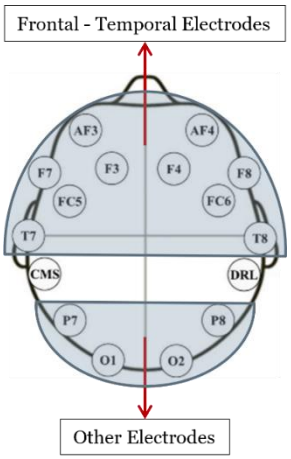

Figure 6.25 Grouped electrodes for this study

For the classification, again, the k parameter was chosen as 1. Then, the gamma, beta and alpha powers of F and T electrodes were used as the features. The obtained accuracy was 77.2%. When the other ones were chosen, the accuracy was 69.4% which was smaller.

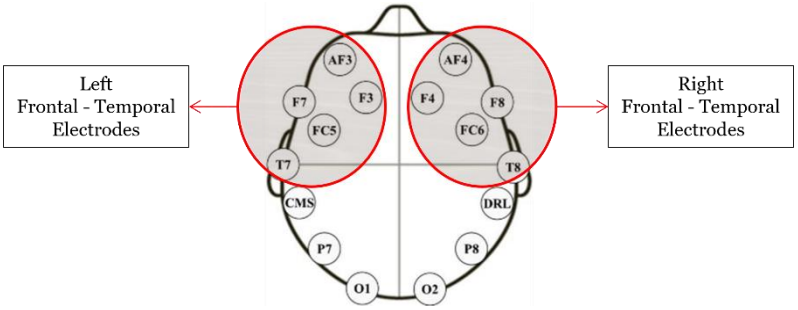

Figure 6.26 Electrodes grouped according to bilateral lobes

After that, at the final step of the classifications with KNN, the difference between left and right lobes was observed. The F and T electrodes were grouped as in Figure 6.26. Then, the powers of the right side probes (AF3, F7, F3, FC5, and T7) and the powers of the left side probes (AF4, F8, F4, FC6, and T8) were used as the features. As a result, the accuracy of the right side was 71% while the accuracy of the left side was 75.6%. So, it was observed that left side is more informative.

Table 6.17 Accuracies of all classifications with KNN

Features	**Accuracy (%)**
All features	73.8
MP of all waves and electrodes	72.3
MP differences of all waves and electrodes	74.2
MP differences of high frequency waves of all electrodes	**77.2**
MP differences of low frequency waves of all electrodes	72
MP differences of high frequency waves of electrodes in F and T lobes	**77.2**
MP differences of high frequency waves of electrodes in other lobes	69.4
MP differences of high frequency waves of electrodes in right F and T lobes	75.6
MP differences of high frequency waves of electrodes in left F and T lobes	71

In Table 6.17, all the accuracy percentages of the classifications done with KNN are given. To classify happiness from all other emotions with higher accuracy and fewer features was accomplished when the MP differences of gamma, beta, and alpha waves of electrodes in F and T lobes were used as the features. For this classification, an accuracy of 77.2% was obtained when the k value was 1.

6.2.2.2. Classification with Support Vector Machine

In the SVM classification method, firstly, the linear and Gaussian SVM were compared to classify the happiness emotion. The used features were MP difference of all waves of all electrodes, and the obtained accuracies for linear and Gaussian SVM were 68.7% and 80.1%, respectively. Since the Gaussian SVM provided higher accuracy, this method was also used in subsequent classifications.

After that, MP difference of F and T electrodes were selected as the features, and accuracy of 80.2% were observed. However, when the features were selected as the MP difference of other electrodes, the accuracy was decreased to 71.2%. Hence, in the next study, the right and left lobes compared for MP difference of F and T electrodes. However, this time, a higher accuracy than before could not be obtained, with 78.9% accuracy from the left side features and 79.2% accuracy from the right side features.

Table 6.18 Accuracies of all classifications with SVM

Features	**SVM type**	**Accuracy (%)**
All MP differences	Linear	68.7
All MP differences	Gaussian	80.1
MP differences of electrodes in F and T lobes	Gaussian	**80.2**
MP differences of electrodes in other lobes	Gaussian	71.2
MP differences of electrodes in left F and T lobes	Gaussian	78.9
MP differences of electrodes in right F and T lobes	Gaussian	79.2

In Table 6.18, all accuracy results from the classifications with SVM are given. It was observed that the highest accuracy among all KNN and SVM classifications for

happiness was obtained when the features were selected as MP differences of electrodes in F and T lobes and classified with Gaussian SVM.

6.2.3 Studies with Dataset Triggered with Questions

The emotion dataset obtained by asking questions to the participants was analyzed using the information obtained from the studies accomplished with the DEAP dataset. Firstly, the recorded dataset was preprocessed with the mentioned steps in Figure 6.23. The brain waves are then filtered from BPFs with cutoff frequencies of the respective wave. Then, for each second, the Hjorth parameters are calculated. Since the sampling frequency of the signals is 128 Hz, the feature signal is calculated with a window with a size of 128 elements and a shift of 64 elements. Afterward, a person-based emotion detection application was done in accordance with the flow diagram given in Figure 6.17. Thus, the EEG dataset analysis is accomplished by using the results obtained from the studies done with the DEAP dataset and the change in the calculated mobility feature signal with respect to time.

An example of the applications is as follows. With the EEG dataset recorded while asking questions, the changes in the mobility parameter of brain waves are obtained, as in Figure 6.27. Firstly, emotions intended to trigger are classified as 2D. Among the questions asked to this participant, thinking about a happy memory (moments highlighted in blue) triggers HAHV and examining a painting (moments highlighted in green) triggers LAHV emotions.

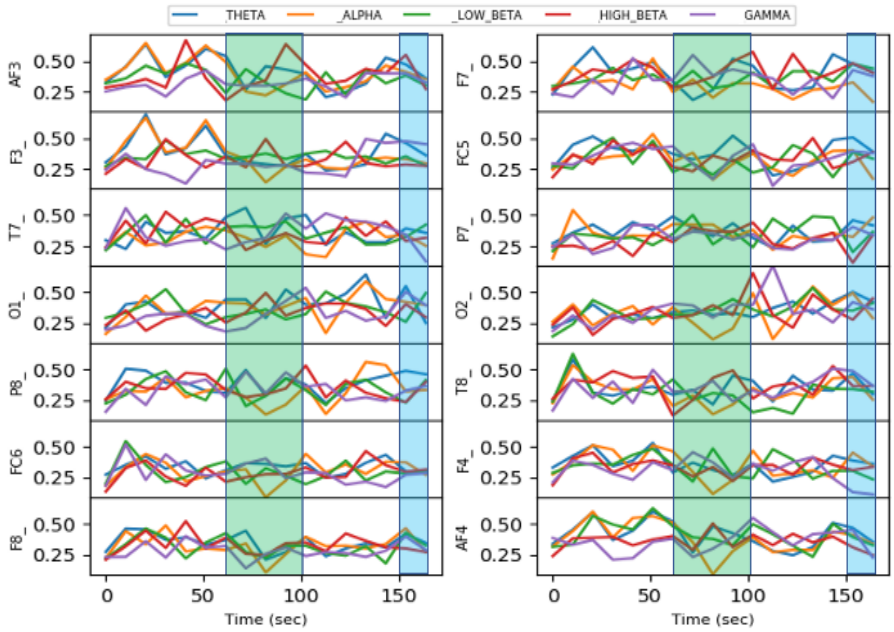

Figure 6.27 Changes in mobility of brain waves in time

Then the results in Figure 6.27 and Table 6.15 were compared. An increase in the mobility of the T7 gamma wave was observed in the moments highlighted in green. However, the Pz and PO3 channels determined for HAHV are not available in this EEG study data system. However, the O1 electrode, which is closest to those electrodes (Figure 6.1), was used in the analysis. In the moments highlighted in blue, a decrease in theta wave in O1 was observed. Thus, it has been observed that the results obtained from the DEAP dataset also agree with other studies at certain points.

Table 6.19 An example results of a person-based emotion detection using the dataset recorded with the designed system

		Theta	Alpha	Low Beta	High Beta	Gamma
Electrode with highest difference	Arousal	AF4	O2	T8	AF3	AF3
	Valence	AF4	O2	AF3	AF3	AF3
Accuracy (%)	Arousal	72.73	59.09	50	81.82	**90.91**
	Valence	58.82	35.29	76.47	88.24	**94.12**

Secondly, analyzes were done for 1D emotions. For this, the moments highlighted in blue labelled as HA for arousal and HV for valence, and the moments highlighted in green labelled as LA for arousal and HV for valence. After the features were

calculated for five separate brain waves, the electrodes with the maximum value difference for low and high emotions were determined as in Table 6.19. The results for the mobility feature of this participant gives better results than other Hjorth parameters. From the classifications done with gamma wave, the highest accuracy was obtained with 94.12% for the valence and 90.91% for the arousal. It was observed that the AF3 electrode had high informativeness for this participant.

6.2.4 Studies with Dataset of Neurological Disorder

The last of the studies carried out within the scope of the thesis is FOG detection. In this section, firstly, the interface created to analyze with EEG signals is explained. Then, Hjorth parameters, indices calculated for concentration and anxiety, and FOG determination studies were carried out.

6.2.4.1. GUI Designed for EEG Analysis and FOG Detection

A GUI is designed to facilitate EEG analysis studies on FOG. This GUI works offline with the recorded EEG and button data. The programming language of it is Python, and the operating system of the computer is Linux Ubuntu. The used libraries for the GUI and usage functions of these libraries are as follows: Tkinter GUI toolkit for its design, Matplotlib library for graphical plotting, and SciPy library for signal operations, and NumPy for mathematical operations.

In Figure 6.28, the initial screenshot of the interface that opens when the program is run is given. The EEG channels to be observed (1. Select EEG channels), the date of the measured data (2. Select date), and the patient (3. Select patient) can be selected from the submenus on the left side of the GUI. After clicking the "GET DATA" button, information about the data is given at the bottom on the left. This information is data size (number of samples of each channel), data duration (recording time), and number of FOGs observed during recording. This information is used in the graphic plotting for the analysis to be done. They will be explained in more detail later.

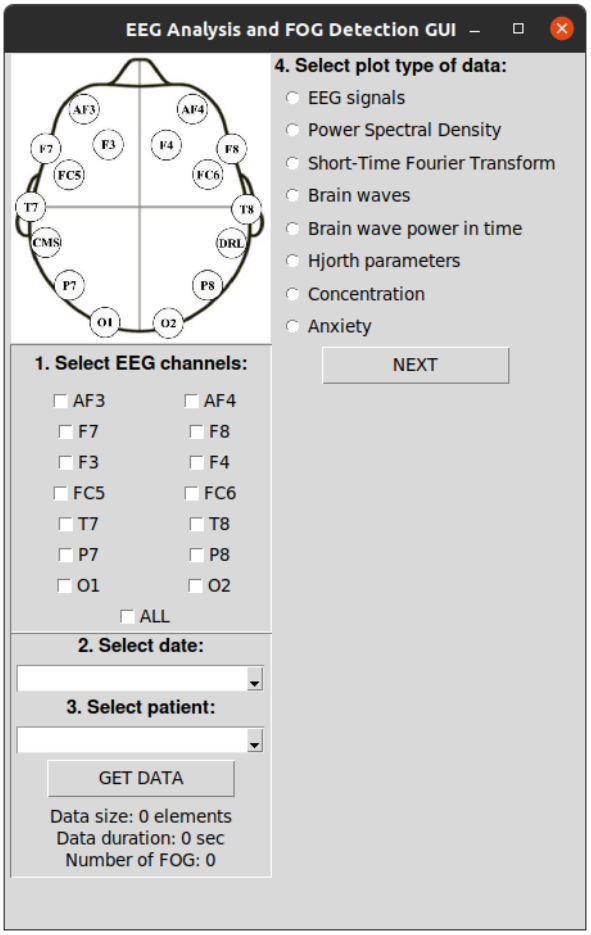

Figure 6.28 EEG Analysis and FOG Detection GUI

The second column has another menu to select the plot type used in the analysis. After choosing the desired plotting option, the " NEXT" button is clicked. Then, the specific plotting settings for the relevant selected plot type are displayed in the empty area on the right side of the GUI in Figure 6.28. A "PLOT" button is also added at the bottom of the newly displayed submenu. When this button is clicked, the plot is displayed on the right side of the GUI.

The options in this menu and their properties are given as follows:

- **EEG signals:** The chosen EEG channel signals are plotted. The signal can be raw or preprocessed signal, and normalization can be applied to the selected data. Optionally, FOG events marked during measurements by an experienced

neurologist can also be included in the plot using button data. In Figure 6.29, the submenu that opens with the selection of EEG signals is given.

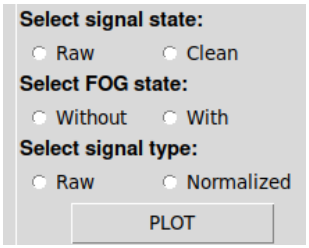

Figure 6.29 Submenu for EEG signals plotting option

- **Power Spectral Density:** With this option, power variation of the EEG signals in the frequency domain, in other words, PSD can be plotted for a determined frequency range. In Figure 6.30, the submenu that opens with the selection of PSD is given.

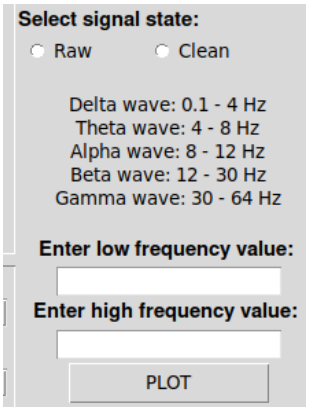

Figure 6.30 Submenu for PSD plotting option

- **Short-Time Fourier Transform:** The spectrogram of the STFT can be drawn, which allows to observe the power changes of the frequency components of the raw or preprocessed EEG signals depending on time. In the submenu that opens with this selection, there are options to choose whether the signal is plotted as raw or preprocessed.

- **Brain waves:** After this option is selected, the low and high cut-off frequencies of the band-pass filter are entered by the user to plot the desired

brain waves. The brain waves which are filtered EEG signals in the selected frequency range are plotted, and if the patient was in the FOG state during measurement, these events are highlighted. In the opened submenu, the frequency ranges of the main brain waves are additionally given.

A sample GUI screenshot for the “Brain waves” option is given in Figure 6.31. As can be seen from this screenshot, the date of data was 2019.01.30 and the participant was selected as the 3rd patient. The chosen channels are F4, FC5, T7, and T8. Then, from the submenu of the brain waves option, the frequency range of these waves was entered as 15-20 Hz.

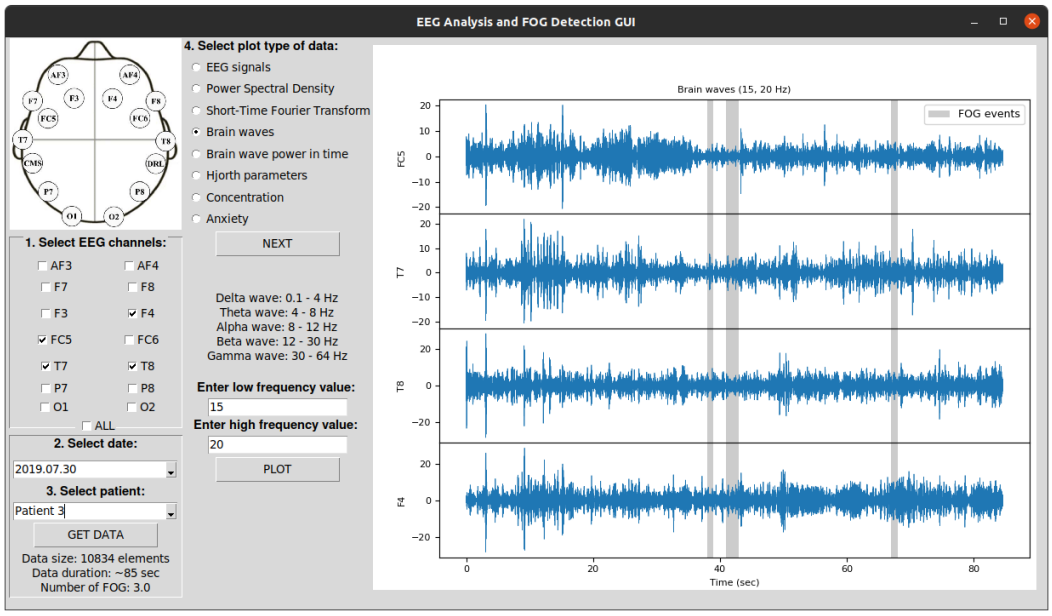

Figure 6.31 Example for EEG channel and data selection to analysis brain waves

- **Brain wave power in time:** This option helps to plot the power signals of the selected electrodes for brain waves whose frequency ranges are entered by the user. Thus, the interaction between FOG events and signals powers can be compared in the analysis. The submenu that opens with the “Brain waves” option is also opened in this selection.

- **Hjorth parameters:** The activity, mobility, or complexity feature from the Hjorth parameters is calculated according to the user's choice and the signals are plotted for each selected channel. In addition, there are two different drawing settings: time state and threshold state. In Figure 6.32, its menu is given.

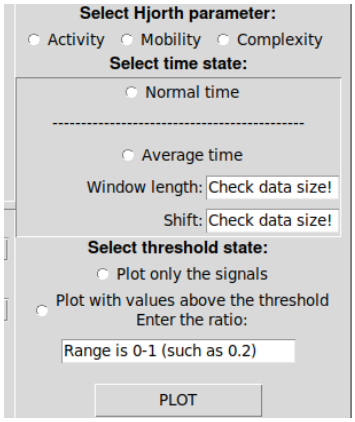

Figure 6.32 Submenu for Hjorth parameters plotting option

In the time state setting, the average signal is calculated using the window size and shift values entered by the user with the average time option, but the normal time option helps to plot the original signal. As an example, in Figure 6.33, the original signal according to the normal time and the average calculated signal according to the entered values are given.

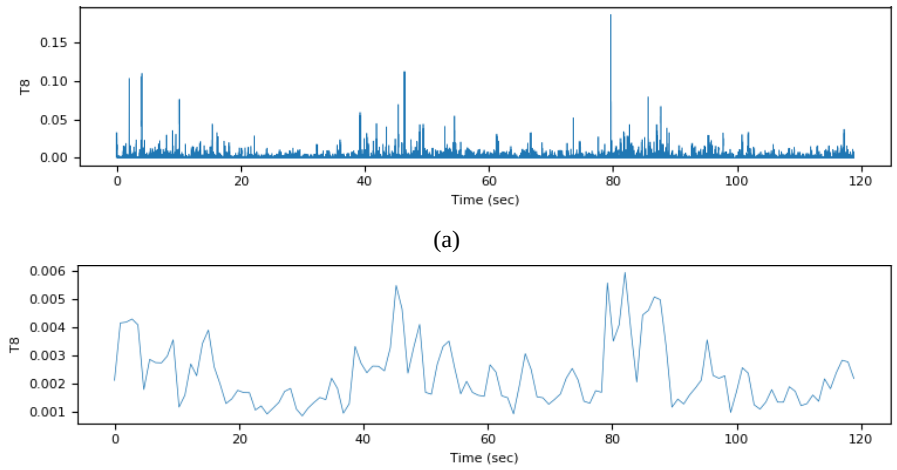

Figure 6.33 Example for time state setting, (a) Normal time option selected signal, (b) Average time option selected signal for window length is 200 and shift is 100

Additionally, the "Plot with values above the threshold" option in the threshold setting allows marking the points above the calculated value by using the threshold ratio determined by the user in the time state adjusted signal. The threshold value is calculated with the Equation (6.9). The x_{mean} value in this equation is calculated with (3.4). Also, “THR” is the threshold ratio value determined from the interface.

$$threshold\ value = x_{mean} \times THR \tag{6.9}$$

- **Concentration:** Concentration mental state indexes are calculated for each second and appended to an array to plot concentration change signals of each channel. For the calculation the Equation (3.16) is used. As with the Hjorth parameters option, there are time and threshold settings in its submenu. However, this time, for the average time option, the window length of the segment whose average value is going to be calculated and the window shifting number are entered considering the data duration information given on the first column of the GUI by the user. Since the sampling frequency of the concentration signal is 1 Hz, its length is smaller than the original EEG signal and equal to the data duration.

- **Anxiety:** Similar to the “Concentration” option, the anxiety signals are drawn, and the plot properties can be determined. The anxiety signal is calculated with the Equation (3.17) . The same submenu in Figure 6.32 is opened with this option. The adaptive thresholding method is performed for Hjorth parameters but also for concentration and anxiety options on the GUI.

For now, these properties only work with offline data. However, the GUI can be improved for use in real-time measurement analysis in future studies.

6.2.4.2. FOG Detection with Concentration Mental State Index

Within the scope of the thesis, the dataset recorded from Parkinson's patients with the data acquisition system was used in all FOG detection studies. In the first FOG detection study, the concentration index, which is found in the literature, is used. This index is calculated by Equation (3.16) for each channel. The concentration signals are generated with the "Concentration" option on the designed GUI, and the thresholding method is applied to these signals. The points above the determined threshold value are marked on the drawn signal by using the thresholding setting.

The comparison between FOG events and the ratio of the average power of the low beta brain wave to the theta wave band power is analyzed by this method. At first, concentration signals with different threshold ratio values for the “Normal time” selection were calculated from the recorded signals for all channels. From the obtained drawings, the points that exceeded the threshold value in the signal were examined 5 seconds before the FOG, during the FOG, and 5 seconds after the FOG. For these three cases, 127 FOG events were investigated. The changes in the concentration signal for each electrode were examined, and the maximum number of FOG detections done among all electrodes is given as a percentage in Table 6.20. Based on these results, it is understood that more FOG detections can be done within 5 seconds after FOG occurs.

Table 6.20 Highest detection percentages from all FOGs for different time categories in concentration analysis

Time category	Percentage of highest number of detection (%)
Pre-FOG	75.59
During	77.17
Post-FOG	82.68

In Table 6.21, FOG detection percentages are given based on the highest number of detections for all THR values in the relevant time category (i.e., pre-FOG, during and post-FOG). The highest detection percentages in the relevant time category are

highlighted in gray. In addition, the value of the electrode with the highest percentage for each THR value is also written in red.

Table 6.21 Percentage of observed increases in the concentration signal

Time category	THR	AF3	F7	F3	FC5	T7	P7	O1	O2	P8	T8	FC6	F4	F8	AF4
Pre-FOG	1.5	56	52	53	49	64	55	51	53	48	55	64	60	58	**66**
	1.6	49	42	44	41	51	50	45	47	30	44	55	**57**	54	**57**
	1.7	36	32	40	35	45	43	34	41	23	40	47	44	**48**	46
	1.8	26	25	30	32	36	**39**	26	30	19	30	35	34	35	36
During	1.5	63	66	54	65	68	68	65	68	69	70	68	63	70	**73**
	1.6	55	59	46	52	61	57	61	56	61	61	61	53	59	**62**
	1.7	49	55	40	47	51	47	55	51	55	48	**56**	48	51	55
	1.8	42	**49**	35	41	45	42	42	44	44	40	47	39	47	46
Post-FOG	1.5	60	56	47	55	59	64	48	54	60	60	**70**	62	55	69
	1.6	53	41	37	41	48	54	39	41	46	48	**60**	50	42	56
	1.7	41	38	30	35	33	47	28	37	38	35	**48**	41	36	44
	1.8	30	34	27	29	30	36	24	30	28	28	**37**	32	28	30

When all time categories in this table are examined in general, it is observed that more detection is done with the electrodes in the right lobe. AF4, F4 and F8 electrodes in the right lobe and P7 electrode in the left lobe gave positive results for the detections, in the results of 5 seconds before the FOG occurs. During FOG, AF4 and FC6 electrodes in the right lobe and F7 electrodes in the left lobe provide a high detection percentage. Finally, for the detections after the occurrence of FOG, the highest detection percentage was obtained with FC6 for all THR values.

Detections were done by changing the THR, that is, the threshold ratio value. An increase in this value means an increase in the threshold value. Therefore, as expected, the number of detections decreased as the value increased. However, even if there is no FOG with low value THR, an increase in the concentration signal occurs and these points are marked. For example, in Figure 6.34 the concentration signals of a person's P8 and F8 channels are given for different THR values. When the THR value is 1.5, there are marked moments higher than the calculated threshold value much before and after the FOG moments.

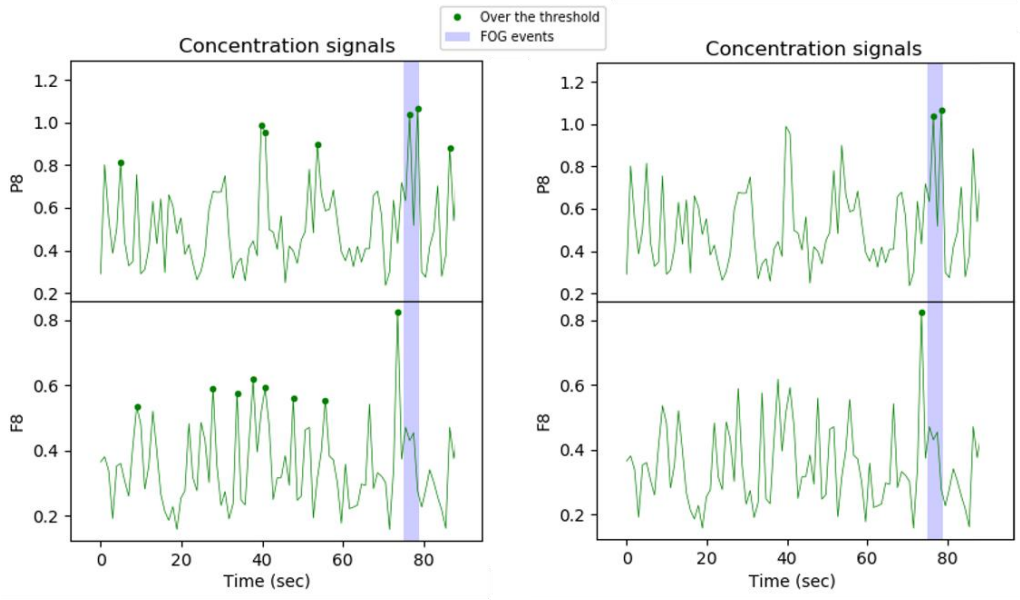

Figure 6.34 Examples for FOG detection for different THR values (a) THR = 1.5 (b) THR = 1.8

For this reason, and when the results of the detections were examined, it was observed that more logical detections were done for the value of 1.7. However, since there is still a difference between the participants, the more appropriate THR value should be adjusted on an individual basis.

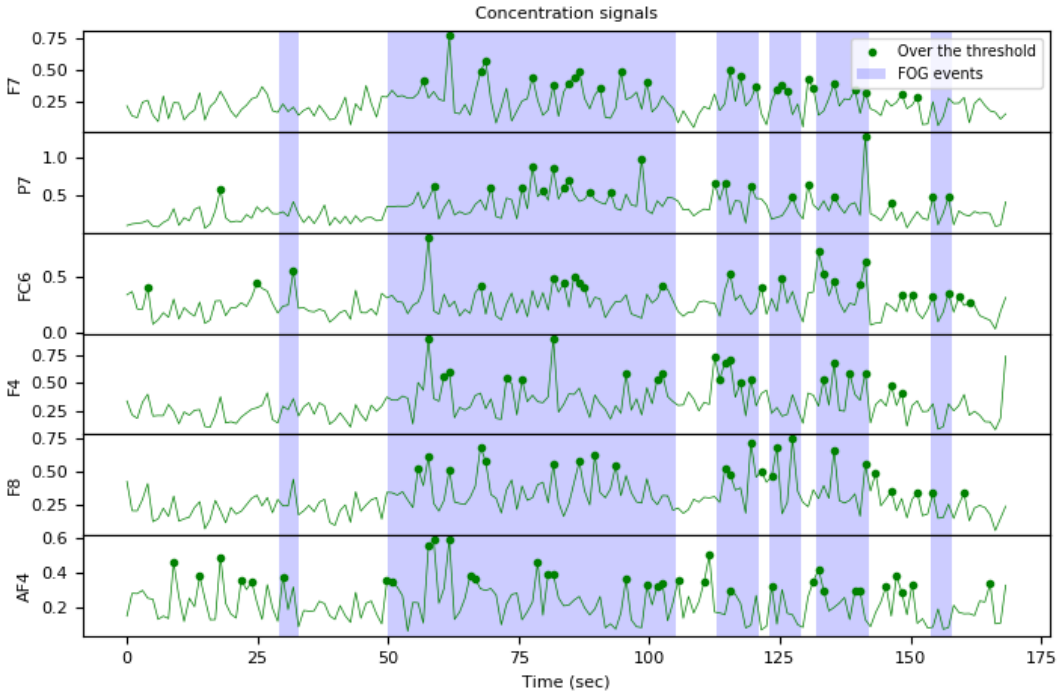

Figure 6.35 An example for detection with normal time

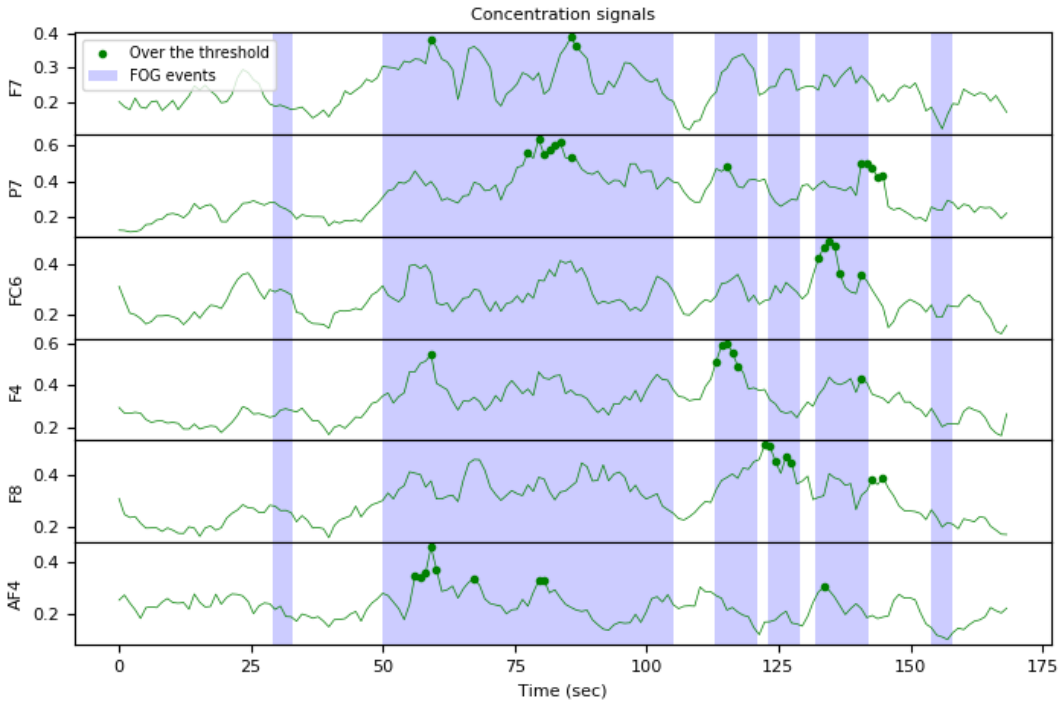

Figure 6.36 The same example but this time for average time

Studies were carried out using the “Average time” selection on the GUI. An example of this is given in Figure 6.35 and Figure 6.36. In Figure 6.35, an example detection done with normal time is given while the average time is applied to this in Figure 6.36. The electrodes (i.e., F7, P7, FC6, F4, F8 and AF4 electrodes) observed to give a high detection percentage in Table 6.21 are examined here. For the normal one, the THR value is set to 1.5 from the equal state settings. For the average one, the window size value is set to 5 and the shift value is set to 1 from the time state settings, and the THR value is set to 1.5. Moments highlighted on the graphs show when FOG events occur, and the dots on the signals indicate the moments that exceed the calculated threshold value. In this example, it can be observed that the threshold value is generally exceeded during and after the FOG.

This "Average time" selection has been included in the studies in order to prevent spikes in signals over time. Thus, it is aimed to avoid signal increases that occur except for the FOG.

6.2.4.3. FOG Detection with Anxiety Emotion Index

In the next study, analysis was done according to changes in anxiety levels. As mentioned before, the ratio in Equation (3.17) was created within the scope of this thesis by using the information obtained in the literature. This equation was formed as the ratio of the average power of the high beta brain wave to the average power of the theta waveband, based on the situations determined to occur in the brain waves in the case of anxiety.

As in the analysis with concentration, only the increases that occurred about 5 seconds before, during and after 5 seconds of occurrence of FOG were considered. As a consequence, the percentage of the highest detection number for 127 FOGs obtained in each time category is given in Table 6.22. As obtained from the results of the studies with the concentration signals, the highest detection percentage was obtained for after the FOG formation.

Table 6.22 Highest detection percentages from all FOGs for different time categories in anxiety analysis

Time category	Percentage of highest number of detection (%)
Pre-FOG	75.59
During	76.38
Post-FOG	81.1

Within the framework of these situations, the percentages of the increasing detections for all time categories are given in Table 6.23. As in the concentration, the percentages are calculated according to the highest detection number of the relevant category.

Table 6.23 Percentage of observed increases in the anxiety signal

Time category	THR	AF3	F7	F3	FC5	T7	P7	O1	O2	P8	T8	FC6	F4	F8	AF4
Pre-FOG	1.5	63	60	55	61	60	53	51	55	60	57	57	**74**	64	65
	1.6	50	49	49	50	54	38	41	48	47	46	52	**61**	49	54
	1.7	36	31	42	43	48	35	30	40	33	36	42	**51**	40	43
	1.8	28	24	33	36	43	29	26	30	26	32	35	**47**	33	34
During	1.5	68	**77**	65	69	71	70	70	70	**77**	66	70	74	73	72
	1.6	61	**68**	57	56	65	58	64	66	65	60	66	65	64	65
	1.7	58	**61**	49	48	58	52	54	54	53	52	57	59	54	57
	1.8	49	**55**	47	42	53	47	47	47	41	43	**55**	53	45	51
Post-FOG	1.5	61	59	50	60	55	59	50	62	62	59	63	**70**	61	68
	1.6	50	46	45	53	48	45	46	52	55	52	55	57	51	**60**
	1.7	39	36	35	48	41	40	39	42	44	39	41	47	43	**53**
	1.8	31	34	27	35	37	31	34	33	38	30	39	41	34	**43**

Unlike the results obtained from the concentration signals, the increase in the anxiety signals, especially during the FOG, mostly occurred in the left lobe, and the highest percentage for all THR values belonged to the F7 electrode. The F4 electrode in the right lobe before FOG occurs and the AF4 electrode after FOG occurs had the highest detection number for almost all THR values. In both these cases, it can be seen that the right lobes have the highest percentage, as in the concentration.

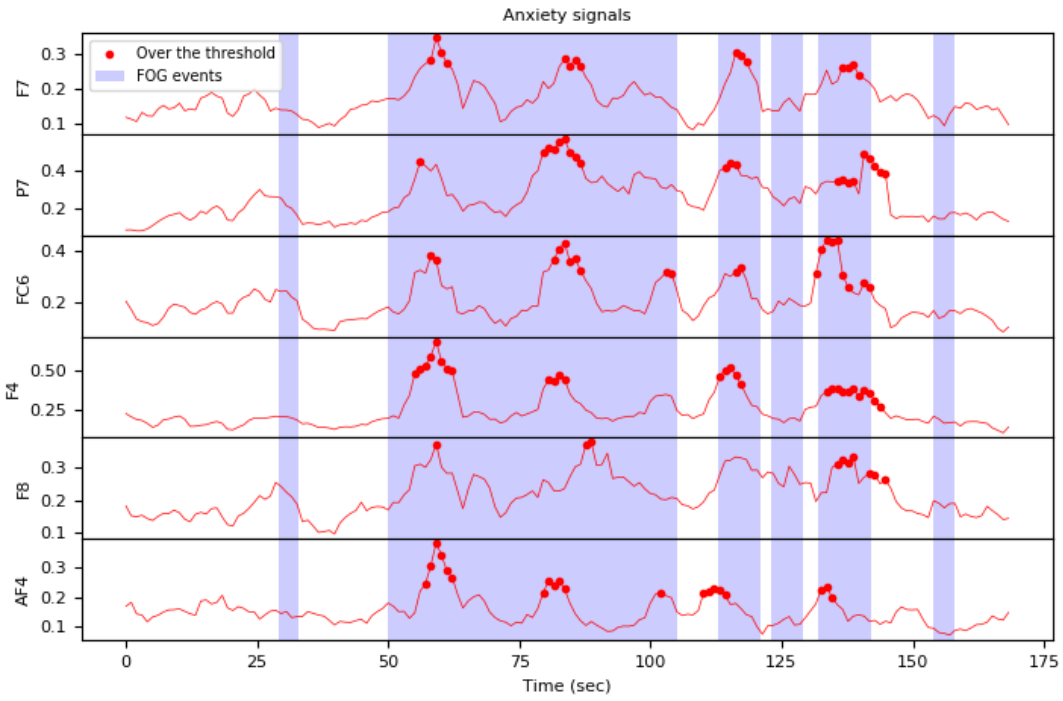

Figure 6.37 The same example for average time with anxiety signals

In the detections done with anxiety signals, the average time application was also carried out. In Figure 6.37, anxiety signals were calculated for the data of the sample in Figure 6.36. To compare the concentration and anxiety results, the examined electrodes were not changed to F7, P8, FC6, F4, and AF4 in Table 6.23, which was observed to give a high detection percentage for anxiety. Here, too, the window size is 5, the shift is 1, and the THR value is 1.5.

6.2.4.4. FOG Detection with Hjorth Parameters

Hjorth parameters were used in the last study with the dataset recorded from the patients. From the preprocessed signals, the gamma waves were extracted. The similar steps as in previous detection studies with concentration and anxiety signals were then applied. First, the signal of the activity feature is calculated with a window with a size of 128 elements and a shift of 64 elements. Then, thresholding method was applied for THR values between 0.7 and 1.1. The controlled time categories were determined as 5 seconds before the FOG, during the FOG, and 5 seconds after the FOG, as in previous studies. In Table 6.24, the accuracy percentages are given. Among all detections done with activity, the highest percentage of accuracy was 74%, obtained from T8 during FOG and with the THR value of 0.7. High accuracy was obtained with the data from the T8 electrode for the increases in the activity value before and during the FOG. However, the AF4 electrode gave better results for the increments after FOG occurs. In addition to these, it has been observed that choosing the THR value as 0.7 provides both high and reasonable results.

Table 6.24 Percentage of observed increases in the activity signal

Time category	THR	AF3	F7	F3	FC5	T7	P7	O1	O2	P8	T8	FC6	F4	F8	AF4
Pre-FOG	0.7	51	54	38	44	46	34	39	47	62	**69**	62	46	61	61
	0.8	45	43	29	33	39	27	35	38	48	**56**	47	41	52	51
	0.9	35	34	24	28	34	18	31	31	39	**48**	42	37	42	43
	1	30	31	20	25	31	14	26	26	29	**39**	31	31	33	38
	1.1	25	29	20	25	27	13	19	22	20	32	27	29	30	**35**
During	0.7	53	59	47	57	51	34	44	50	59	**74**	67	47	69	73
	0.8	50	53	40	48	45	25	36	45	50	**65**	55	45	61	**65**
	0.9	45	45	33	44	42	24	34	40	45	57	51	37	46	**60**
	1	40	45	32	41	35	22	29	34	38	**53**	44	34	38	51
	1.1	36	39	26	37	32	20	25	25	34	**48**	35	32	33	46
Post-FOG	0.7	54	56	37	54	54	32	38	48	63	62	58	40	57	**68**
	0.8	47	47	30	42	41	26	36	42	51	51	44	36	47	**62**
	0.9	40	40	28	34	34	20	29	31	42	41	37	30	39	**55**
	1	36	37	25	32	27	18	25	28	32	38	30	27	35	**46**
	1.1	30	31	22	27	22	15	16	26	24	36	28	25	31	**41**

After that, detections were done with the mobility parameter. Accuracies are given in Table 6.25. Here, only results are given for the THR value equal to 1, because for other values the results are not better than this. In both detections, 95% accuracy was obtained with the O1 and F4 electrodes for the detections done before the FOG and with the FC5, FC6, and AF4 electrodes for the detections done during the FOG. The highest accuracy for this feature was obtained from FC5 and T7 electrodes for the detections done after FOG occurs, and it was 96%.

Table 6.25 Percentage of observed increases in the mobility signal

Time category	THR	AF3	F7	F3	FC5	T7	P7	O1	O2	P8	T8	FC6	F4	F8	AF4
Pre-FOG	1	88	94	92	91	91	92	**95**	94	92	92	87	**95**	91	94
During	1	93	92	93	**95**	90	93	94	94	90	91	**95**	90	91	**95**
Post-FOG	1	93	92	90	**96**	94	**96**	92	92	92	89	91	92	87	95

For the complexity parameter, the detections were done when the THR is equal to 1. As given in Table 6.26, the highest percentage of accuracy obtained for all time categories is equal and 92%. Electrodes O2 for pre-FOG, F7 and O1 during FOG, and F3 and FC5 for post-FOG provided the highest accuracy for the respective time category.

Table 6.26 Percentage of observed increases in the complexity signal

Time category	THR	AF3	F7	F3	FC5	T7	P7	O1	O2	P8	T8	FC6	F4	F8	AF4
Pre-FOG	1	86	86	91	91	89	87	88	**92**	87	89	86	90	85	84
During	1	91	**92**	88	88	90	86	**92**	89	86	85	88	88	89	87
Post-FOG	1	90	86	**92**	**92**	86	87	83	90	91	90	88	88	89	85

As a result of all the work done with the Hjorth parameters, the best results for different time categories have always been obtained with the mobility feature. However, the informative electrodes differ for pre-FOG, during and post-FOG detections.

CHAPTER SEVEN
CONCLUSION AND DISCUSSION

This thesis focuses on EEG signals produced because of electrical activities in the brain and can be measured practically without any surgery. In the literature, it has been observed that there are studies with features extracted from EEG signals, and they are related to emotion based on arousal and valence, and detection of disorders. The features that are widely used in the literature and also used in this thesis are: mean value, standard deviation, power, and Hjorth parameters. EEG signals are also used in studies for the. In these studies, the previously mentioned features are used.

In this thesis, several different studies about emotions and disorders were carried out in parallel. These studies and the resulting inferences are given below.

- **Emotion studies with the dataset in the literature:** To understand the effects of emotions on the brain, analyzes were done with the DEAP dataset from the literature. EEG signals were recorded while the participants were watching music videos, and then a SAM was conducted to understand the triggered emotion. In the scope of the thesis, after the reliable participants were chosen and the classification of the video emotion was accomplished, firstly, the changes in time of the amplitudes of the EEG signals were examined. It has been observed that different changes can occur over time for different emotions. Then, in order not to depend on time, the average of the EEG signals was calculated, and the amplitudes were examined. From here, the electrodes with the highest amplitude for 2D emotions were determined as in Table 6.5.

- **Developing an algorithm for the selection of personalized informative electrodes on emotion detection:** Firstly, to understand the effect of different features and brain waves, the comparison studies were done with the DEAP dataset. From the comparison results of the mean value feature given in Table 6.6, the electrodes with the highest value for each emotion were determined.

With the standard deviation value, the electrodes not very reliable were identified from Figure 6.14. Average Hjorth parameter values were examined for each arousal and valence emotion as in Figure 6.15 and Figure 6.16. Then, 1D emotion classification was done by using the threshold value method with the features calculated as the majority and personally. The results of these are given in Table 6.8 and Table 6.9, respectively. From these results, it is observed that the mobility feature provides a higher percentage of accuracy. Based on this, the comparisons of theta, alpha, low beta, high beta, and gamma waves were also done with mobility. Better results given in Table 6.12 were obtained with person-based features. Consequently, the gamma wave for arousal and the high beta wave for valence emotion were determined as more informative. From all these results, it was observed that the highest accuracies were obtained with person-based features, so an algorithm in Figure 6.20 was developed.

- **Designing and implementing a data acquisition system:** A data recording system has been established for studies on emotion and disease detection. The block diagram of this system is given in Figure 4.1. With this system, which includes different sensors, acceleration of motion and marking data can be recorded as well as EEG signals. Afterwards, datasets were recorded for three different methods with this system. In addition to the recordings done for mental state and emotions during the examination of the images and answering the questions, recordings were taken from the patients while performing a specific task for PD, a neurological disease. Detailed explanations about the system and its operation are given in chapter four, and explanations about recording implementations are given in chapter five.

- **Mental state and emotion studies with the recorded datasets:** For the analysis of emotions triggered by images and questions, the recorded datasets were analyzed with different methods. For emotions triggered by images, the indexes of concentration mental state and anxiety emotion, which are also given in the literature, were calculated, and then, interpreted according to the

change in the signals over time (Figure 6.24). Then, the feeling of happiness was classified among all other emotions by using different features from signal powers in two basic machine learning methods such as KNN and SVM. The minimum number of features and the high percentage of accuracy were obtained using the KNN method (Table 6.17). The higher percentage of accuracy as a result of both methods was obtained when the features are MP differences of electrodes in frontal and temporal lobes and classified with Gaussian SVM (Table 6.18). For emotions triggered by questions, the developed algorithm for the selection of personalized informative electrodes and some results of the studies with the DEAP dataset were tested.

- **Disorder detection by the help of emotion and mental states:** First of all, a multi-functional interface has been developed to facilitate analysis. With this, besides examining the EEG signals with different methods, analyzes can be done by calculating different features. For the diseases, first, pre-FOG, during, and post-FOG detection studies were carried out with the adaptive thresholding method with the increase in concentration and anxiety levels of the data obtained from PD patients. The highest detection rate from the concentration was obtained by the thresholding method with a THR value of 1.5 for the signals of the AF4 channel during FOG (Table 6.21). By using anxiety signals, most of during FOG was also detected, but this time the data obtained from channels F7 and P8 gave good results (Table 6.23). Finally, in studies with Hjorth parameters, even higher percentages for pre-FOG, during, and post-FOG were obtained with the mobility feature (Table 6.25).

As can be seen from these results, it is not necessary to carry out studies using the data provided by all the electrodes in an EEG device. These electrodes can be selected on an individual basis for the studies to be carried out and can be reduced to the use of very few electrodes. Personalized informative electrode selection algorithm, which is one of the studies in this thesis, has also been developed for this purpose. Although the algorithm was used only for emotion detection in this study, it can be used for other studies in the future. Thus, more comfortable use of EEG

devices for long-term measurements will be possible by reducing the number of electrodes. In addition to all these, with devices to be designed with fewer electrodes, the cost of the device will be lower and the number of channels of the data to be examined will be reduced only as channels determined to be more informative, data pollution will be eliminated, and signal processing processes will be accelerated.

With the help of the information and experience about EEG signals and some diseases in this study, personal diagnostic and stimulation devices can be developed. Elder persons, who suffer those diseases related to brain disorders or malfunctioning, may live in more comfort by detecting and preventing some effects of diseases before the attack occurs. At the same time, lots of applications can be developed related to brain activity and emotion extraction for any area of medical and consumer product marketing.

An issue that should be mentioned based on the results is the levels of obtained accuracy percentages. Further studies can be organized to investigate more about the reasons for low accuracy results. There are several possibilities for this. First, differences were observed in the ratings and EEG signal responses in individuals from the studies conducted with the DEAP dataset. However, studies to prevent this situation were carried out as mentioned before, and improvements were observed in the results. The reason for the low percentage of studies with the recorded dataset may be the small size of the data. Finally, there may have been errors in marking the FOG events in disease detection studies, either due to the experienced user's incorrect use of the button or due to delays in the system.

REFERENCES

Acharya, J. N., & Acharya, V. J. (2019). Overview of EEG montages and principles of localization. *Journal of Clinical Neurophysiology*, 36(5), 325-329. http://dx.doi.org/10.1097/WNP.0000000000000538

Acharya, J. N., Hani, A. J., Cheek, J., Thirumala, P., & Tsuchida, T. N. (2016). American clinical neurophysiology society guideline 2: guidelines for standard electrode position nomenclature. *The Neurodiagnostic Journal*, *56*(4), 245-252. https://doi.org/10.1080/21646821.2016.1245558

Adolphs, R. (2002). Recognizing emotion from facial expressions: psychological and neurological mechanisms. *Behavioral and cognitive neuroscience reviews*, *1*(1), 21-62. https://doi.org/10.1177/1534582302001001003

Al-Qammaz, A. Y., Yusof, Y., & Ahamd, F. K. (2017, July). An enhanced discrete wavelet packet transform for feature extraction in electroencephalogram signals. In *Proceedings of the International Conference on Imaging, Signal Processing and Communication* (pp. 88-93). https://doi.org/10.1145/3132300.3132303

Alexander, C. K., & Sadiku, M. N. O. (2009). *Fundamentals of electric circuits* (4th ed.). McGraw-Hill Higher Education, Boston.

Anderer, P., Roberts, S., Schlögl, A., Gruber, G., Klösch, G., Herrmann, W., Rappelsberger, P., Filz, O., Barbanoji, M. J., Dorffner, G., & Saletu, B. (1999). Artifact processing in computerized analysis of sleep EEG–a review. *Neuropsychobiology*, *40*(3), 150-157. https://doi.org/10.1159/000026613

Apaydın, H., Özekmekci, S., Oğuz, S., & Zileli, İ. (2013). *Parkinson hastalığı: hasta ve yakınları için el Kitabı* (5th ed.). Parkinson Hastalığı Derneği.

Bachlin, M., Plotnik, M., Roggen, D., Maidan, I., Hausdorff, J. M., Giladi, N., & Troster, G. (2009). Wearable assistant for Parkinson's disease patients with the freezing of gait symptom. *IEEE Transactions on Information Technology in Biomedicine*, *14*(2), 436-446.

Bal, R. (2021). Uyarılabilir Hücre: Dinlenim Zar Potansiyeli ve Aksiyon Potansiyeli. In E. Ağar (Eds.), *İnsan fizyolojisi* (1st ed., pp. 71-95). İstanbul Medikal Sağlık ve Yayıncılık.

Bansal, D., & Mahajan, R. (2019). EEG-based brain-computer interfacing (BCI). *EEG-based brain-computer interfaces. Elsevier, Amsterdam*, 21-71. https://doi.org/10.1016/B978-0-12-814687-3.00002-8

Basu, S., Bag, A., Aftabuddin, M., Mahadevappa, M., Mukherjee, J., & Guha, R. (2016, December). Effects of emotion on physiological signals. In *2016 IEEE Annual India Conference (INDICON)* (pp. 1-6). IEEE. https://doi.org/10.1109/INDICON.2016.7839091

Bazgir, O., Mohammadi, Z., & Habibi, S. A. H. (2018, November). Emotion recognition with machine learning using EEG signals. In *2018 25th national and 3rd international iranian conference on biomedical engineering (ICBME)* (pp. 1-5). IEEE. https://doi.org/10.1109/ICBME.2018.8703559

Bear, M. F., Connors, B. W., & Paradiso, M. A. (2016). *Neuroscience: Exploring the Brain* (4th ed.). Wolters Kluwer.

Bek, S. & Genç, B. O. (2021). Yeni Nöbet Sınıflaması. In İ. Öztura, G. Kutlu, İ. Tezer, K. Ağan, & Ö. Çokar (Eds.), *Epilepsi Tanı ve Tedavileri* (1st ed., pp. 4-11). İstanbul Galenos Yayınevi.

Bhagawati, A. J., & Chutia, R. (2016). Design of single channel portable eeg signal acquisition system for brain computer interface application. *International Journal*

of Biomedical Engineering and Science (IJBES 2016), *3*(1), 37-44. https://doi.org/10.5121/ijbes.2016.3103

Bitar, H. & Tepe, C. (2021). Design and Implementation of Prototype for Portable and Wireless EEG Device. Avrupa Bilim ve Teknoloji Dergisi, Ejosat Special Issue 2021 (ISMSIT), (29), 225-230. https://doi.org/10.31590/ejosat.1016694

Bloem, B. R., Hausdorff, J. M., Visser, J. E., & Giladi, N. (2004). Falls and freezing of gait in Parkinson's disease: a review of two interconnected, episodic phenomena. *Movement disorders: official journal of the Movement Disorder Society*, *19*(8), 871-884. https://doi.org/10.1002/mds.20115

Bradley, M. M., & Lang, P. J. (1994). Measuring emotion: the self-assessment manikin and the semantic differential. *Journal of behavior therapy and experimental psychiatry*, *25*(1), 49-59. https://doi.org/10.1016/0005-7916(94)90063-9

Bridi, J. C., & Hirth, F. (2018). Mechanisms of α-synuclein induced synaptopathy in Parkinson's disease. *Frontiers in neuroscience*, *12*, 80. https://doi.org/10.3389/fnins.2018.00080

Britton, J. W., Frey, L. C., Hopp, J. L., Korb, P., Koubeissi, M. Z., Lievens, W. E., Pestana-Knight, E. M., & St Louis, E. K. St. (2016). *Electroencephalography (EEG): an introductory text and atlas of normal and abnormal findings in adults, children, and infants*. American Epilepsy Society.

Byun, S. W., Lee, S. P., & Han, H. S. (2017, August). Feature selection and comparison for the emotion recognition according to music listening. In *2017 international conference on robotics and automation sciences (ICRAS)* (pp. 172-176). IEEE. https://doi.org/10.1109/ICRAS.2017.8071939

Chaudhary, U., Birbaumer, N., & Curado, M. R. (2015). Brain-machine interface (BMI) in paralysis. *Annals of physical and rehabilitation medicine*, *58*(1), 9-13. https://doi.org/10.1016/j.rehab.2014.11.002

Chaudhary, U., Birbaumer, N., & Ramos-Murguialday, A. (2016). Brain–computer interfaces for communication and rehabilitation. *Nature Reviews Neurology*, *12*(9), 513-525. https://doi.org/10.1038/nrneurol.2016.113

Choi, T. J., Kim, J. O., Jin, S. M., & Yoon, G. (2014). Determination of the concentrated state using multiple EEG channels. *International Journal of Computer, Electrical, Automation, Control and Information Engineering*, *8*(8), 1373-1376.

Cimtay, Y., & Ekmekcioglu, E. (2020). Investigating the use of pretrained convolutional neural network on cross-subject and cross-dataset EEG emotion recognition. *Sensors*, *20*(7), 2034. https://doi.org/10.3390/s20072034

Clark, I., Biscay, R., Echeverría, M., & Virués, T. (1995). Multiresolution decomposition of non-stationary EEG signals: a preliminary study. *Computers in biology and medicine*, *25*(4), 373-382. https://doi.org/10.1016/0010-4825(95)00014-U

Coşgun, E., Çelebi, A., & Güllü, M. K. (2021). A channel selection method for epilepsy seizure prediction. In *2021 International Conference on INnovations in Intelligent SysTems and Applications (INISTA)*, 1-5. https://doi.org/10.1109/INISTA52262.2021.9548583

Coyle, D., Garcia, J., Satti, A. R., & McGinnity, T. M. (2011, April). EEG-based continuous control of a game using a 3 channel motor imagery BCI: BCI game. In *2011 IEEE Symposium on Computational Intelligence, Cognitive Algorithms, Mind, and Brain (CCMB)* (pp. 1-7). IEEE. https://doi.org/10.1109/CCMB.2011.5952128

Deak, A. (2011). Brain and emotion: Cognitive neuroscience of emotions. *Review of psychology*, *18*(2), 71-80. https://hrcak.srce.hr/81460

Demiralp, T. (2021). Sinir Sisteminin Genel Organizasyonu. In E. Ağar (Eds.), *İnsan fizyolojisi* (1st ed., pp. 523-562). İstanbul Medikal Sağlık ve Yayıncılık.

Duan, R. N., Zhu, J. Y., & Lu, B. L. (2013, November). Differential entropy feature for EEG-based emotion classification. In *2013 6th International IEEE/EMBS Conference on Neural Engineering (NER)* (pp. 81-84). IEEE. https://doi.org/10.1109/NER.2013.6695876

Emotiv. (2021, May 21). *The introductory guide to EEG (Electroencephalography)*. https://www.emotiv.com/eeg-guide/

Emotiv. (2022, April 7). *EPOC+ User Manual: Technical Specifications*. https://emotiv.gitbook.io/epoc-user-manual/introduction-1/technical_specifications.

Gérard, M., Bayot, M., Derambure, P., Dujardin, K., Defebvre, L., Betrouni, N., & Delval, A. (2022). EEG-based functional connectivity and executive control in patients with Parkinson's disease and freezing of gait. *Clinical Neurophysiology*, *137*, 207-215. https://doi.org/10.1016/j.clinph.2022.01.128

Ghadiri, Z., Nourafza, N., & Rasoolian, A. (2019). Study of Interactive Systems Based on Brain and Computer Interfaces. *Electronic Business*, *18*(8). http://doi.org/10.31224/osf.io/qg8er

Gorgoni, M., Ferlazzo, F., Ferrara, M., Moroni, F., D'Atri, A., Fanelli, S., Torriglia, I. G., Lauri, G., Marzano, C., Rossini, P. M., & De Gennaro, L. (2014). Topographic electroencephalogram changes associated with psychomotor

vigilance task performance after sleep deprivation. *Sleep medicine, 15*(9), 1132-1139. https://doi.org/10.1016/j.sleep.2014.04.022

Guyton, A. C., & Hall, J. E. (2006). *Textbook of medical physiology* (11th ed.). Elsevier Saunders, Amsterdam.

Hagen, E., Næss, S., Ness, T. V., & Einevoll, G. T. (2018). Multimodal modeling of neural network activity: Computing LFP, ECoG, EEG, and MEG signals with LFPy 2.0. *Frontiers in neuroinformatics*, *12*, 92. https://doi.org/10.3389/fninf.2018.00092

Hamann, S. (2012). Mapping discrete and dimensional emotions onto the brain: controversies and consensus. *Trends in cognitive sciences, 16*(9), 458-466. https://doi.org/10.1016/j.tics.2012.07.006

Handojoseno, A. A., Shine, J. M., Nguyen, T. N., Tran, Y., Lewis, S. J., & Nguyen, H. T. (2012, August). The detection of Freezing of Gait in Parkinson's disease patients using EEG signals based on Wavelet decomposition. In *2012 Annual International Conference of the IEEE Engineering in Medicine and Biology Society* (pp. 69-72). IEEE. https://doi.org/10.1109/EMBC.2012.6345873

Handojoseno, A. A., Shine, J. M., Gilat, M., Nguyen, T. N., Tran, Y., Lewis, S. J., & Nguyen, H. T. (2014, August). Prediction of freezing of gait using analysis of brain effective connectivity. In *2014 36th Annual International Conference of the IEEE Engineering in Medicine and Biology Society* (pp. 4119-4122). IEEE. https://doi.org/10.1109/EMBC.2014.6944530

Handojoseno, A. A., Naik, G. R., Gilat, M., Shine, J. M., Nguyen, T. N., Ly, Q. T., Lewis, S. J. G., & Nguyen, H. T. (2018). Prediction of freezing of gait in patients with Parkinson’s disease using EEG signals. https://doi.org/10.3233/978-1-61499-845-7-124

Heckbert, P. (1995). Fourier transforms and the fast Fourier transform (FFT) algorithm. *Computer Graphics*, *2*, 15-463.

Herrington, J. D., Mohanty, A., Koven, N. S., Fisher, J. E., Stewart, J. L., Banich, M. T., Webb, A. G., Miller, G. A., & Heller, W. (2005). Emotion-modulated performance and activity in left dorsolateral prefrontal cortex. *Emotion*, *5*(2), 200-207. https://psycnet.apa.org/doi/10.1037/1528-3542.5.2.200

Higuchi, T. (1988). Approach to an irregular time series on the basis of the fractal theory. *Physica D: Nonlinear Phenomena*, *31*(2), 277-283. https://doi.org/10.1016/0167-2789(88)90081-4

Hjorth, B. (1970). EEG analysis based on time domain properties. *Electroencephalography and clinical neurophysiology*, *29*(3), 306-310. https://doi.org/10.1016/0013-4694(70)90143-4

Islam, M. K., Rastegarnia, A., & Yang, Z. (2016). Methods for artifact detection and removal from scalp EEG: A review. *Neurophysiologie Clinique/Clinical Neurophysiology*, *46*(4-5), 287-305.

Jatupaiboon, N., Pan-ngum, S., & Israsena, P. (2013). Real-time EEG-based happiness detection system. *The Scientific World Journal*, *2013*. https://doi.org/10.1155/2013/618649

Jatupaiboon, N., Pan-ngum, S., & Israsena, P. (2013, May). Emotion classification using minimal EEG channels and frequency bands. In *The 2013 10th international joint conference on Computer Science and Software Engineering (JCSSE)* (pp. 21-24). IEEE. https://doi.org/10.1109/JCSSE.2013.6567313

Jiang, X., Bian, G. B., & Tian, Z. (2019). Removal of artifacts from EEG signals: a review. *Sensors*, *19*(5), 987. https://doi.org/10.3390/s19050987

K and H products. (n.d.). Experiment 4: Electroencephalogram (EEG) Measurement. In *KL-730 Biomedical Measurement Training System Experiment Manual*.

Katsigiannis, S., & Ramzan, N. (2017). DREAMER: A database for emotion recognition through EEG and ECG signals from wireless low-cost off-the-shelf devices. *IEEE journal of biomedical and health informatics*, *22*(1), 98-107. https://doi.org/10.1109/JBHI.2017.2688239

Kerous, B., Skola, F., & Liarokapis, F. (2018). EEG-based BCI and video games: a progress report. *Virtual Reality*, *22*(2), 119-135. https://doi.org/10.1007/s10055-017-0328-x

Kıymık, M. K., Güler, İ., Dizibüyük, A., & Akın, M. (2005). Comparison of STFT and wavelet transform methods in determining epileptic seizure activity in EEG signals for real-time application. *Computers in biology and medicine*, *35*(7), 603-616. https://doi.org/10.1016/j.compbiomed.2004.05.001

Kim, S. P. (2018). Preprocessing of eeg. In *Computational EEG Analysis* (pp. 15-33). Springer, Singapore. https://doi.org/10.1007/978-981-13-0908-3_2

Kim, Y. J., Park, S. W., Yeom, H. G., Bang, M. S., Kim, J. S., Chung, C. K., & Kim, S. (2015). A study on a robot arm driven by three-dimensional trajectories predicted from non-invasive neural signals. *Biomedical engineering online*, *14*(1), 1-19. https://doi.org/10.1186/s12938-015-0075-8

Kimmatkar, N. V., & Babu, B. V. (2021). Novel approach for emotion detection and stabilizing mental state by using machine learning techniques. *Computers*, *10*(3), 37. https://doi.org/10.3390/computers10030037

Kuran, E. C., Er, M. B., & Kuran, U. (2021). Epileptic Seizure Detection via EEG Signals with Feature Extraction Technique Based on Cubic Spline Interpolation.

In *2021 29th Signal Processing and Communications Applications Conference (SIU)*, 1-4.

Koelstra, S., Muhl, C., Soleymani, M., Lee, J. S., Yazdani, A., Ebrahimi, T., et al. (2011). DEAP: A database for emotion analysis; using physiological signals. *IEEE transactions on affective computing, 3*(1), 18-31. https://doi.org/10.1109/T-AFFC.2011.15

Krishnan, S. (2021). *Biomedical signal analysis for connected healthcare*. Academic Press.

Lang, P. J., Bradley, M. M., & Cuthbert, B. N. (2005). *International affective picture system (IAPS): Affective ratings of pictures and instruction manual* (pp. A-8). Gainesville, FL: NIMH, Center for the Study of Emotion & Attention.

Li, Z., Xu, J., & Zhu, T. (2015). Prediction of brain states of concentration and relaxation in real time with portable electroencephalographs. *arXiv preprint arXiv:1509.07642*. https://doi.org/10.48550/arXiv.1509.07642

Lin, C. T., Lin, F. C., Chen, S. A., Lu, S. W., Chen, T. C., & Ko, L. W. (2010). EEG-based brain-computer interface for smart living environmental auto-adjustment. *Journal of Medical and Biological Engineering*, *30*(4), 237-245.

Lin, Y. P., Wang, C. H., Wu, T. L., Jeng, S. K., & Chen, J. H. (2007, October). Multilayer perceptron for EEG signal classification during listening to emotional music. In *TENCON 2007-2007 IEEE region 10 conference* (pp. 1-3). IEEE. https://doi.org/10.1109/TENCON.2007.4428831

Liu, N. H., Chiang, C. Y., & Chu, H. C. (2013). Recognizing the degree of human attention using EEG signals from mobile sensors. *sensors*, *13*(8), 10273-10286. https://doi.org/10.3390/s130810273

Madden, K., & Savard, G. K. (1995). Effects of mental state on heart rate and blood pressure variability in men and women. *Clinical Physiology*, *15*(6), 557-569. https://doi.org/10.1111/j.1475-097X.1995.tb00544.x

Malmivuo, J., & Plonsey, R. (1995). *Bioelectromagnetism: principles and applications of bioelectric and biomagnetic fields*. Oxford University Press, USA.

Maskeliunas, R., Damasevicius, R., Martisius, I., & Vasiljevas, M. (2016). Consumer-grade EEG devices: are they usable for control tasks?. *PeerJ*, *4*, e1746. https://doi.org/10.7717/peerj.1746

Moore, S. T., MacDougall, H. G., & Ondo, W. G. (2008). Ambulatory monitoring of freezing of gait in Parkinson's disease. *Journal of neuroscience methods*, *167*(2), 340-348. https://doi.org/10.1016/j.jneumeth.2007.08.023

Murugappan, M., Ramachandran, N., & Sazali, Y. (2010). Classification of human emotion from EEG using discrete wavelet transform. *Journal of biomedical science and engineering*, *3*(04), 390. http://dx.doi.org/10.4236/jbise.2010.34054

Musk, E., & Neuralink (2019). An integrated brain-machine interface platform with thousands of channels. *Journal of medical Internet research*, *21*(10), e16194. https://doi.org/10.2196/16194

Nutt, J. G., Bloem, B. R., Giladi, N., Hallett, M., Horak, F. B., & Nieuwboer, A. (2011). Freezing of gait: moving forward on a mysterious clinical phenomenon. *The Lancet Neurology*, *10*(8), 734-744. https://doi.org/10.1016/S1474-4422(11)70143-0

Oh, S. H., Lee, Y. R., & Kim, H. N. (2014). A novel EEG feature extraction method using Hjorth parameter. *International Journal of Electronics and Electrical Engineering*, *2*(2), 106-110. http://dx.doi.org/10.12720/ijeee.2.2.106-110

Oostenveld, R., & Praamstra, P. (2001). The five percent electrode system for high-resolution EEG and ERP measurements. *Clinical neurophysiology*, *112*(4), 713-719. https://doi.org/10.1016/S1388-2457(00)00527-7

Oppenheim, A. V., Buck, J., Daniel, M., Willsky, A. S., Nawab, S. H., & Singer, A. (1997). *Signals & systems*. Pearson Educación.

Plutchik, R. (2001). The nature of emotions: Human emotions have deep evolutionary roots, a fact that may explain their complexity and provide tools for clinical practice. *American scientist*, *89*(4), 344-350.

Posada-Quintero, H. F., Reljin, N., Bolkhovsky, J. B., Orjuela-Cañón, A. D., & Chon, K. H. (2019). Brain activity correlates with cognitive performance deterioration during sleep deprivation. *Frontiers in neuroscience, 13*, 1001. https://doi.org/10.3389/fnins.2019.01001

Proakis, J. G., & Manolakis, D. G. (1996). *Digital signal processing: principles, algorithms, and applications* (3rd ed.). Prentice Hall International, USA.

Rabbani, M. H. R., & Islam, S. M. R. (2019). Detection of Different Brain Diseases from EEG Signals Using Hidden Markov Model. *International Journal of Image, Graphics and Signal Processing*, *10*(10), 16. https://doi.org/10.5815/ijigsp.2019.10.03

Rahman, M. M., Sarkar, A. K., Hossain, M. A., Hossain, M. S., Islam, M. R., Hossain, M. B., Quinn, J. M. W., & Moni, M. A. (2021). Recognition of human emotions using EEG signals: A review. *Computers in Biology and Medicine*, *136*, 104696. https://doi.org/10.1016/j.compbiomed.2021.104696

Rahman, S., Griffin, H. J., Quinn, N. P., & Jahanshahi, M. (2008). The factors that induce or overcome freezing of gait in Parkinson's disease. *Behavioural neurology*, *19*(3), 127-136. https://doi.org/10.1155/2008/456298

Ray, W. J., & Cole, H. W. (1985). EEG alpha activity reflects attentional demands, and beta activity reflects emotional and cognitive processes. *Science*, *228*(4700), 750-752. https://doi.org/10.1126/science.3992243

Rubin, D., L., Greenspan, H., & Brinkley, J., F., (2014). Biomedical imaging informatics. In E. H. Shortliffe, & J. J. Cimino (Eds.), *Biomedical informatics:* Computer Applications in health care and biomedicine (pp. 285–328). Springer. https://doi.org/10.1007/978-1-4471-4474-8

Russell, J. A. (1980). A circumplex model of affect. *Journal of personality and social psychology*, *39*(6), 1161. https://doi.org/10.1037/h0077714

Sarno, R., Munawar, M., & Nugraha, B. (2016). Real-time electroencephalography-based emotion recognition system. Int. Rev. Comput. Softw. IRECOS, 11(5), 456-465. https://doi.org/10.15866/irecos.v11i5.9334

Schaafsma, J. D., Balash, Y., Gurevich, T., Bartels, A. L., Hausdorff, J. M., & Giladi, N. (2003). Characterization of freezing of gait subtypes and the response of each to levodopa in Parkinson's disease. *European journal of neurology*, *10*(4), 391-398. https://doi.org/10.1046/j.1468-1331.2003.00611.x

Seiffert, C., Khoshgoftaar, T. M., Van Hulse, J., & Napolitano, A. (2008, December). RUSBoost: Improving classification performance when training data is skewed. In *2008 19th international conference on pattern recognition* (pp. 1-4). IEEE. https://doi.org/10.1109/ICPR.2008.4761297

Seo, S. H., Lee, J. T., & Crisan, M. (2010). Stress and EEG. *Convergence and hybrid information technologies*, *27*.

Shahnaz, C., Masud, S. B., & Hasan, S. S. (2016, November). Emotion recognition based on wavelet analysis of Empirical Mode Decomposed EEG signals

responsive to music videos. In *2016 IEEE Region 10 Conference (TENCON)* (pp. 424-427). IEEE. https://doi.org/10.1109/TENCON.2016.7848034

Shine, J. M., Handojoseno, A. M. A., Nguyen, T. N., Tran, Y., Naismith, S. L., Nguyen, H., & Lewis, S. J. G. (2014). Abnormal patterns of theta frequency oscillations during the temporal evolution of freezing of gait in Parkinson's disease. *Clinical Neurophysiology*, *125*(3), 569-576. https://doi.org/10.1016/j.clinph.2013.09.006

Silicon Laboratories. (2017). *Single-chip USB to UART bridge CP2102/9 datasheet*. Revised January 20, 2017.

Soleymani, M., Lichtenauer, J., Pun, T., & Pantic, M. (2011). A multimodal database for affect recognition and implicit tagging. *IEEE transactions on affective computing*, *3*(1), 42-55. https://doi.org/10.1109/T-AFFC.2011.25

Srinivasan, R., Tucker, D. M., & Murias, M. (1998). Estimating the spatial Nyquist of the human EEG. *Behavior Research Methods, Instruments, & Computers*, *30*(1), 8-19.

Suhaimi, N. S., Mountstephens, J., & Teo, J. (2020). EEG-based emotion recognition: a state-of-the-art review of current trends and opportunities. *Computational intelligence and neuroscience*, *2020*. https://doi.org/10.1155/2020/8875426

Şen, B., & Peker, M. (2013). Novel approaches for automated epileptic diagnosis using FCBF selection and classification algorithms. *Turkish Journal of Electrical Engineering & Computer Sciences*, *21*(Sup. 1), 2092-2109. https://doi.org/10.3906/elk-1203-9

Thammasan, N., Moriyama, K., Fukui, K. I., & Numao, M. (2017). Familiarity effects in EEG-based emotion recognition. *Brain informatics*, *4*(1), 39-50. https://doi.org/10.1007/s40708-016-0051-5

Toresano, L. O. H. Z., Wijaya, S. K., Prawito, Sudarmaji, A., Syakura, A., & Badri, C. (2017, February). Data acquisition instrument for EEG based on embedded system. In *AIP Conference Proceedings* (Vol. 1817, No. 1, p. 040009). AIP Publishing LLC. https://doi.org/10.1063/1.4976794

Torres, E. P., Torres, E. A., Hernández-Álvarez, M., & Yoo, S. G. (2020). EEG-based BCI emotion recognition: A survey. *Sensors*, *20*(18), 5083. https://doi.org/10.3390/s20185083

Trnka, R., Hasto, J., Cabelkova, I., Kuska, M., Tavel, P., & Nikolai, T. (2018). Amygdala and emotionality in Parkinson's disease: An integrative review of the neuropsychological evidence. *Neuroendocrinology Letters*, 39(2).

Urigüen, J. A., & Garcia-Zapirain, B. (2015). EEG artifact removal—state-of-the-art and guidelines. *Journal of neural engineering*, *12*(3), 031001. http://doi.org/10.1088/1741-2560/12/3/031001

Vaid, S., Singh, P., & Kaur, C. (2015, February). EEG signal analysis for BCI interface: A review. In *2015 fifth international conference on advanced computing & communication technologies* (pp. 143-147). IEEE. https://doi.org/10.1109/ACCT.2015.72

van Mierlo, T. J., Chung, C., Foncke, E. M., Berendse, H. W., & van den Heuvel, O. A. (2015). Depressive symptoms in Parkinson's disease are related to decreased hippocampus and amygdala volume. *Movement Disorders*, *30*(2), 245-252. https://doi.org/10.1002/mds.26112

Vasiljevic, G. A. M., & de Miranda, L. C. (2020). Brain–computer interface games based on consumer-grade EEG Devices: A systematic literature review. *International Journal of Human–Computer Interaction*, *36*(2), 105-142. https://doi.org/10.1080/10447318.2019.1612213

Vriend, C., Boedhoe, P. S., Rutten, S., Berendse, H. W., van der Werf, Y. D., & van den Heuvel, O. A. (2016). A smaller amygdala is associated with anxiety in Parkinson's disease: a combined FreeSurfer—VBM study. *Journal of Neurology, Neurosurgery & Psychiatry*, *87*(5), 493-500. https://doi.org/10.1111/bph.13509

Waldert, S. (2016). Invasive vs. non-invasive neuronal signals for brain-machine interfaces: Will one prevail?. *Frontiers in neuroscience*, *10*, 295. https://doi.org/10.3389/fnins.2016.00295

Wang, Y., Beuving, F., Nonnekes, J., Cohen, M. X., Long, X., Aarts, R. M., & Van Wezel, R. (2020, July). Freezing of gait detection in Parkinson's disease via multimodal analysis of EEG and accelerometer signals. In *2020 42nd Annual International Conference of the IEEE Engineering in Medicine & Biology Society (EMBC)* (pp. 847-850). IEEE. https://doi.org/10.1109/EMBC44109.2020.9175288

Webster, J. G. (2009). *Medical instrumentation: application and design* (2nd ed.). John Wiley & Sons.

Wong, K. F. K., Galka, A., Yamashita, O., & Ozaki, T. (2006). Modelling non-stationary variance in EEG time series by state space GARCH model. *Computers in biology and medicine*, *36*(12), 1327-1335. https://doi.org/10.1016/j.compbiomed.2005.10.001

World Health Organization. (2006). *Neurological disorders: public health challenges*. World Health Organization.

Wróbel, G. (2018). The structure of the brain and human behaviour. *Journal of Education, Health and Sport*, *8*(1), 37-51. https://doi.org/10.5281/zenodo.1145427

Wu, S., Xu, X., Shu, L., & Hu, B. (2017, November). Estimation of valence of emotion using two frontal EEG channels. In *2017 IEEE international conference on bioinformatics and biomedicine (BIBM)* (pp. 1127-1130). IEEE. https://doi.org/10.1109/BIBM.2017.8217815

Xsens Technologies B.V. (2018). *MTw Awinda User Manual*. https://www.xsens.com/hubfs/Downloads/Manuals/MTw_Awinda_User_Manual.pdf

Yang, X., Gao, M., Shi, J., Ye, H., & Chen, S. (2017). Modulating the activity of the DLPFC and OFC has distinct effects on risk and ambiguity decision-making: A tDCS study. *Frontiers in psychology*, *8*, 1417. https://doi.org/10.3389/fpsyg.2017.01417

You, S. D. (2021). Classification of Relaxation and Concentration Mental States with EEG. *Information*, *12*(5), 187. https://doi.org/10.3390/info12050187

Yurdem, B., Ozkurt, A., Eliiyi, U., Kahraman, T., Duran, G., Colakoglu, B. D., Keskinoglu, P., & Genc, A. (2020). Emotion and brain state based freezing of gait occurrence analysis with electroencephalography data. *Gait & Posture*, *81*, 403. https://doi.org/10.1016/j.gaitpost.2020.08.101

Yürdem, B., & Özkurt, A. (2022, September). Algorithm of Informative Electrode Selection in Person Based Emotion Detection with Hjorth Parameters Obtained from EEG Signals. In *2022 Innovations in Intelligent Systems and Applications Conference (ASYU)* (pp. 1-5). IEEE. https://doi.org/10.1109/ASYU56188.2022.9925425

Yürdem, B., Akpinar, B., & Özkurt, A. (2019, November). EEG Data Acquisition and Analysis for Human Emotions. In *2019 11th International Conference on Electrical and Electronics Engineering (ELECO)* (pp. 432-436). IEEE. https://doi.org/10.23919/ELECO47770.2019.8990539

Zheng, W. L., & Lu, B. L. (2015). Investigating critical frequency bands and channels for EEG-based emotion recognition with deep neural networks. *IEEE Transactions on autonomous mental development*, *7*(3), 162-175. https://doi.org/10.1109/TAMD.2015.2431497

Zhang, Y., Ji, X., & Zhang, S. (2016). An approach to EEG-based emotion recognition using combined feature extraction method. *Neuroscience letters*, *633*, 152-157. https://doi.org/10.1016/j.neulet.2016.09.037

Zucco, C., Calabrese, B., & Cannataro, M. (2019, July). Emotion Mining: from Unimodal to Multimodal Approaches. In *International Workshop on Brain-Inspired Computing* (pp. 143-158). Springer, Cham. https://doi.org/10.1007/978-3-030-82427-3_11